

AD-A196 526

2

NAVAL POSTGRADUATE SCHOOL

Monterey, California



DTIC FILE COPY

THESIS

DTIC
ELECTE
AUG 08 1988
S H D

TRANSISTOR SIZING IN THE DESIGN OF
HIGH-SPEED CMOS SUPER BUFFERS

by

Gordon R. Steele

March 1988

Co-advisor:

D.E. Kirk

Co-advisor:

H.H. Loomis, Jr.

Approved for public release; distribution is unlimited.

12 8 28 030

UNCLASSIFIED

SECURITY CLASSIFICATION OF THIS PAGE

REPORT DOCUMENTATION PAGE

1a. REPORT SECURITY CLASSIFICATION (UNCLASSIFIED)			1b. RESTRICTIVE MARKINGS		
2a. SECURITY CLASSIFICATION AUTHORITY			3. DISTRIBUTION/AVAILABILITY OF REPORT Approved for public release; distribution is unlimited		
2b. DECLASSIFICATION/DOWNGRADING SCHEDULE			5. MONITORING ORGANIZATION REPORT NUMBER(S)		
4. PERFORMING ORGANIZATION REPORT NUMBER(S)			5. MONITORING ORGANIZATION REPORT NUMBER(S)		
6a. NAME OF PERFORMING ORGANIZATION Naval Postgraduate School		6b. OFFICE SYMBOL (If applicable) 62	7a. NAME OF MONITORING ORGANIZATION Naval Postgraduate School		
6c. ADDRESS (City, State, and ZIP Code) Monterey, California 93943-5000			7b. ADDRESS (City, State, and ZIP Code) Monterey, California 93943-5000		
8a. NAME OF FUNDING/SPONSORING ORGANIZATION		8b. OFFICE SYMBOL (If applicable)	9. PROCUREMENT INSTRUMENT IDENTIFICATION NUMBER		
8c. ADDRESS (City, State, and ZIP Code)			10. SOURCE OF FUNDING NUMBERS		
			PROGRAM ELEMENT NO.	PROJECT NO.	TASK NO.
			WORK UNIT ACCESSION NO.		
11. TITLE (Include Security Classification) TRANSISTOR SIZING IN THE DESIGN OF HIGH-SPEED CMOS SUPER BUFFERS (U)					
12. PERSONAL AUTHOR(S) Steele, Gordon R.					
13a. TYPE OF REPORT Master's Thesis		13b. TIME COVERED FROM _____ TO _____		14. DATE OF REPORT (Year, Month, Day) 1988 March	
				15. PAGE COUNT 145	
16. SUPPLEMENTARY NOTATION The views in this thesis are those of the author and do not reflect the official policy or position of the Department of Defense or the U.S. Government.					
17. COSATI CODES			18. SUBJECT TERMS (Continue on reverse if necessary and identify by block number)		
FIELD	GROUP	SUB-GROUP	MacPITTS; Silicon Compiler; CMOS; VLSI; Super Buffer; Transistor Sizing; High-Speed CMOS		
19. ABSTRACT (Continue on reverse if necessary and identify by block number) An algorithm for sizing transistors for static Complementary-symmetry Metal-Oxide-Semiconductor (CMOS) integrated circuit logic design using silicon gate enhancement mode Field-Effect Transistors (FET) is derived and implemented in software. The algorithm is applied to the mask level hardware design of a three micron minimum feature size p well high-speed super buffer. A software representation of the super buffer can be used for the automated design of custom Very-Large-Scale Integrated (VLSI) circuits.					
20. DISTRIBUTION/AVAILABILITY OF ABSTRACT <input checked="" type="checkbox"/> UNCLASSIFIED/UNLIMITED <input type="checkbox"/> SAME AS RPT <input type="checkbox"/> DTIC USERS			21. ABSTRACT SECURITY CLASSIFICATION (UNCLASSIFIED)		
22a. NAME OF RESPONSIBLE INDIVIDUAL H.H. Loomis, Jr.			22b. TELEPHONE (Include Area Code) (408) 646-3214		22c. OFFICE SYMBOL 62LM

DD FORM 1473, 84 MAR

83 APR edition may be used until exhausted.

All other editions are obsolete

SECURITY CLASSIFICATION OF THIS PAGE

U.S. Government Printing Office: 1986-608-24.

Approved for public release; distribution is unlimited

Transistor Sizing in the Design of
High-Speed CMOS Super Buffers

by

Gordon R. Steele
Captain, United States Marine Corps
B.S.F.S., Georgetown University, 1981

Submitted in partial fulfillment of the
requirements for the degree of

MASTER OF SCIENCE IN ELECTRICAL ENGINEERING

from the

NAVAL POSTGRADUATE SCHOOL

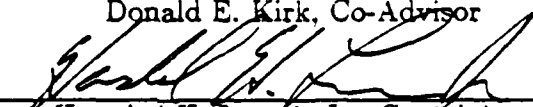
March 1988

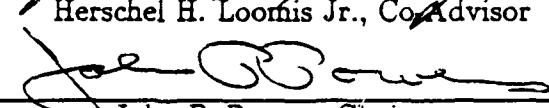
Author:

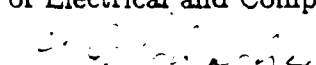

Gordon R. Steele

Approved by:


Donald E. Kirk, Co-Advisor


Herschel H. Loomis Jr., Co-Advisor


John P. Powers, Chairman
Department of Electrical and Computer Engineering


Gordon E. Schacher, Dean of Science and Engineering

ABSTRACT

An algorithm for sizing transistors for static Complementary-symmetry Metal-Oxide-Semiconductor (CMOS) integrated circuit logic design using silicon gate enhancement mode Field-Effect Transistors (FET) is derived and implemented in software. The algorithm is applied to the mask level hardware design of a three micron minimum feature size p well high-speed super buffer. A software representation of the super buffer can be used for the automated design of custom Very-Large-Scale-Integrated (VLSI) circuits.

QUALITY
INSPECTED
2

Accession For	
NTIS GRA&I	<input checked="checked" type="checkbox"/>
DTIC TAB	<input type="checkbox"/>
Unannounced	<input type="checkbox"/>
Justification	
By	
Distribution/	
Availability Codes	
Dist	Avail and/or Special
A-1	

TABLE OF CONTENTS

I.	INTRODUCTION	1
II.	SIZING OF SILICON GATE ENHANCEMENT MODE METAL-OXIDE- SEMICONDUCTOR FIELD-EFFECT TRANSISTORS IN STATIC CMOS LOGIC DESIGN	6
A.	CHARACTERISTICS OF STATIC CMOS CIRCUIT DESIGN	6
B.	DERIVATION OF EQUATIONS FOR TRANSISTOR SIZING IN A STA- TIC CMOS INVERTER	9
1.	Overview	9
2.	Rise Time and Fall Time Determination	10
3.	Capacitive Loading	26
a.	Diffusion to Substrate Capacitance of the Interconnection Node	27
b.	Gate Capacitance of the Next Stage	34
c.	Routing Capacitance	37
4.	Finding W_p and W_n	37
5.	Drain Resistance	39
6.	Theoretical Bounds on Inverter Performance	42
C.	EXTENSION OF THE STATIC CMOS INVERTER TRANSISTOR SIZ- ING EQUATIONS TO GENERAL STATIC CMOS LOGIC DESIGN	45
D.	EXTENSION OF THE TRANSISTOR SIZING EQUATIONS TO NON- RECTANGULAR TRANSISTORS	50

E. CHAPTER SUMMARY	51
III. DESIGN OF A HIGH-SPEED STATIC CMOS SUPER BUFFER FOR THE MONTEREY SILICON COMPILER	53
A. BACKGROUND	53
B. DESIGN OF THE SUPER BUFFER	57
C. SIMULATION OF THE SUPER BUFFER	68
D. MASK LEVEL SUPER BUFFER IMPLEMENTATION	73
E. PERFORMANCE OF THE SUPER BUFFER IN MULTI-BIT DATA- PATH CIRCUITS	76
IV. CONCLUSIONS	84
A. SUMMARY	84
B. RECOMMENDATIONS	85
1. Effects of a Non-Ideal Input Square Wave	86
2. Empirical Adjustment of Drain Current Equations	86
3. Channel Length Modulation	87
4. Body Effect	87
5. Accuracy in Computation and Fabrication	87
6. Stage Ratio	88
7. Suggested Modifications to the Monterey Silicon Compiler	88
APPENDIX A: STATIC CMOS INVERTER TRANSISTOR SIZING PROGRAMS	90
APPENDIX B: STATIC CMOS SUPER BUFFER PSPICE DECK	121

LIST OF REFERENCES	125
BIBLIOGRAPHY	127
INITIAL DISTRIBUTION LIST	130

LIST OF TABLES

2.1 MOSFET Drain Current Equations (from MicroSim Corporation's PSpice) ..	13
2.2 PSpice MOSFET Model Parameters (from MicroSim Corporation's PSpice) ..	15
2.3 MOSFET Temperature Effects (from MicroSim Corporation's PSpice) ...	16
2.4 Important Equations for the Static CMOS Inverter	39
2.5 Important Equations for General Static CMOS Logic Design	50
3.1 Summary of Rise and Fall Time Data for the Super Buffer	73
3.2 Summary of Delay Time Data for the Super Buffer	74
3.3 Summary of Rise and Fall Time Data for the Super Buffer in Multi-Bit Data Path Circuits with $V_{DD} = 6$ Volts	80
3.4 Summary of Delay Time Data for the Super Buffer in Multi-Bit Data Path Circuits with $V_{dd} = 6$ Volts	81
4.1 Monterey Silicon Compiler NMOS Logic Cells Requiring CMOS Replacements	85
A.1 SPICE Fabrication Parameter Data Register Allocation	93
A.2 Data Register Allocation for Variables Other than SPICE Fabrication Parameters	94

LIST OF FIGURES

2.1 Schematic of a Possible p Block Configuration in a Static CMOS Logic Gate	6
2.2 Schematic of a Possible n Block Configuration in a Static CMOS Logic Gate	7
2.3 Interconnection of p and n Blocks in Static CMOS Logic Gates with Capacitive Loading	8
2.4 Schematic of a Static CMOS Inverter without Capacitive Loading	8
2.5 Switch Level Idealization of MOSFET Behavior	10
2.6 Switch Level Idealization of Static CMOS Inverter Behavior	11
2.7 Current Flow in MOSFETs	14
2.8 Schematic of a Static CMOS Inverter with Capacitive Loading	17
2.9 Effects of the Rising Edge of a Pulsed Input on a Static CMOS Inverter	18
2.10 Effects of the Falling Edge of a Pulsed Input on a Static CMOS Inverter	20
2.11 Idealized Physical MOSFET	23
2.12 Effects of Lateral Diffusion of Doping Ions on a Physical MOSFET	24
2.13 Drain Diffusion Area Dimensions	28
2.14 Bulk-Drain Depletion Capacitance and Metal to Diffusion Contact Capacitance	29
2.15 Mask Level Layout of a Static CMOS Inverter	33
2.16 Load MOSFET Channel Dimensions	35

2.17 Load MOSFET Gate Capacitance	36
2.18 Drain Diffusion Region and Resistive Equivalent	40
2.19 Drain Diffusion Region with a Single Metal to Diffusion Contact Area and Resistive Equivalent	41
2.20 Drain Diffusion Region with N Metal to Diffusion Contact Areas and Resistive Equivalent	43
2.21 Static CMOS Compound Gate Implementation of $F = \overline{((A \cdot B) + (C \cdot D))}$	46
2.22 Manhattan Geometry Star Configured MOSFET	51
2.23 Circular MOSFET	51
3.1 Employment of Super Buffer within the Monterey Silicon Compiler Architecture	55
3.2 Mask Level Integrated Circuit Layout of CMOS Register	60
3.3 Schematic of Static CMOS Super Buffer	67
3.4 PSpice PROBE Postprocessor Simulation of Voltage Waveforms Presented to and Produced by the Input Stage of the Super Buffer Using MOSFET Level Two Model	69
3.5 PSpice PROBE Postprocessor Simulation of Voltage Waveforms Presented to and Produced by the Output Stage of the Super Buffer Using MOSFET Level Two Model	71
3.6 PSpice PROBE Postprocessor Simulation of Voltage Waveforms Presented to the Input Stage of the Super Buffer and Produced by the Output Stage of the Super Buffer Using MOSFET Level Two Model	72
3.7 Mask Level Integrated Circuit Layout of Static CMOS Super Buffer	75
3.8 Example of a Portion of a Microchip Designed with the Monterey Silicon Compiler Showing Placement of the Static CMOS Super Buffer Below a CMOS Register	77

3.9 Four Bit Shifter Hybrid Microchip Designed with the Monterey Silicon Compiler	78
3.10 CMOS Input Pad Replacement for the Monterey Silicon Compiler	79
3.11 Eight Bit Taxi Meter Hybrid Microchip Designed with the Monterey Silicon Compiler	83
A.1 Interrelationships of Transistor Sizing Programs	91

ACKNOWLEDGMENTS

My deepest and most sincere thanks for the support I have received in the pursuit of my studies go to my wife, Anne, and my children, Andrew and Julia. I would also like to express my appreciation to Dr. Donald Kirk and to Dr. Herschel Loomis of the Naval Postgraduate School for the assistance and guidance that they provided to me in conducting the research and the writing of this thesis.

I. INTRODUCTION

The MacPITTS silicon compiler is a tool for the automated design of complete, Very-Large-Scale Integrated (VLSI) microchips that was created at the Massachusetts Institute of Technology Lincoln Laboratory in the early 1980's [Massachusetts Institute of Technology 1982 Conference on Advanced Research in VLSI, 1982, pp. 28-29]. To use MacPITTS a design engineer specifies the desired logic behavior of a complete microchip in a source program written in a high level algorithmic language. Writing this program is the only task that the design engineer need perform—the entire design process is then performed by the compiler. The compiler extracts information from this program which it uses to create a mask level layout in Caltech Intermediate Form (CIF). The layout when specified in this form is suitable for use by silicon foundries for the fabrication of an actual microchip.

Use of a silicon compiler provides dramatic design time savings over handcrafting layouts. The design—simulate—redesign cycle that occurs before fabrication of handcrafted layouts is lengthy and therefore expensive. Handcrafted designs that take many months of man-hours to complete using computer based engineering design tools may be completed in a much shorter time by using a silicon compiler. Most VLSI designs today contain 20,000 to 50,000 devices. When human engineers design these large chips they partition and design the project in teams. Integrating the subsystems into a final working design requires close coordination throughout the design process and a uniform approach on the part of all the design teams. Using a silicon compiler to design automatically institutes uniformity in the design process. The compiler uses embedded techniques and rigorous checking

and verification of design practices to ensure that the resulting circuit is "correct by construction." These embedded functions often incorporate the practices of expert integrated circuit designers. A good compiler can verify the functionality and timing of a design after it has been implemented. Some can provide real-time checking, verification and implementation strategies that flag potential errors and hazards and prevent them from being entered into the design. All of these features of silicon compilers contribute to the production of designs that are as correct as possible before fabrication. This is extremely important in VLSI design because it is difficult and costly to isolate design errors on a finished microchip. [Pollack, Erickson, and Mazor, 1986, pp. 79-80]

The MacPITTS Silicon Compiler is actually a collection of programs each of which performs a specific function. The base language of these programs is Franz Lisp with extended functions for geometric cell layout provided by the Massachusetts Institute of Technology Lincoln Laboratory language L5 and by MacPITTS itself. One way in which the programs can be categorized is to lump together all those that are dependent upon a particular microchip fabrication technology and those that are not. By altering only the technology dependent programs to reflect the design rules of a desired technology the rest of the compiler can become technology independent. This is a very desirable feature in the fast moving electronics industry because a favored technology today may be outmoded tomorrow. The technology dependent programs in the original MacPITTS compiler were based on n channel Metal-Oxide-Semiconductor (NMOS) technology. NMOS has since been largely replaced by Complementary-symmetry Metal-Oxide-Semiconductor (CMOS) technology as the commercial technology of choice for low power consumption VLSI applications. This transition in industry has occurred largely because

CMOS technology has matured to the point that it now rivals NMOS in switching speed yet consumes only a fraction of the power required by NMOS circuitry. It is therefore a logical step to modify the technology dependent portions of the MacPITTS Silicon Compiler to support CMOS design rules.

One of the major technology dependent portions of MacPITTS is the body of code within it that defines the geometric layout of logic cells. The compiler selects, places, and interconnects these cells in such a way that the result is a design for a physically achievable microchip that will behave as specified by the word picture that the design engineer presents to the compiler in his or her source program. These cells reside in what is essentially a library.

An ongoing project at the Naval Postgraduate School in Monterey, California, has been the addition of a CMOS option to the technology dependent portions of the MacPITTS Silicon Compiler. Since the work has progressed to the point that the present compiler is a significant departure from the original MacPITTS the hybrid NMOS/CMOS compiler is now referred to as the Monterey Silicon Compiler.

The immediate goal of the research documented in this thesis is to create and insert into the Monterey Silicon Compiler code a mask level integrated circuit design of a high-speed static CMOS super buffer to replace the existing NMOS version. In the Monterey Silicon Compiler architecture the super buffer is that part of the branching fan-out tree that feeds clock signals from off-chip to various parts of a VLSI circuit. Since the super buffer is a gate in the path of incoming clock signals it must be guaranteed to function within specified timing constraints under given loading lest the operation of an entire chip fail due to the inability of the clock circuit to drive the on chip storage registers within an acceptable amount of time delay. From the designer's point of view the timing characteristics

of enhancement Metal-Oxide-Semiconductor Field-Effect Transistors (MOSFET), of which the super buffer is made, are controlled chiefly by the mask geometry of the MOSFETs. Therefore, a major portion of this research is devoted to an analysis of transistor sizing for static CMOS logic gates constructed from silicon gate enhancement MOSFETs.

Transistor sizing is the principal means by which an integrated circuit design engineer can influence the timing of a MOSFET. In a silicon compiler the design engineer is a computer. Typically, human engineers achieve desired timing through a design—simulate—redesign iterative method based on rules of thumb that are handed down by successful engineers to junior engineers. A silicon compiler that strives to optimize signal input to signal output delay time on a microchip cannot work in this way—it must be given explicit instructions on how to decide what transistor sizes are required to drive a given load, with a given supply voltage and operating temperature, within a specified delay time. Chapter II, which deals with the transistor sizing problem, is an original contribution to the field of time delay optimization in silicon compiler generated custom CMOS VLSI circuits. A coherent body of mathematical equations that detail how to size transistors to achieve desired timing parameters under known loading conditions, operating temperature, and supply voltage is derived in Chapter II. The equations are applicable to general static CMOS design.

Although the Monterey Silicon Compiler is not capable of designing a circuit that is constructed specifically to achieve a designer specified time delay this is a topic applicable to the general field of silicon compilation. The equations in Chapter II are useful to the Monterey Silicon Compiler as a design tool for the construction of the individual logic cells in the library that the compiler uses to build an integrated circuit floorplan. The equations developed are implemented in

a computer program that is included in Appendix A. The program is used to apply the equations to a design problem, the design of the super buffer, in Chapter III. The resulting mask level design is simulated with a SPICE MOSFET model that is independent of the transistor sizing equations to verify the correctness of the approach. The design is translated into L5 code and inserted into the Monterey Silicon Compiler code for use in the automated design of custom CMOS VLSI circuits. The design of the super buffer moves the Monterey Silicon Compiler project one step closer to completion.

II. SIZING OF SILICON GATE ENHANCEMENT MODE METAL-OXIDE-SEMICONDUCTOR FIELD-EFFECT TRANSISTORS IN STATIC CMOS LOGIC DESIGN

A. CHARACTERISTICS OF STATIC CMOS CIRCUIT DESIGN

Static CMOS Logic gates are made from two distinct blocks of devices that are connected together. Within one block are series combinations of p MOSFETs or parallel combinations of p MOSFETs or both. The MOSFETs in the p block are connected to a supply voltage.

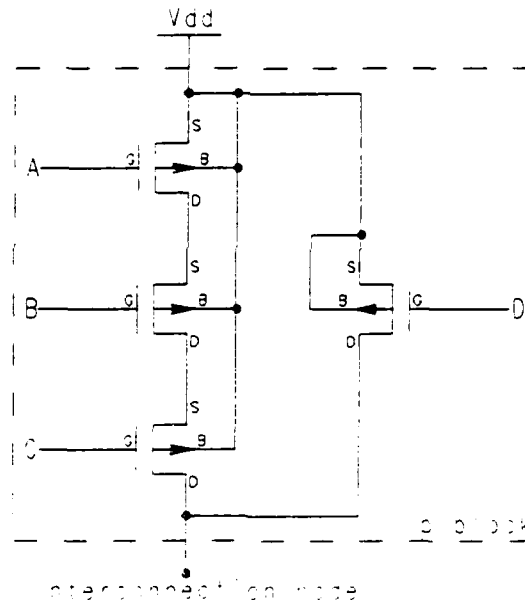


Figure 2.1 Schematic of a Possible p Block Configuration in a Static CMOS Logic Gate

Figure 2.1 shows an example of a possible p block configuration [Weste and Eshraghian, 1985, p. 16]. Within the other block are series combinations of n MOSFETs or parallel combinations of n MOSFETs or both. The MOSFETs in

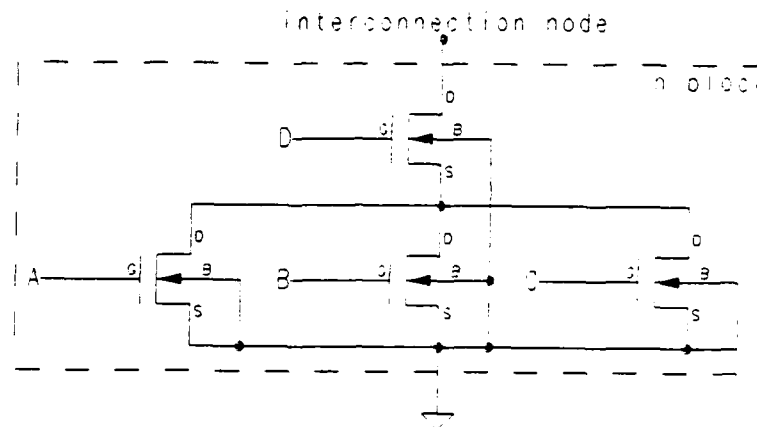


Figure 2.2 Schematic of a Possible n Block Configuration in a Static CMOS Logic Gate

the n block are connected to ground. Figure 2.2 shows an example of a possible n block configuration. [Weste and Eshraghian, 1985, p. 16]

Any load capacitance to be driven by a static CMOS logic gate is attached to the node defined by the interconnection of the p and n blocks. Figure 2.3 shows the interconnection of the two blocks with a capacitive load attached.

The simplest static CMOS logic gate is an inverter. The inverter shown in Figure 2.4 consists of a single p MOSFET and a single n MOSFET. In an ideal sense, each p MOSFET in a static CMOS logic gate may be thought of as a switch along a path connecting the supply voltage to the load capacitance [Weste and Eshraghian, 1985, p. 7]. Similarly, each n MOSFET may be thought of as a switch along a path connecting the load capacitance to ground.

Figure 2.5 illustrates that a MOSFET that is conducting can be thought of as a closed switch and that a MOSFET that is in cutoff can be thought of as an open switch. Therefore, the voltage across the terminals of the load capacitance

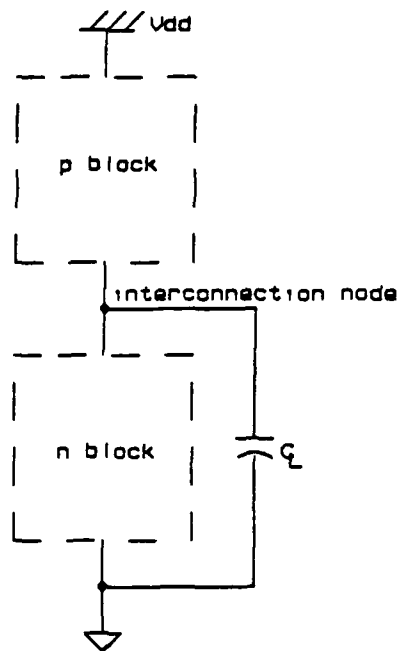


Figure 2.3 Interconnection of p and n Blocks in Static CMOS Logic Gates with Capacitive Loading

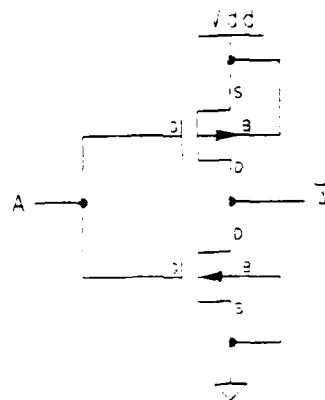


Figure 2.4 Schematic of a Static CMOS Inverter without Capacitive Loading

will be driven to the logic high level if enough switches in the p block are closed to create at least one complete path from the supply voltage to the load capacitance and enough switches in the n block are opened to sever all paths between the load capacitance and ground. Figure 2.6.a illustrates this switch level behavior for the inverter in Figure 2.4. The voltage across the terminals of the load capacitance will be driven to the logic low level if enough switches in the n block are closed to create at least one path from the load capacitance to ground and enough switches in the p block are opened to sever all paths between the supply voltage and the load. Figure 2.6.b illustrates this switch level behavior for the inverter in Figure 2.4.

B. DERIVATION OF EQUATIONS FOR TRANSISTOR SIZING IN A STATIC CMOS INVERTER

1. Overview

In the physical world MOSFETs are not ideal switches. In addition to the capacitive load that they must drive they have internal parasitic capacitances and resistances that must also be driven. These parasitic capacitances and resistances are chiefly determined by operating temperature, various parameters associated with the fabrication process, and the physical dimensions of the MOSFETs. Only the third factor, the physical dimensions of the MOSFETs, is under the control of a circuit designer.

It is essential that the circuit designer, be it a human or an automated CAD tool like a silicon compiler, have a method to determine the physical dimensions of the MOSFETs in a static CMOS logic gate that are required to drive the load. The method presented here finds the dimensions of the p and n MOSFETs in the inverter of Figure 2.4 that are required to drive the parasitics and known capacitive load within a designer specified time constraint. The inverter is used

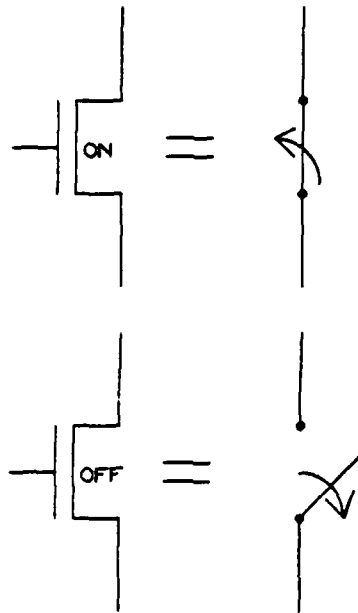


Figure 2.5 Switch Level Idealization of MOSFET Behavior

for the development of this method because it is the simplest static CMOS logic gate and as such the method developed for the inverter can be easily extended to general static CMOS logic design, the topic of Section C.

2. Rise Time and Fall Time Determination

Table 2.1 gives the ideal (first order) equations of the Shichman-Hodges model describing the behavior of MOSFETs in their three regions of operation: cutoff region, linear region, and saturation region [Hodges and Jackson, 1983, p. 51, and MicroSim Corp., 1987, p. 78]. Table 2.1 refers to the variable $KP\{T\}$. KP is one of the 58 variables used in the SPICE circuit simulation program, a standard CAD tool for the design and simulation of MOSFET circuits. Table 2.2 presents only those MOSFET model parameters used in this thesis as defined in MicroSim Corporation's PSpice program documentation [MicroSim Corp., 1987,

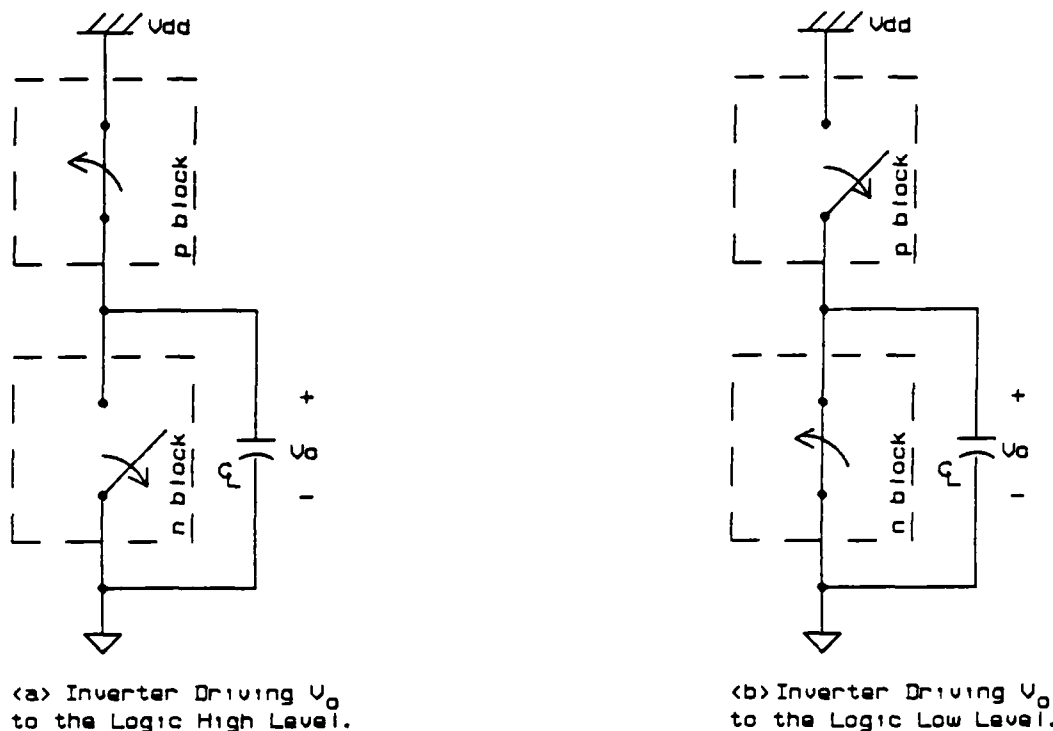


Figure 2.6 Switch Level Idealization of Static CMOS Inverter Behavior

pp. 74-76]. The model parameters can be grouped into two broad categories: those that represent the mask geometry of the on-chip devices and those that represent the electrical and metallurgical properties of the chip due to the particular type of fabrication process used to construct the microchip.¹ As stated in Section B.1,

¹ A good discussion of the physical meaning of the SPICE MOSFET model parameters can be found in, "The Simulation of MOS Integrated Circuits Using SPICE2, Memorandum No. M80/7, February, 1980", by Vladimirescu and Liu. The paper is available through the Electronics Research Laboratory Industrial Support Office at the University of California at Berkeley.

the circuit designer is able to modify parameters in the first category but not those in the second.

Some of these parameters are temperature dependent. The effects of temperature on those SPICE MOSFET model parameters used in this thesis are defined by the equations in Table 2.3. These equations are drawn from the program documentation for PSpice by MicroSim Corporation. [MicroSim Corp., 1987, p. 80]

Note that positive drain current in an n channel enhancement MOSFET flows from drain to source. This is illustrated in Figure 2.7.a. In a p channel enhancement MOSFET it flows from source to drain [Sedra and Smith, 1982, p. 311]. This is illustrated in Figure 2.7.b.

Section B.1 states that the load on a MOSFET is capacitive. Switching from one logic level to another therefore involves the charging or discharging of the parasitic and load capacitors and this requires time. The time that it takes a voltage waveform to rise from 10% to 90% of its steady state value is defined to be its rise time, denoted t_r . Fall time, denoted t_f , is defined to be the time it takes a voltage waveform to fall from 90% to 10% of its steady state value. [Weste and Eshraghian, 1985, p. 137]

The following discussion is based on a method of finding the rise and fall time of a static CMOS inverter proposed by Weste and Eshraghian [Weste and Eshraghian, 1985, pp. 137-140]. Given the circuit of Figure 2.8 in which C_L is initially charged so that $V_0 = V_{dd}$, a pulse of magnitude V_{dd} is applied to V_{in} . The effect of the pulse on the circuit's behavior is plotted in Figure 2.9.a. In this figure the regions of operation of the n MOSFET and p MOSFET are labeled in accordance with the definitions of the regions presented in Table 2.1. From Figure 2.9.a it is evident that the p MOSFET immediately enters the cutoff region where

**TABLE 2.1 MOSFET DRAIN CURRENT EQUATIONS
(FROM MICROSIM CORPORATION'S PSPICE)**

DEVICE TYPE	REGION	DRAIN CURRENT
n	$Vds_n \geq 0$ $Vgs_n - Vto_n\{T\} < 0$ [cutoff region]	$I_{\text{drain}_n} = 0$
n	$Vds_n \geq 0$ $Vds_n < Vgs_n - Vto_n\{T\}$ [linear region]	$I_{\text{drain}_n} = \left(\frac{W_n}{L_{\text{eff}_n}} \right) \cdot \left(\frac{KP_n\{T\}}{2} \right) \cdot Vds_n \cdot (2 \cdot (Vgs_n - Vto_n\{T\}) - Vds_n)$
n	$Vds_n \geq 0$ $0 \leq Vgs_n - Vto_n\{T\} \leq Vds_n$ [saturation region]	$I_{\text{drain}_n} = \left(\frac{W_n}{L_{\text{eff}_n}} \right) \cdot \left(\frac{KP_n\{T\}}{2} \right) \cdot (Vgs_n - Vto_n\{T\})^2$
p	$ Vds_p \geq 0$ $ Vgs_p - Vto_p\{T\} < 0$ [cutoff region]	$I_{\text{drain}_p} = 0$
p	$ Vds_p \geq 0$ $ Vds_p < Vgs_p - Vto_p\{T\} $ [linear region]	$I_{\text{drain}_p} = \left(\frac{W_p}{L_{\text{eff}_p}} \right) \cdot \left(\frac{KP_p\{T\}}{2} \right) \cdot Vds_p \cdot (2 \cdot (Vgs_p - Vto_p\{T\}) - Vds_p)$
p	$ Vds_p \geq 0$ $0 \leq Vgs_p - Vto_p\{T\} \leq Vds_p $ [saturation region]	$I_{\text{drain}_p} = \left(\frac{W_p}{L_{\text{eff}_p}} \right) \cdot \left(\frac{KP_p\{T\}}{2} \right) \cdot (Vgs_p - Vto_p\{T\})^2$

where:

$$Vto_n\{T\} = VTO_n + GAMMA_n \cdot \left((PHI_n\{T\} + |Vbs_n|)^{1/2} - (PHI_n\{T\})^{1/2} \right); Vbs_n \leq 0$$

$$|Vto_p\{T\}| = |VTO_p| + GAMMA_p \cdot \left((PHI_p\{T\} + Vbs_p)^{1/2} - (PHI_p\{T\})^{1/2} \right); Vbs_p \geq 0$$

$$* L_{\text{eff}_n} = L_n - 2 \cdot LD_n$$

$$† L_{\text{eff}_p} = L_p - 2 \cdot LD_p$$

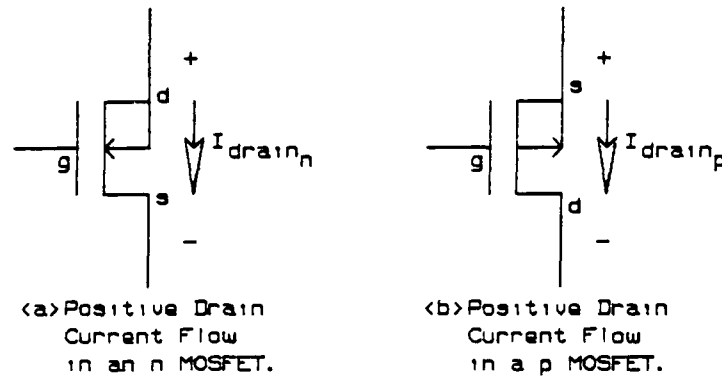


Figure 2.7 Current Flow in MOSFETs

$I_{\text{drain}_p} = 0$. The n MOSFET passes through two regions as V_0 falls: the saturation region, then the linear region. It is possible then to redraw Figure 2.8 as Figure 2.9.b during fall time with the understanding that I_{drain_n} is dependent upon the region of operation of the n MOSFET as the capacitor voltage, V_0 , falls. Indeed, this is the reason for the use of a dependent current source symbol in Figure 2.9.b. From Weste and Eshraghian [Weste and Eshraghian, 1985, p. 139]:

“... it is evident that the fall time, t_f , consists of two intervals:

1. t_{f_1} = period during which the capacitor voltage, V_0 , drops from $0.9 \cdot V_{dd}$ to $(V_{dd} - V_{to_n}\{T\})$ [$I_{\text{drain}_n} \equiv \text{saturation current}$].
2. t_{f_2} = period during which the capacitor voltage, V_0 , drops from $(V_{dd} - V_{to_n}\{T\})$ to $0.1 \cdot V_{dd}$ [$I_{\text{drain}_n} \equiv \text{linear current}$].”

Figure 2.9.b can now be used to write an equation at the interconnection node based on Kirchhoff's current law: ²

$$I_{\text{drain}_n} - (-i_c) = 0$$

² Current flow convention: Current flowing out of a node is positive, current flowing into a node is negative.

TABLE 2.2 PSPICE MOSFET MODEL PARAMETERS
(FROM MICROSIM CORPORATION'S PSPICE)

L	channel length	meter
W	channel width	meter
AD	drain diffusion area	square meter
AS	source diffusion area	square meter
PD	drain diffusion perimeter	meter
PS	source diffusion perimeter	meter
LEVEL	model type (1, 2, or 3)	
LD	lateral diffusion	meter
VTO	0-bias threshold voltage	volt
KP	transconductance	amp/volt ²
GAMMA	bulk threshold parameter	volt ^{1/2}
PHI	surface potential	volt
LAMBDA	channel-length modulation	volt ⁻¹
RD	drain ohmic resistance	ohm
RS	source ohmic resistance	ohm
RSH	drain, source diffusion sheet resistance	ohm/sq.
PB	bulk junction potential	volt
CJ	bulk junction 0-bias bottom capacitance/area	farad/meter ²
CJSW	bulk junction 0-bias perimeter capacitance/length	farad/meter
MJ	bulk junction bottom grading	
MJSW	bulk junction sidewall grading	
FC	bulk junction fwd-bias cap. coef	
CGSO	G-S overlap cap./channel width	farad/meter
CGDO	G-D overlap cap./channel width	farad/meter
NSUB	substrate doping density	1/cm ³
NSS	surface state density	1/cm ²
NFS	fast surface state density	1/cm ²
TOX	oxide thickness	meter
TPG	gate material: +1 = opposite of substrate -1 = same as substrate 0 = aluminum	
XJ	metallurgical junction depth	meter
UO	surface mobility	cm ² /volt-sec
UCRIT	mobility degradation critical field	volt/cm
UEXP	mobility degradation exponent	
VMAX	max. drift velocity	meter/sec
NEFF	channel charge coef.	
DELTA	width effect on threshold	

TABLE 2.3 MOSFET TEMPERATURE EFFECTS
(FROM MICROSIM CORPOPATION'S PSPICE)

$$EG\{T\} = 1.16 - (0.000702 \cdot T^2) / (T + 1108)$$

$$PB\{T\} = PB \cdot T/Tnom - 3 \cdot Vt \cdot \ln(T/Tnom) - EG\{T\} + Eg\{Tnom\} \cdot T/Tnom$$

$$PHI\{T\} = PHI \cdot T/Tnom - 3 \cdot Vt \cdot \ln(T/Tnom) - EG\{T\} + Eg\{Tnom\} \cdot T/Tnom$$

$$CJ\{T\} = CJ \cdot (1 + MJ \cdot (.0004 \cdot (T - Tnom) + (1 - PB\{T\}/PB)))$$

$$CJSW\{T\} = CJSW \cdot (1 + MJSW \cdot (.0004 \cdot (T - Tnom) + (1 - PB\{T\}/PB)))$$

$$KP\{T\} = KP \cdot (T/Tnom)^{-3/2}$$

$$UO\{T\} = UO \cdot (T/Tnom)^{-3/2}$$

$$\epsilon_{rel,oxide}\{T\} = (KP\{T\} \cdot 100 \cdot TOX) / (UO\{T\} \cdot \epsilon_0)$$

Note:

All temperatures in degrees Kelvin

$Tnom$ = nominal temperature (assumed to be 300.15 K)

ϵ_0 = Electric Field Constant (permittivity of vacuum) $[\frac{F}{cm}]$

$Vt = K \cdot T/q$ (thermal voltage)

K = Boltzmann's constant

q = electron charge

T = operating temperature

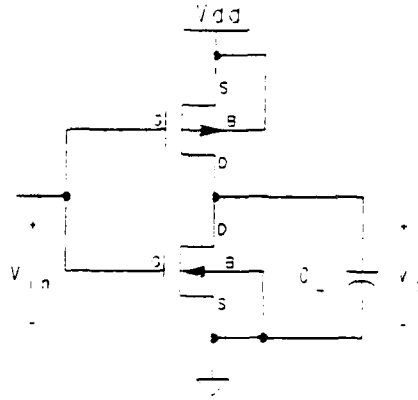


Figure 2.8 Schematic of a Static CMOS Inverter with Capacitive Loading

$$I_{\text{drain}_n} + C_L \cdot \frac{dV_0}{dt} = 0 \quad ; \quad i_c = C_L \cdot \frac{dV_0}{dt} \quad (2.1)$$

Applying equation (2.1) to the first interval where I_{drain_n} = saturation current gives:

$$\left(\frac{W_n}{L_{\text{eff}_n}} \right) \cdot \left(\frac{KP_n\{T\}}{2} \right) \cdot (V_{gs_n} - V_{to_n}\{T\})^2 + C_L \cdot \frac{dV_0}{dt} = 0$$

After substituting $V_{ds_n} = V_0$ and $V_{gs_n} = V_{in} = V_{dd}$ and some algebraic manipulation this equation becomes:

$$dt = - \frac{2 \cdot C_L}{\left(\frac{W_n}{L_{\text{eff}_n}} \right) \cdot (KP_n\{T\}) \cdot (V_{dd} - V_{to_n}\{T\})^2} \cdot dV_0 \quad (2.2)$$

Integrating the left side of equation (2.2) from $t = t_1$ to $t = t_2$ and the right side over the corresponding output voltages $V_0 = 0.9V_{dd}$ to $V_0 = V_{dd} - V_{to_n}\{T\}$ gives:

$$t_{f1} = \frac{2 \cdot C_L \cdot (V_{to_n}\{T\} - 0.1 \cdot V_{dd})}{\left(\frac{W_n}{L_{\text{eff}_n}} \right) \cdot (KP_n\{T\}) \cdot (V_{dd} - V_{to_n}\{T\})^2} \quad (2.3)$$

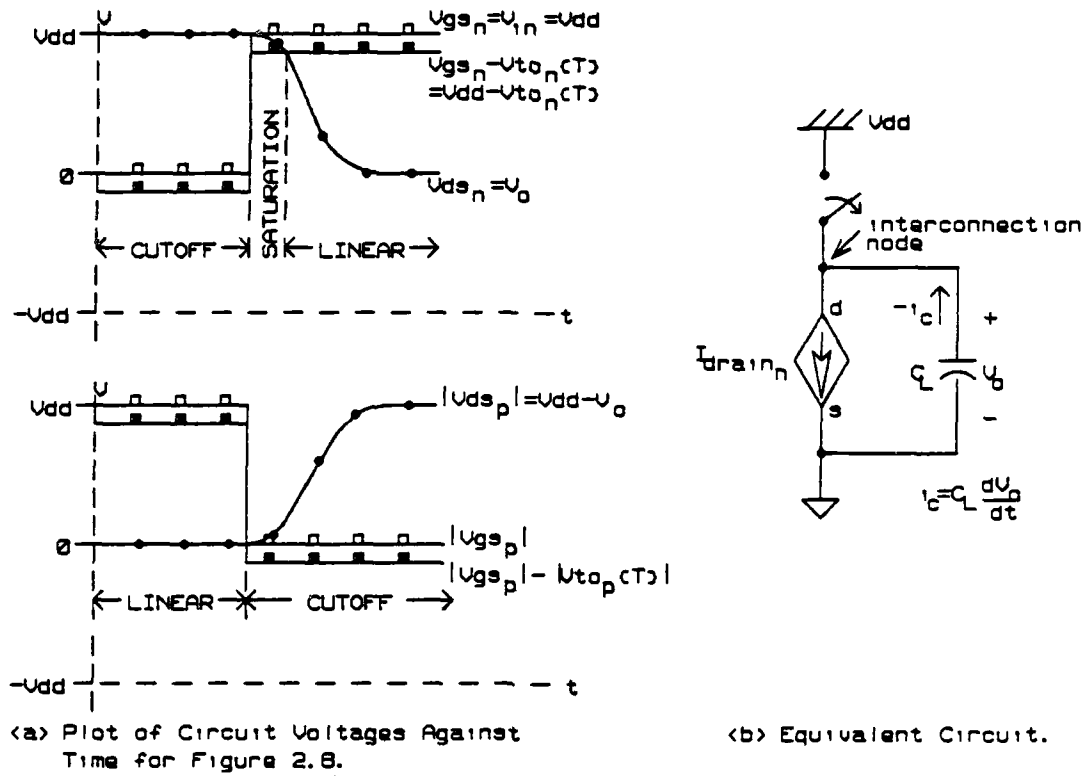


Figure 2.9 Effects of the Rising Edge of a Pulsed Input on a Static CMOS Inverter

Equation (2.1) may be applied to the second interval where I_{drain_n} = linear current:

$$\left(\frac{W_n}{L_{effn}} \right) \cdot \left(\frac{KP_n\{T\}}{2} \right) \cdot V_{ds_n} \cdot (2 \cdot (V_{gs_n} - V_{to_n}\{T\}) - V_{ds_n}) + C_L \cdot \frac{dV_o}{dt} = 0 \quad (2.4)$$

Again substituting $V_{ds_n} = V_o$ and $V_{gs_n} = V_{in} = V_{DD}$ and performing some algebra gives:

$$dt = \frac{2 \cdot C_L}{\left(\frac{W_n}{L_{effn}} \right) \cdot (KP_n\{T\}) \cdot (V_o^2 - 2 \cdot V_o)} \cdot dV_o \quad (2.5)$$

Integrating the left side of equation (2.5) from $t = t_2$ to $t = t_3$ and the right side over the corresponding output voltages $V_0 = Vdd - Vto_n\{T\}$ to $V_0 = 0.1Vdd$ gives:

$$t_{f2} = \frac{C_L}{\left(\frac{W_n}{L_{effn}}\right) \cdot (KP_n\{T\}) \cdot (Vdd - Vto_n\{T\})} \cdot \log_e \left(\frac{19 \cdot Vdd - 20 \cdot Vto_n\{T\}}{Vdd} \right) \quad (2.6)$$

The total fall time, t_f , is found by summing equations (2.3) and (2.6):

$$t_f = t_{f1} + t_{f2} = \frac{2 \cdot C_L}{\left(\frac{W_n}{L_{effn}}\right) \cdot (KP_n\{T\}) \cdot (Vdd - Vto_n\{T\})} \cdot \left[\frac{(Vto_n\{T\} - 0.1 \cdot Vdd)}{(Vdd - Vto_n\{T\})} + \frac{1}{2} \cdot \log_e \left(\frac{19 \cdot Vdd - 20 \cdot Vto_n\{T\}}{Vdd} \right) \right] \quad (2.7)$$

A similar procedure may be applied to find the rise time, t_r . Given the circuit of Figure 2.8 in which C_L is initially discharged so that $V_0 = 0$, the input voltage instantaneously falls from $V_{in} = Vdd$ to $V_{in} = 0$. The effect of the input voltage on the circuit's behavior is plotted in Figure 2.10.a. In this figure the regions of operation of the n and p MOSFETs are labeled in accordance with the definitions of the regions presented in Table 2.1. From the figure it is evident that the n MOSFET immediately enters the cutoff region where $I_{drainn} = 0$. The p MOSFET passes through two regions, as V_0 rises: the saturation region then the linear region. It is possible then to redraw Figure 2.8 as Figure 2.10.b during rise time with the understanding that I_{drainp} is dependent upon the region of operation of the p MOSFET as the capacitor voltage, V_0 , rises. Figure 2.10.b can be used to write an equation at the interconnection node based on Kirchoff's Current law:

$$-I_{drainp} + i_c = 0 \quad (2.8)$$

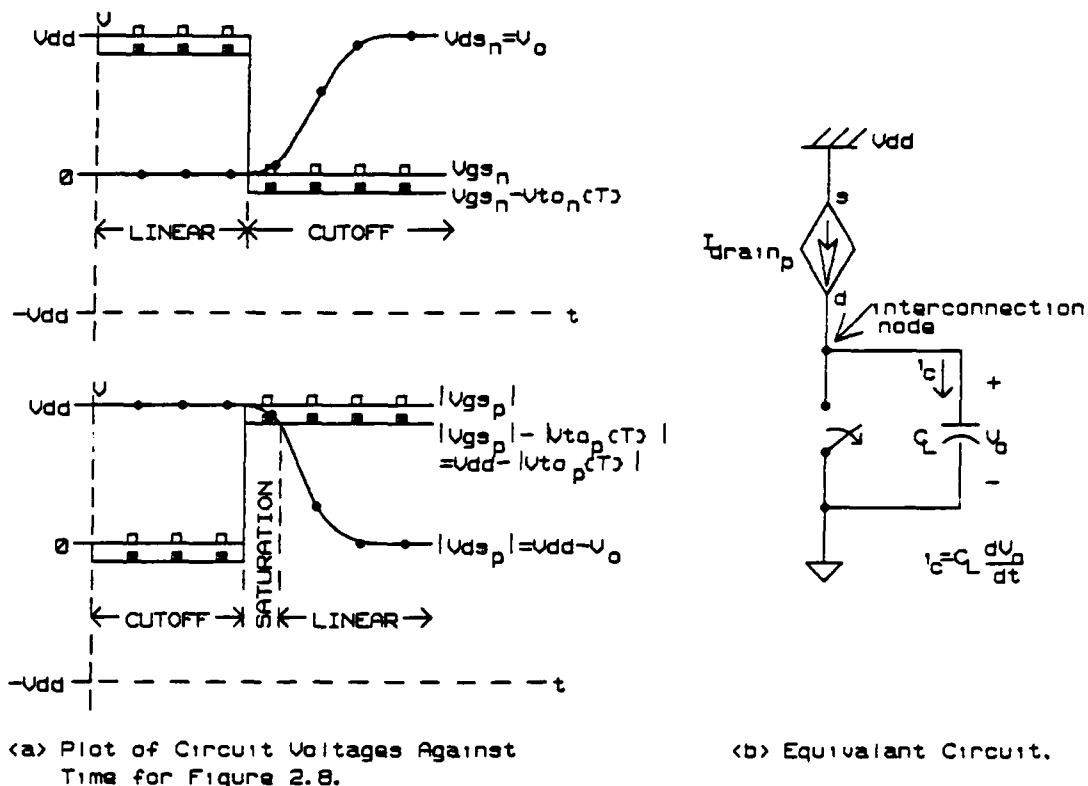


Figure 2.10 Effects of the Falling Edge of a Pulsed Input on a Static CMOS Inverter

Since the p MOSFET passes through two regions of operation during the rise time, equation (2.8) must be applied separately to each region and the separate results are summed together. The lower voltage limit in the time span denoted t_{r1} is $0.1V_{dd}$. The upper limit may be found from Figure 2.10.a. In Figure 2.10.a. the p MOSFET crosses over from the saturation region to the linear region when:

$$|Vds_p| = |Vgs_p| - |Vto_p\{T\}| \quad (2.9)$$

But

$$|Vds_p| = Vdd - V_0 \quad (2.10)$$

$$|Vgs_p| - |Vto_p\{T\}| = Vdd - |Vto_p\{T\}| \quad (2.11)$$

Substituting equations (2.10) and (2.11) into (2.9) and solving for V_0 gives:

$$V_0 = |Vto_p\{T\}| \quad (2.12)$$

Thus the rise time intervals t_{r1} and t_{r2} are defined:

1. t_{r1} = period during which the capacitor voltage, V_0 , rises from $0.1Vdd$ to $|Vto_p\{T\}|$ [$I_{drainp} \equiv$ saturation current].
2. t_{r2} = period during which the capacitor voltage, V_0 , rises from $|Vto_p\{T\}|$ to $0.9Vdd$ [$I_{drainp} \equiv$ linear current].

The drain current equations are substituted into equation (2.8) for the two regions of operation of the p MOSFET in identical fashion to the procedure used in determining t_f for the n MOSFET. The result is:

$$t_r = t_{r1} + t_{r2} = \frac{2 \cdot C_L}{\left(\frac{W_p}{L_{effp}}\right) \cdot (KP_p\{T\}) \cdot (Vdd - |Vto_p\{T\}|)} \cdot \left[\frac{(|Vto_p\{T\}| - 0.1 \cdot Vdd)}{(Vdd - |Vto_p\{T\}|)} + \frac{1}{2} \cdot \log_e \left(\frac{19 \cdot Vdd - 20 \cdot |Vto_p\{T\}|}{Vdd} \right) \right] \quad (2.13)$$

Figure 2.11 shows an idealized MOSFET where L and W are the length and width of the channel, respectively. In the fabrication process that produces

this ideal MOSFET doping ions diffuse only vertically down into the substrate through designer specified windows in the mask that define the source and drain regions. Figure 2.12 shows the result of a more true to life fabrication process. In this process the doping ions diffuse not only vertically down into the substrate but laterally under the edges of the window as well. The effect is that the drain and source regions are bloated in all directions by an amount LD . Since this lateral diffusion also occurs at both ends of the channel, the channel length is effectively reduced by $2 \cdot LD$. The effective channel length is denoted L_{eff} in Table 2.1 and in equations (2.7) and (2.13). For short channel devices this decrease in channel length can have a significant impact on drain current.

Rewriting equations (2.7) and (2.13) in terms of effective channel length gives:

$$t_f = \frac{2 \cdot C_L}{\left(\frac{W_n}{L_n - 2 \cdot LD_n}\right) \cdot (KP_n\{T\}) \cdot (Vdd - Vto_n\{T\})} \cdot \left[\frac{(Vto_n\{T\} - 0.1 \cdot Vdd)}{(Vdd - Vto_n\{T\})} + \frac{1}{2} \cdot \log_e \left(\frac{19 \cdot Vdd - 20 \cdot Vto_n\{T\}}{Vdd} \right) \right] \quad (2.14)$$

$$t_r = \frac{2 \cdot C_L}{\left(\frac{W_p}{L_p - 2 \cdot LD_p}\right) \cdot (KP_p\{T\}) \cdot (Vdd - |Vto_p\{T\}|)} \cdot \left[\frac{(|Vto_p\{T\}| - 0.1 \cdot Vdd)}{(Vdd - |Vto_p\{T\}|)} + \frac{1}{2} \cdot \log_e \left(\frac{19 \cdot Vdd - 20 \cdot |Vto_p\{T\}|}{Vdd} \right) \right] \quad (2.15)$$

where $Vto_n\{T\}$ and $|Vto_p\{T\}|$ are defined in Table 2.1 and $KP_n\{T\}$ and $KP_p\{T\}$ are defined in Table 2.3.

Delay time, denoted t_d , is the time it takes a logic transition to pass from the input of a gate to its output. In fully restored CMOS logic t_d is explicitly defined to be the amount of time that elapses between the moment that the input

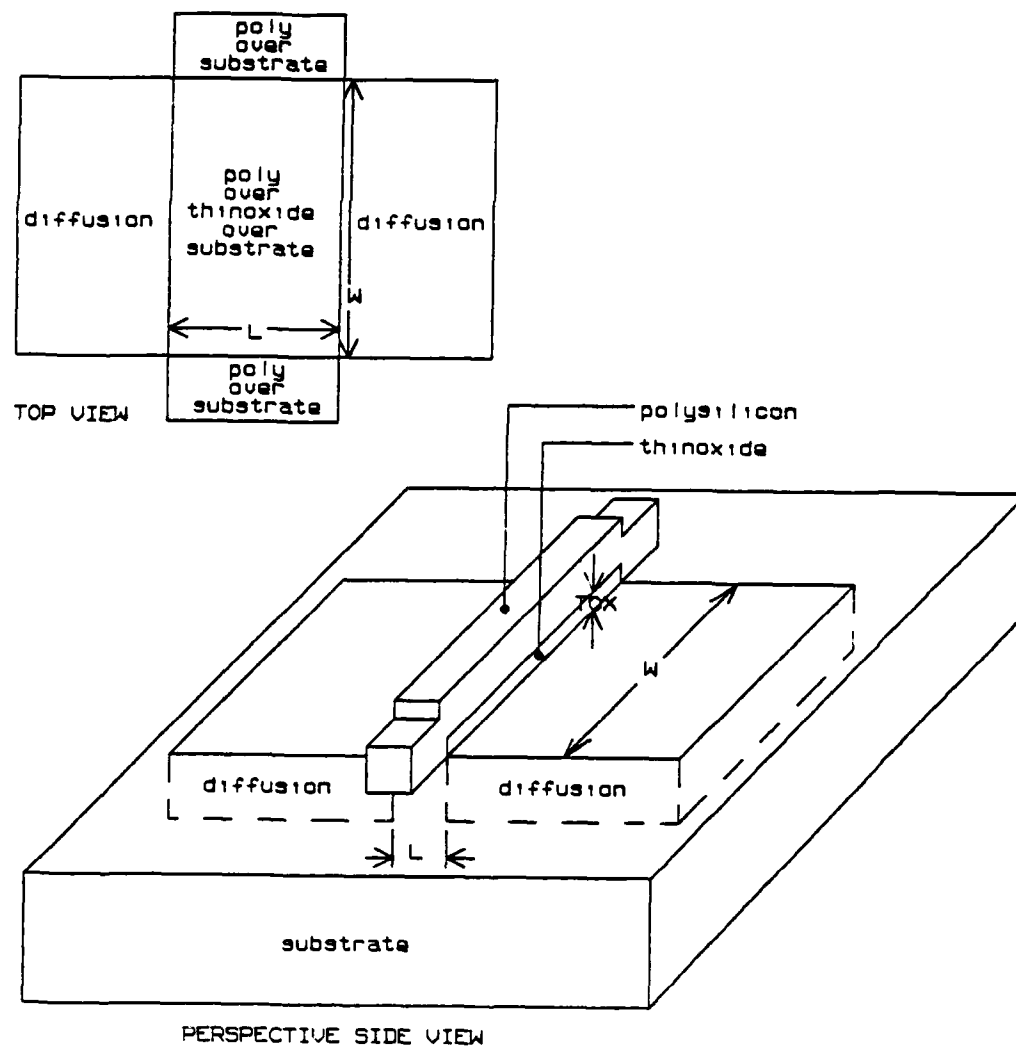


Figure 2.11 Idealized Physical MOSFET

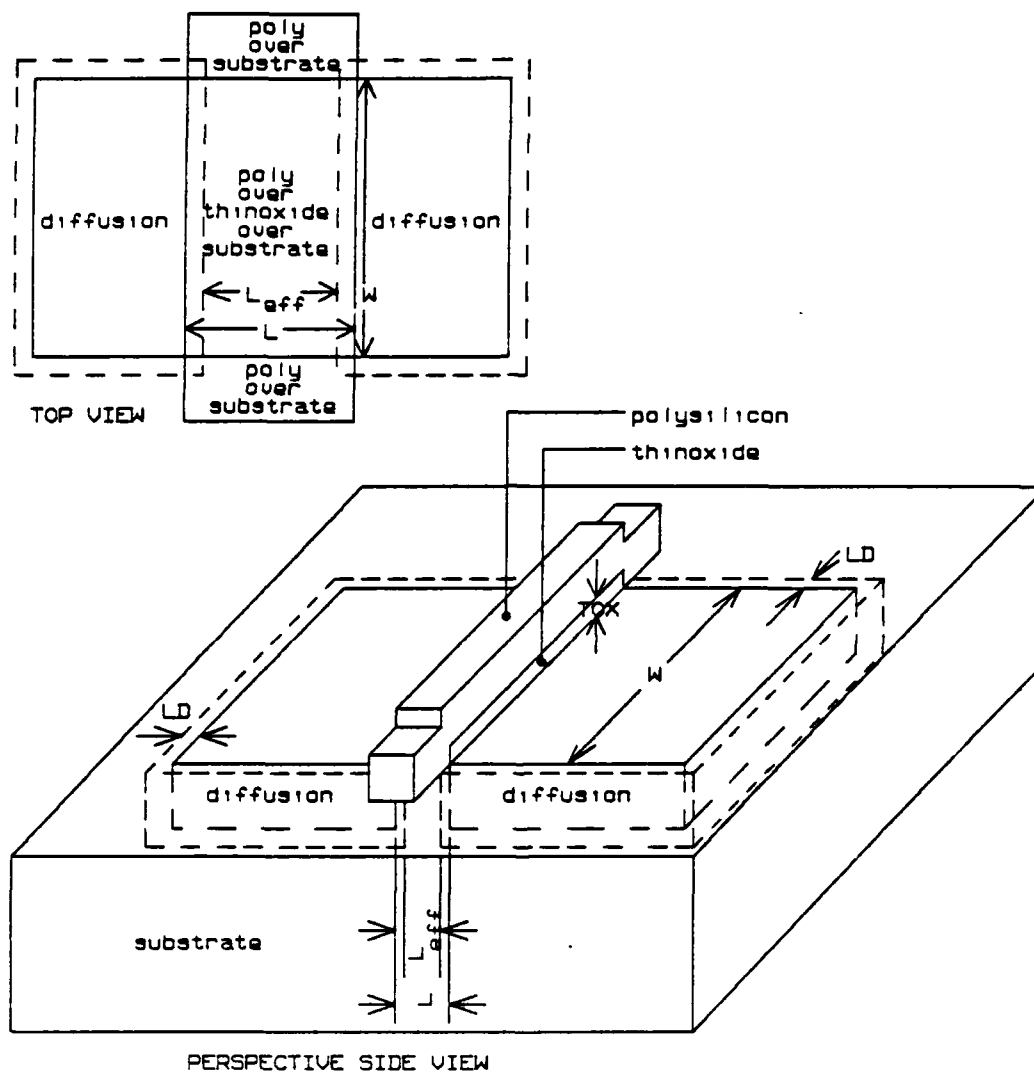


Figure 2.12 Effects of Lateral Diffusion of Doping Ions on a Physical MOSFET

signal to a gate transitions through $Vdd/2$ and the moment that the output affected by that input transitions through $Vdd/2$ [Weste and Eshraghian, 1985, p. 141]:

$$t_{d_{avg}} = \frac{t_r + t_f}{4} \quad (2.16)$$

One of the more attractive feature of CMOS circuits is that symmetric output sourcing and sinking currents are easily achieved resulting in equal rise and fall times. When this is achieved $t_{d_{avg}}$ becomes:

$$t_{d_{avg}} = \frac{t_r}{2} = \frac{t_f}{2} \quad (2.17)$$

To achieve $t_r = t_f$ for the inverter in Figure 2.8 equations (2.14) and (2.15) are set equal to one another then W_n is solved for. The result is:

$$W_n = W_p \cdot A \quad (2.18)$$

where

$$A = \frac{(L_n - 2 \cdot LD_n) \cdot (KP_p\{T\}) \cdot (Vdd - |Vto_p\{T\}|)}{(L_p - 2 \cdot LD_p) \cdot (KP_n\{T\}) \cdot (Vdd - Vto_n\{T\})} \cdot \frac{\left[\frac{(Vto_n\{T\} - 0.1 \cdot Vdd)}{(Vdd - Vto_n\{T\})} + \frac{1}{2} \cdot \log_e \left(\frac{19 \cdot Vdd - 20 \cdot Vto_n\{T\}}{Vdd} \right) \right]}{\left[\frac{(|Vto_p\{T\}| - 0.1 \cdot Vdd)}{(Vdd - |Vto_p\{T\}|)} + \frac{1}{2} \cdot \log_e \left(\frac{19 \cdot Vdd - 20 \cdot |Vto_p\{T\}|}{Vdd} \right) \right]} \quad (2.19)$$

In the drain current equations of Table 2.1 it is evident that as the channel length, L , is decreased drain current increases. To maximize speed, L should be the minimum channel length permitted by the design rules of the particular technology being used. This length is usually the same as the minimum feature size of the technology.

Keeping in mind the previous paragraph on the selection of L_n and L_p , all the values on the right side of equation (2.18) are now known except for W_p . Once W_p is found, a W_n that results in $t_f \simeq t_r$ and $t_{d_{avg}} \simeq \frac{t_f}{2} \simeq \frac{t_r}{2}$ can be readily obtained from equation (2.18). Finding W_p is dealt with in Section 4.

3. Capacitive Loading

The load capacitance, C_L , has been referred to in Section B.2, but not yet described. The term C_L represents three parallel capacitances [Weste and Eshraghian, 1985, p. 123]:

$$C_L = Cbd_{total} + C \sum_{\substack{\text{load} \\ \text{devices}}} \text{gate} + C_r \quad (2.20)$$

where

$Cbd_{total} \equiv$ the diffusion capacitance of the drain
regions connected to the output

$C \sum_{\substack{\text{load} \\ \text{devices}}} \text{gate} \equiv$ gate capacitance of the load devices connected
to the output of the gate under design

$C_r \equiv$ routing capacitance of the interconnect
between the p block, the n block, and the load

It should be noted that in the definition of the term Cbd_{total} the word region is plural. That is to say that in Figure 2.8 each transistor, when active, must drive not only its own drain diffusion to substrate capacitance but also that of the other transistor that is connected to it. This is so because the drains are connected together resulting in parallel capacitances. Cbd_{total} , $C \sum_{\substack{\text{load} \\ \text{devices}}} \text{gate}$, and C_r are described in the next three subsections.

a. Diffusion to Substrate Capacitance of the Interconnection Node

Figure 2.13 shows a drain area diffused into the substrate and bloated by an amount LD in all horizontal directions. To the top of the figure would be the channel, but the channel, gate, and source have been removed to make clear that only the drain area is being considered here. At the bottom end of the drain is an area of diffusion that protrudes. This area has been reserved for a metal to diffusion surface contact. Similar contacts may be placed alongside this contact at the bottom end of the drain or on the sides of the drain or both (but obviously not at the channel end). The important drain area dimensions shown in Figure 2.13 are:

$$\begin{aligned} W_{d,eff} &\equiv \text{Effective diffusion width} = W + 2 \cdot LD \\ L_{d,eff} &\equiv \text{Effective diffusion length} = L_{d,mask} + 2 \cdot LD \\ &\quad \text{where } L_{d,mask} \text{ is the mask level diffusion length} \\ W_{c,eff} &\equiv \text{effective contact width} = W_c + 2 \cdot LD \\ &\quad \text{where } W_c \text{ is the mask level contact width} \\ L_c &\equiv \text{mask level contact length} \end{aligned}$$

In Figure 2.13 the length of the contact area at the bottom edge of the diffusion runs from top to bottom, and the contact width runs from left to right. If contacts were placed along the sides of the diffusion area shown in Figure 2.13 their lengths would run from left to right in the figure while their widths would run from top to bottom. These dimensions are just the reverse of the dimensions of the contact along the bottom edge of the diffusion area in Figure 2.13.

From Figure 2.13 the drain area is defined:

$$AD = W_{d,eff} \cdot L_{d,eff} + N \cdot W_{c,eff} \cdot L_c \quad (2.21)$$

where N is the number of metal to diffusion contacts placed around the diffusion area.

From Figure 2.13 the drain perimeter is defined:

$$PD = 2 \cdot (W_{d,eff} + L_{d,eff} + N \cdot L_c) = 2 \cdot W_{d,eff} + 2 \cdot (L_{d,eff} + N \cdot L_c) \quad (2.22)$$

where N is as defined in equation (2.21)

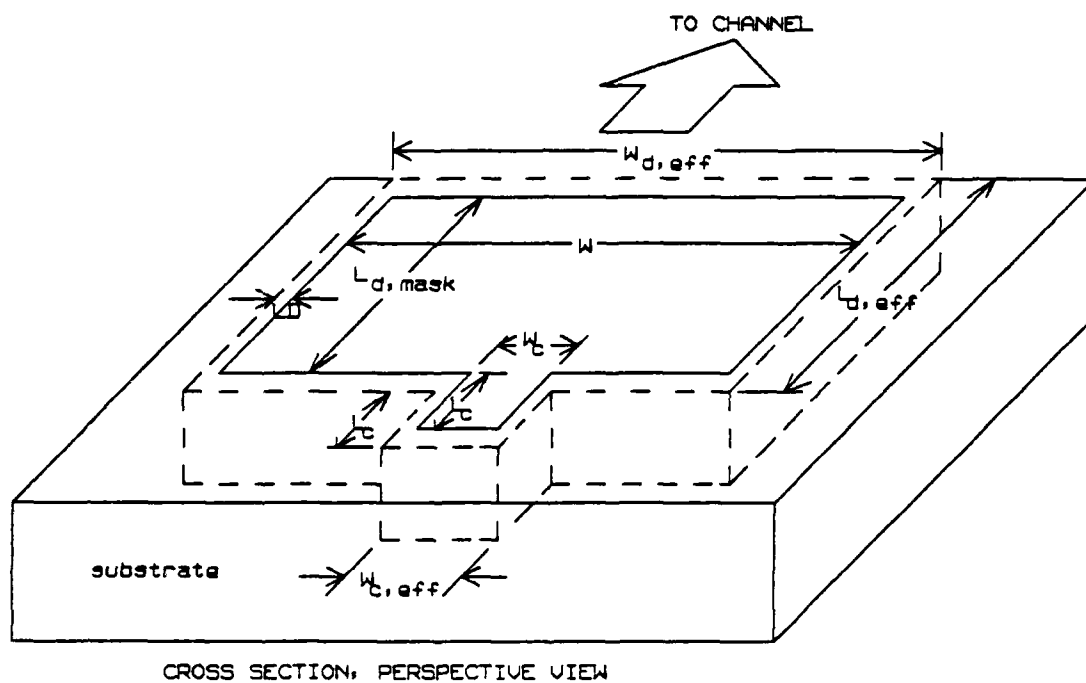


Figure 2.13 Drain Diffusion Area Dimensions

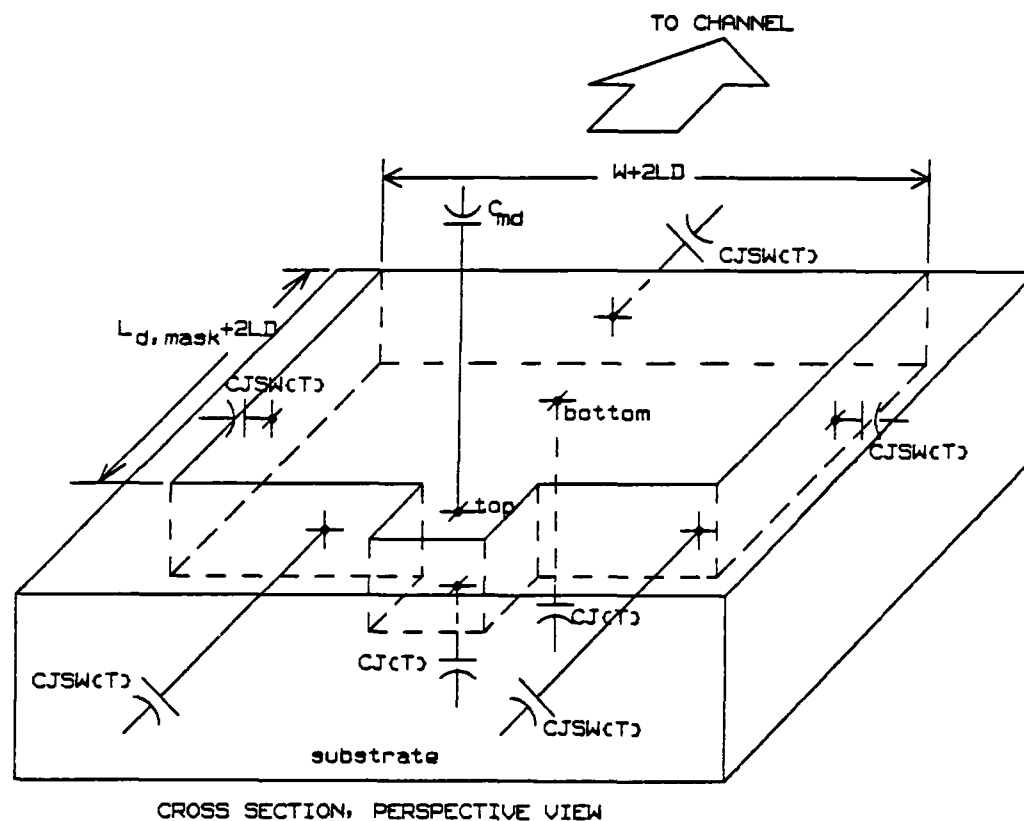


Figure 2.14 Bulk-Drain Depletion Capacitance and Metal to Diffusion Contact Capacitance

Figure 2.14 shows the three capacitances of concern in calculating C_{bd} . $CJ\{T\}$ and $CJSW\{T\}$ in Figure 2.14 are defined in Tables 2.2 and 2.3. C_{md} is the capacitance that results by bringing metal into contact with the protrusion areas—like the one at the bottom edge of the diffusion in Figure 2.14—that are reserved for metal to diffusion contacts.

Having defined the dimensions of the drain diffusion and its capacitive components, Cbd may now be defined [MicroSim Corp., 1987, p. 79]:

$$\begin{aligned}
 Cbd\{T, Vbd\} &= \text{bulk-drain depletion capacitance} \\
 &\quad + \text{metal to diffusion contact capacitance} \\
 &= \text{bottom junction capacitance} + \text{sidewall capacitance} \\
 &\quad + \text{metal to diffusion contact capacitance} \\
 &= AD \cdot CJ\{T\} \cdot Cbdj\{T, Vbd\} \\
 &\quad + PD \cdot CJSW\{T\} \cdot CbdS\{T, Vbd\} \\
 &\quad + N \cdot L_c \cdot W_c \cdot C_{md}
 \end{aligned} \tag{2.23}$$

Cbd is a function of Vbd because $Cbdj$ and $CbdS$ in equation (2.23) are functions of Vbd . This implies that all three will vary during switching due to variations in bias level. To reduce the difficulty that this introduces in the analysis, values that are dependent on temperature only may be assigned to $Cbdj$ and $CbdS$ if the values assigned are chosen carefully and with good judgment. [McCarthy, 1982, p.58]

MicroSim's PSpice defines $Cbdj\{T, Vbd\}$ and $CbdS\{T, Vbd\}$ [MicroSim Corp., 1987, p. 80]:

$$\begin{aligned}
 Cbdj\{T, Vbd\} &= (1 - FC)^{-(1+MJ)} \\
 &\quad \cdot \left(1 - FC \cdot (1 + MJ) + MJ \cdot |Vbd|/PB\{T\}\right) [\text{dimensionless}]
 \end{aligned} \tag{2.24}$$

$$\begin{aligned}
 CbdS\{T, Vbd\} &= (1 - FC)^{-(1+MJSW)} \\
 &\quad \cdot \left(1 - FC \cdot (1 + MJSW) + MJSW \cdot |Vbd|/PB\{T\}\right) [\text{dimensionless}]
 \end{aligned} \tag{2.25}$$

During switching $0.1 \cdot V_{dd} < |V_{bd}| < 0.9 \cdot V_{dd}$. $|V_{bd}|$ does not dwell at either end of this range any longer than it does at the other. Therefore, C_{bdj} and C_{bds} may be expressed as function of T , independent of V_{bd} by simple averaging:

$$C_{bdj}_{avg}\{T\} = \frac{1}{2} \cdot \left[C_{bdj}\{T, V_{bd}\} \Big|_{V_{bd}=0.9V_{dd}} + C_{bdj}\{T, V_{bd}\} \Big|_{V_{bd}=0.1 \cdot V_{dd}} \right] \quad (2.26)$$

$$C_{bds}_{avg}\{T\} = \frac{1}{2} \cdot \left[C_{bds}\{T, V_{bd}\} \Big|_{V_{bd}=0.9V_{dd}} + C_{bds}\{T, V_{bd}\} \Big|_{V_{bd}=0.1 \cdot V_{dd}} \right] \quad (2.27)$$

Substituting equations (2.26) and (2.27) into equation (2.23) allows C_{bd} to be expressed as a function of temperature only:

$$C_{bd}\{T\} = AD \cdot CJ\{T\} \cdot C_{bdj}_{avg}\{T\} + PD \cdot CJSW\{T\} \cdot C_{bds}_{avg}\{T\} + N \cdot L_c \cdot W_c \cdot C_{md} \quad (2.28)$$

Substituting equations (2.21) and (2.22) for the drain area and drain perimeter into equation (2.28) and grouping terms gives:

$$C_{bd}\{T\} = W_{d,eff} \cdot (L_{d,eff} \cdot CJ\{T\} \cdot C_{bdj}_{avg}\{T\} + 2 \cdot CJSW\{T\} \cdot C_{bds}_{avg}\{T\}) + 2 \cdot (L_{d,eff} + N \cdot L_c) \cdot CJSW\{T\} \cdot C_{bds}_{avg}\{T\} + N \cdot L_c \cdot (W_{c,eff} \cdot CJ\{T\} \cdot C_{bdj}_{avg}\{T\} + W_c \cdot C_{md}) \quad (2.29)$$

Figure 2.15 is a literal translation from the schematic in Figure 2.8 (with no load attached) to a mask level layout. That is to say that the p and n MOSFETs are in the same position with respect to one another in Figure 2.15 as they are in Figure 2.8. Figure 2.15 shows graphically why each transistor drives

not only the load and its own drain diffusion capacitance but the drain diffusion capacitance of the other transistor as well. It is because the two drain areas are hard-wired together.

Since the two capacitances $Cbd_p\{T\}$ and $Cbd_n\{T\}$ are in parallel with one another $Cbd_{total}\{T\}$ becomes:

$$Cbd_{total}\{T\} = Cbd_p\{T\} + Cbd_n\{T\} \quad (2.30)$$

Equation (2.30) can now be fully expanded according to the following procedure:

- 1.) Expand $W_{d,eff}$, $L_{d,eff}$, and $W_{c,eff}$ in equation (2.29) according to their definitions at the beginning of Section B.3.a.
- 2.) Take the expression resulting from step 1 and substitute it into equation (2.30).
- 3.) Make use of equation (2.18) to express n channel widths in terms of p channel widths.
- 4.) Collect terms.

The result is:

$$Cbd_{total}\{T\} = Wp \cdot C + D \quad [\text{farad}] \quad (2.31)$$

where

$$\begin{aligned} C = & \left([L_{d,mask_p} + 2 \cdot LD_p] \cdot CJ_p\{T\} \cdot Cbd_{j,avg,p}\{T\} \right. \\ & + 2 \cdot CJSW_p\{T\} \cdot Cbd_{s,avg,p}\{T\} \\ & + A \cdot [L_{d,mask_n} + 2 \cdot LD_n] \cdot CJ_n\{T\} \cdot Cbd_{j,avg,n}\{T\} \\ & \left. + 2 \cdot A \cdot CJSW_n\{T\} \cdot Cbd_{s,avg,n}\{T\} \right) \end{aligned} \quad (2.32)$$

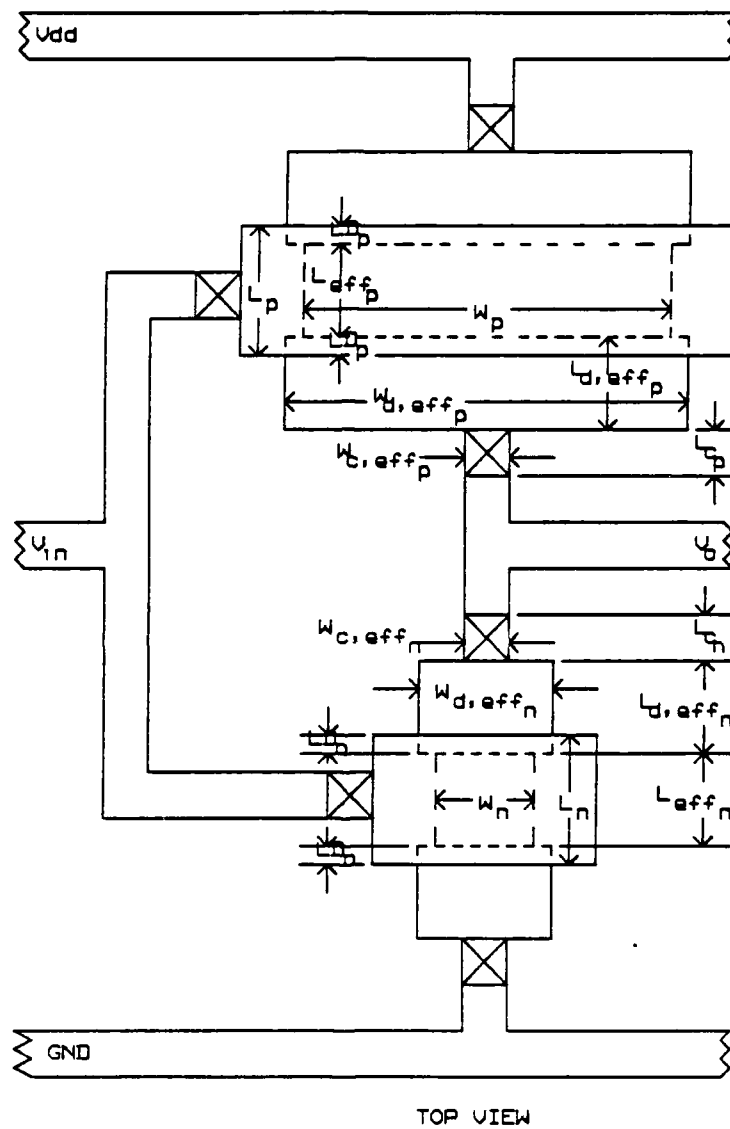


Figure 2.15 Mask Level Layout of a Static CMOS Inverter

$$\begin{aligned}
D = \sum_x & \left[2 \cdot LD_x \cdot \left([L_{d, \text{mask}_x} + 2 \cdot LD_x] \cdot CJ_x\{T\} \cdot Cbdj_{\text{avg},x}\{T\} \right. \right. \\
& + 2 \cdot CJSW_x\{T\} \cdot Cbd_s_{\text{avg},x}\{T\} \Big) \\
& + 2 \cdot \left([L_{d, \text{mask}_x} + 2 \cdot LD_x] + N_x \cdot L_{cx} \right) \cdot CSJW_x\{T\} \cdot Cbd_s_{\text{avg},x}\{T\} \\
& \left. + N_x \cdot L_{cx} \cdot \left([W_{cx} + 2 \cdot LD_x] \cdot CJ_x\{T\} \cdot Cbdj_{\text{avg},x}\{T\} + W_{cx} \cdot C_{mdx} \right) \right]
\end{aligned}$$

for $x = p, n$

(2.33)

and A in equation (2.32) is defined by equation (2.19).

b. Gate Capacitance of the Next Stage

The capacitance of the input gates of the immediate next logic stage is determined in this section. Figure 2.16 shows a single load MOSFET from a top view. The load channel dimensions W_{load} and $L_{ch, \text{load}, \text{eff}}$ are defined in Figure 2.16 where:

$$L_{ch, \text{load}, \text{eff}} = L_{ch, \text{load}, \text{mask}} - 2 \cdot LD$$

Figure 2.17 shows three capacitances formed between the gate material above the surface plane of the wafer and the channel and diffusion areas below. The capacitance Cg is the capacitance that forms between the gate and the substrate. This capacitance is much larger when the load transistor is off than when it is on. In design work it is always safest to estimate capacitive loading conservatively so that a realistic safety margin is allowed for variable operating conditions of a physical device. Since the load capacitance component is largest when the load transistor is off it is best from an engineering standpoint to assume that the physical device

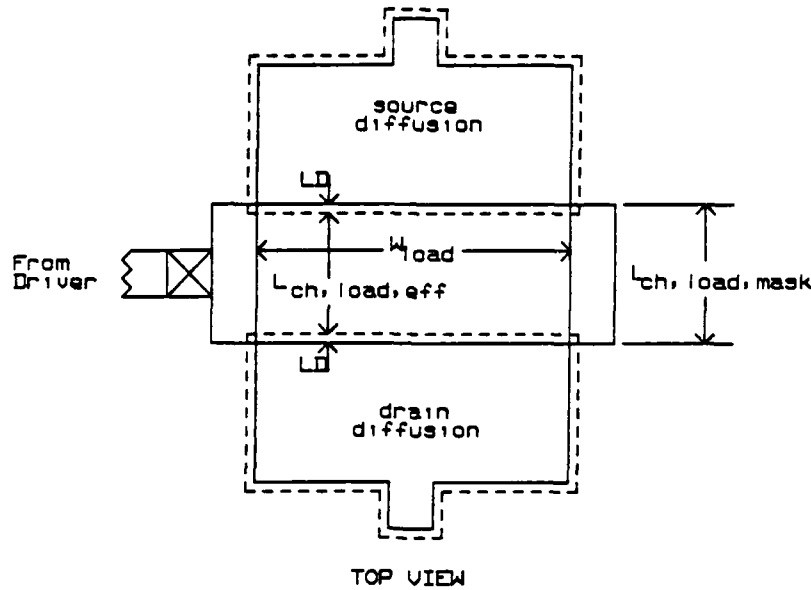


Figure 2.16 Load MOSFET Channel Dimensions

will be operated at low frequency (below 100 Hz).³ For low frequency operation C_g may be estimated from [Weste and Eshraghian, 1985, p. 125]:

$$C_g = \left(\frac{\epsilon_0 \cdot \epsilon_{\text{rel,oxide}} \{T\}}{TOX} \right) \cdot ([L_{\text{ch,load,mask}} - 2 \cdot LD] \cdot W_{\text{load}}) \quad (2.34)$$

C_{gs} and C_{gd} in Figure 2.17 are the capacitances between the gate and the source diffusion and between the gate and drain diffusion. These capacitances are a direct result of the overlapping of the gate and drain and of the gate and source caused by the lateral diffusion of doping ions into the intended channel area

³ Note that channel length becomes shorter when the load device operates in the saturation region. In saturation, $L_{\text{ch,load,eff}} = (L_{\text{ch,load,mask}} - 2 \cdot LD) \cdot (1 - \text{LAMBDA} \cdot |V_{ds}|)$. Since the load device operates in all three regions—cutoff, linear, and saturation—the region chosen for modeling the physical load channel length is that which yields the most conservative estimate for C_g , namely the linear region where $L_{\text{ch,load,eff}} = L_{\text{ch,load,mask}} - 2 \cdot LD$.

as discussed in Section B.2. C_{gs} and C_{gd} are determined from [MicroSim Corp., 1987, p. 80]:

$$C_{gs} = CGSO \cdot W_{load}$$

$$C_{gd} = CGDO \cdot W_{load}$$

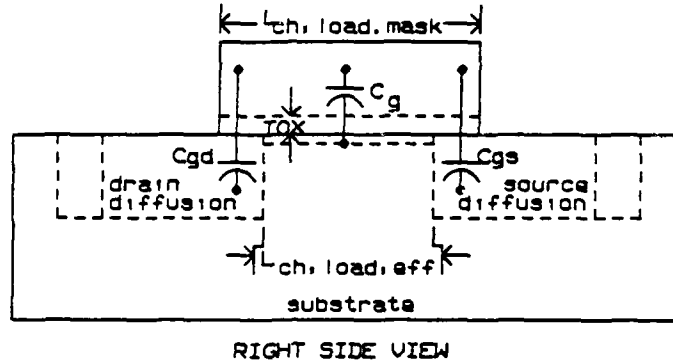


Figure 2.17 Load MOSFET Gate Capacitance

As C_g , C_{gs} , and C_{gd} are in parallel with one another, $C \sum_{load\ devices}^{gate}$ is equal to their sum over all load devices:

$$C \sum_{load\ devices}^{gate} = \sum_{load\ devices} [C_g + C_{gs} + C_{gd}] \quad (2.34)$$

$$= \sum_{load\ devices} \left[\left(\frac{\epsilon_0 \cdot \epsilon_{rel,oxide}\{T\}}{TOX} \right) \cdot (L_{ch,load,mask} - 2 \cdot LD) \cdot W_{load} + CGSO \cdot W_{load} + CGDO \cdot W_{load} \right] \quad (2.35)$$

where all the variables in equation (2.35) are defined in Tables 2.2 and 2.3.

c. Routing Capacitance

Routing capacitance between layers or between a layer and substrate is determined by multiplying the capacitance per unit area measured between the specific layers by the area that is jointly occupied by both layers. Values for these unit area capacitances must be obtained from the fabrication facility being used. Typical values for a 4 micron, two level metal, silicon gate CMOS process are provided in Weste and Eshraghian [Weste and Eshraghian, 1985, p. 135]. An alternate method is to remove C_r from equation (2.20) and compute the delay due to routing capacitance separately. A paper by John L. Wyatt, Jr. entitled, "The Practical Engineer's No-Nonsense Guide to On-Chip Signal Delay Calculation," available through the M.I.T. VLSI memo series gives worst case bounds on delay time due to routing for use in this type of approach [Wyatt, 1987]. Note that the capacitance due to diffusion to metal contacts on the drains wired to the node that connects the p and n blocks is considered separate from C_r , and is developed in Section B.3.a.

4. Finding W_p and W_n

Figure 2.15, which was discussed in Section B.3.a, shows the dimensions W_p and W_n . As discussed in Section B.1, the circuit designer needs to have a method to determine the widths W_p and W_n required to drive the parasitics and known capacitive load within a designer specified time constraint given some expected temperature and supply voltage operating conditions. All that has been accomplished thus far in Chapter II is to gather together the tools necessary to make this calculation. In this section the tools are used together to find W_p and W_n for the static CMOS inverter of Figures 2.8 and 2.15.

Rearranging equation (2.15) to solve for W_p gives:

$$W_p = F \cdot C_L [G + H] \quad (2.36)$$

where:

$$F = \frac{2 \cdot (L_p - 2 \cdot LD_p)}{(t_r) \cdot (KP_p\{T\}) \cdot (Vdd - |Vto_p\{T\}|)} \quad (2.37)$$

$$G = \frac{(|Vto_p\{T\}| - 0.1 \cdot Vdd)}{(Vdd - |Vto_p\{T\}|)} \quad (2.38)$$

$$H = \frac{1}{2} \cdot \log_e \left(\frac{19 \cdot Vdd - 20 \cdot |Vto_p\{T\}|}{Vdd} \right) \quad (2.39)$$

But C_L is itself a function of the unknown W_p since

$$C_L = Cbd_{total} + C \sum_{\text{load devices}} \text{gate} + C_r \quad ; \text{from equation (2.20)} \quad (2.40)$$

$$C_L = C \cdot W_p + D + C \sum_{\text{load devices}} \text{gate} + C_r \quad ; \text{from equation (2.31)} \quad (2.41)$$

Renaming $C \sum_{\text{load devices}} \text{gate}$ and C_r for simplicity:

$$B = C \sum_{\text{load devices}} \text{gate} \quad (2.42)$$

$$E = C_r \quad (2.43)$$

Substituting equations (2.42) and (2.43) into equation (2.41) gives:

$$C_L = C \cdot W_p + D + B + E \quad (2.44)$$

Substituting equation (2.44) into equation (2.36) and solving for W_p gives the final result for the static CMOS inverter:

$$W_p = \frac{F \cdot (G + H) \cdot (B + D + E)}{1 - F \cdot C \cdot (G + H)} \quad (2.45)$$

$$W_n = W_p \cdot A \quad (\text{from equation (2.18)}) \quad (2.46)$$

The equations defining the variables in equations (2.45) and (2.46) are referenced in Table 2.4.

Practical calculation of W_p requires a computer program. A program to calculate W_p , W_n , and all other MOSFET parameters required on a MOSFET card in a PSpice deck is provided in Appendix A. This program is written for an HP41CX with card reader and two extended memory modules.

**TABLE 2.4 IMPORTANT EQUATIONS
FOR THE STATIC CMOS INVERTER**

Variable	Defining Equations(s)
W_p	(2.45)
W_n	(2.46)
A	(2.19)
B	(2.42) and (2.35)
C	(2.32)
D	(2.33)
E	(2.43)
F	(2.37)
G	(2.38)
H	(2.39)

5. Drain Resistance

With respect to the drain diffusion region, only its capacitive value has been determined thus far. Proper modeling of a MOSFET in PSpice requires that the drain resistance be provided as well. Figure 2.18 shows a simple drain diffusion region (substrate omitted from the figure) and its resistive equivalent, RD . The resistance between end faces of the figure can be calculated from [McCarthy, 1982, p. 39]:

$$RD = \bar{\rho} \cdot \frac{\text{drain length}}{\text{end face area}} \quad (2.47)$$

where $\bar{\rho}$ is the average resistivity for the diffusion layer.

In terms of SPICE parameters [McCarthy, 1982, p. 59]:

$$RSH = \frac{\bar{\rho}}{XJ} \quad (2.48)$$

Therefore,

$$\begin{aligned} RD &= \bar{\rho} \cdot \left(\frac{L_{d,eff}}{W_{d,eff} \cdot XJ} \right) \\ RD &= RSH \cdot XJ \cdot \left(\frac{L_{d,eff}}{W_{d,eff} \cdot XJ} \right) \\ RD &= RSH \cdot \left(\frac{L_{d,mask} + 2 \cdot LD}{W + 2 \cdot LD} \right) \end{aligned} \quad (2.49)$$

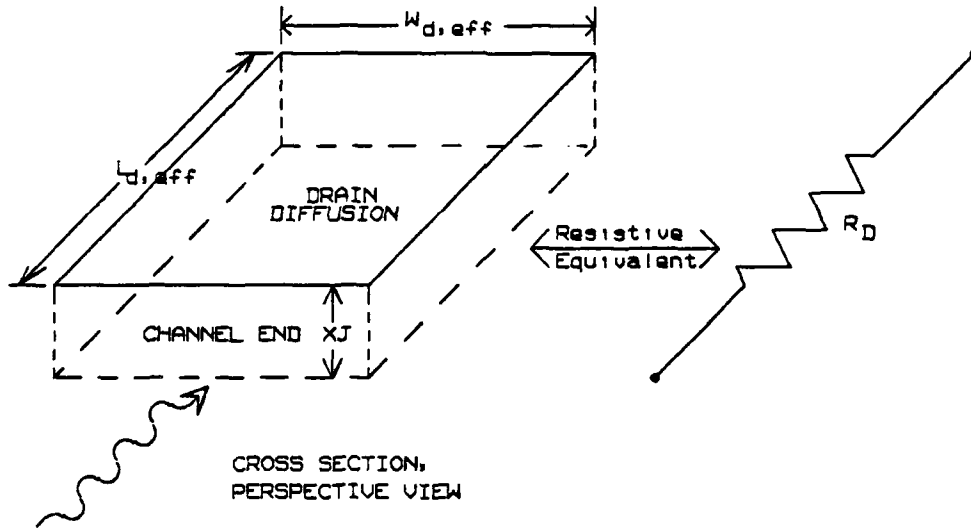


Figure 2.18 Drain Diffusion Region and Resistive Equivalent

Figure 2.19 shows a drain diffusion area with a single contact area defined and a resistive equivalent. Since R and R_c in Figure 2.19 are in series:

$$RD = R + R_c \quad (2.50)$$

$$RD = \bar{\rho} \cdot \left(\frac{L_{d,eff}}{W_{d,eff} \cdot XJ} \right) + \bar{\rho} \cdot \left(\frac{L_c}{W_{c,eff} \cdot XJ} \right)$$

$$RD = RSH \cdot \left[\frac{(L_{d,mask} + 2 \cdot LD)}{(W + 2 \cdot LD)} + \frac{L_c}{W_c + 2 \cdot LD} \right] \quad (2.51)$$

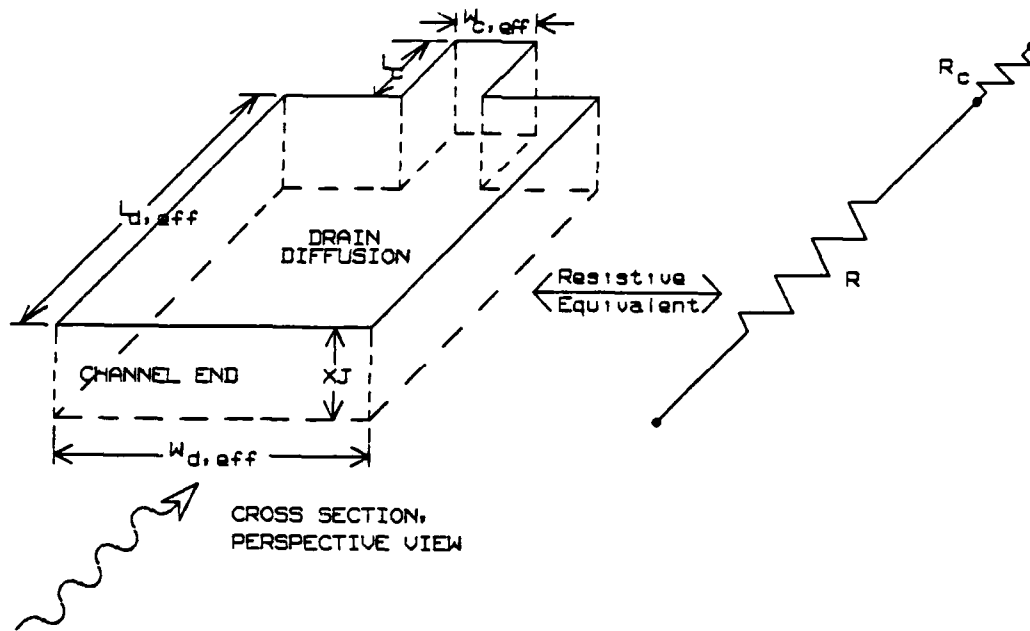


Figure 2.19 Drain Diffusion Region with a Single Metal to Diffusion Contact Area and Resistive Equivalent

Figure 2.20 is an extension of the resistance calculations performed in equations (2.49) and (2.51) to the general case where several contact areas may be placed around the diffusion area. In the figure

$$R_{eq} = \frac{1}{\frac{1}{R_1} + \frac{1}{R_2} + \dots + \frac{1}{R_N}}$$

But assuming that all the contact areas have identical dimensions, $R_1 = R_2 = \dots = R_N = R_c$, where R_c is the resistance of any one contact area and so:

$$R_{eq} = \frac{1}{N} \cdot R_c \quad (2.52)$$

Using the results of equations (2.52) and (2.51) gives the drain resistance for the general case depicted in Figure 2.20:

$$RD = R + R_{eq} = RSH \cdot \left[\left(\frac{L_{d,mask} + 2 \cdot LD}{W + 2 \cdot LD} \right) + \frac{1}{N} \cdot \left(\frac{L_c}{W_c + 2 \cdot LD} \right) \right] \quad (2.53)$$

Given that the contact areas employed by the designer are of the minimum dimensions permitted by the design rules for the technology being used, equations (2.23) in Section B.3.a. and (2.53) in this section confirm an intuitive trade off:

- placing more contact areas decreases drain resistance but increases drain capacitance.
- placing fewer contact areas decreases drain capacitance but increases drain resistance.

6. Theoretical Bounds on Inverter Performance

Equation (2.45) can be manipulated algebraically into the form:

$$W_p = \frac{(F \cdot t_r) \cdot (G + H) \cdot (B + D + E)}{t_r - \frac{2 \cdot (L_p - 2 \cdot LD_p) \cdot C \cdot (G + H)}{(K P_p \{T\}) \cdot (V_{dd} - |V_{to_p}\{T\}|)}} \quad (2.54)$$

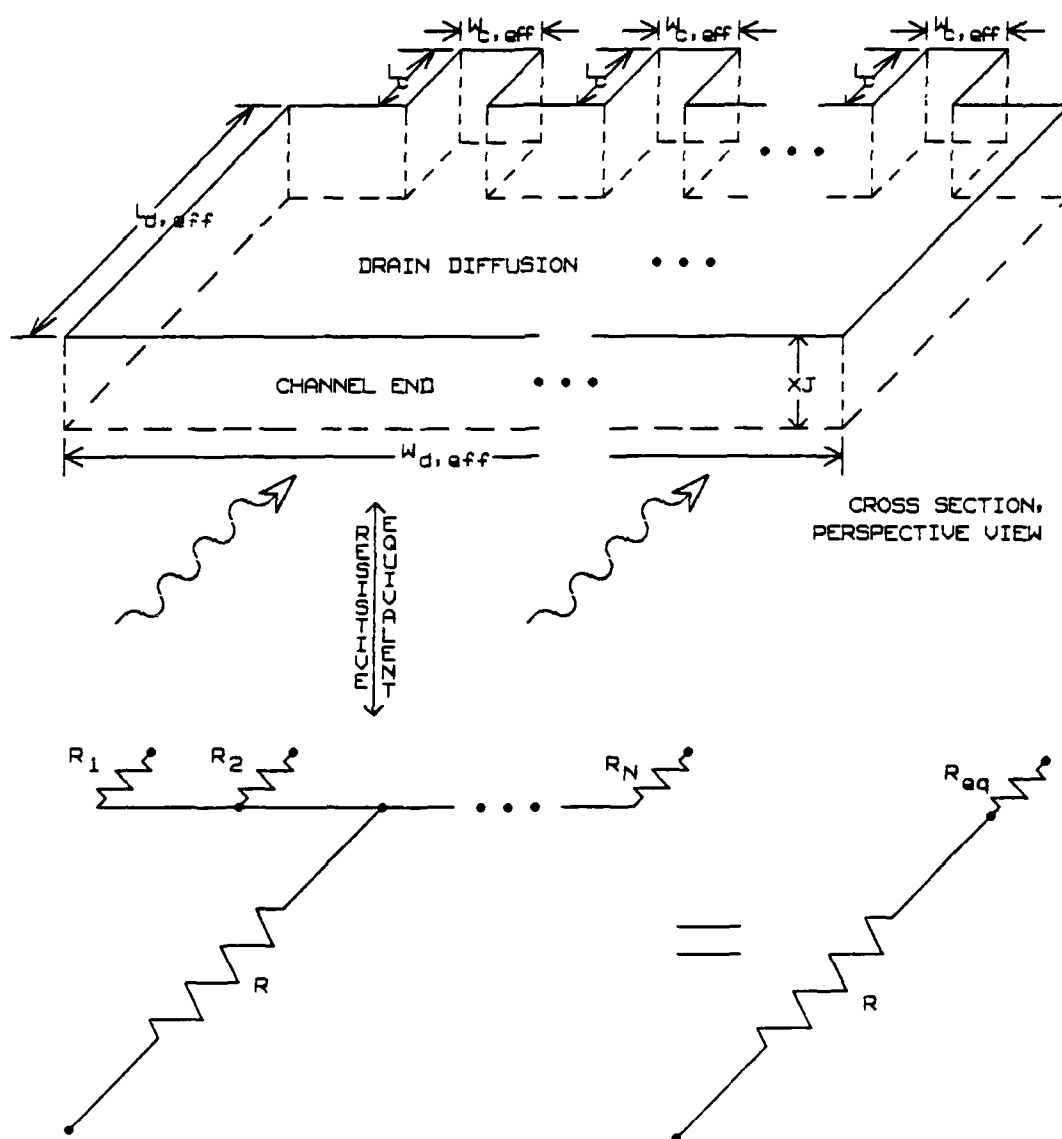


Figure 2.20 Drain Diffusion Region with N Metal to Diffusion Contact Areas and Resistive Equivalent

The denominator of equation (2.54) shows that the p transistor width, W_p , goes to infinity as the denominator goes to zero which occurs at the point where:

$$t_r = \frac{2 \cdot (L_p - 2 \cdot LD_p) \cdot C \cdot (G + H)}{(KP_p\{T\}) \cdot (Vdd - |Vto_p\{T\}|)} \quad (2.55)$$

Obviously the p MOSFET required to source enough current to achieve the rise time defined by equation (2.55) would be so large as to be physically impossible to construct. Therefore, equation (2.55) imposes a theoretical bound on the rise time achievable by a static CMOS inverter of the type shown in Figures 2.8 and 2.15.

If a previously constructed inverter is being examined its minimum theoretical rise time can be determined by rearranging equation (2.45) into the following form.

$$t_r = \frac{2 \cdot (L_p - 2 \cdot LD_p) \cdot (G + H)}{(KP_p\{T\}) \cdot (Vdd - |Vto_p\{T\}|)} \cdot \left[\frac{(B + D + E)}{W_p} + C \right] \quad (2.56)$$

It is important to realize that the inverter being examined may have been constructed such that the variable A in the expression $W_n = W_p \cdot A$ is not defined by equation (2.19). In such a case, the numerical value of A that is obtained from the physical layout of the inverter should be used in the calculation of the variable C in equation (2.56).

For this same inverter that has already been constructed the amount of capacitance that it can drive in t_r seconds can be determined theoretically by manipulating equation (2.45) into the following form:

$$B + E = W_p \cdot \left[\frac{(t_r) \cdot (KP_p\{T\}) \cdot (Vdd - |Vto_p\{T\}|)}{2 \cdot (L_p - 2 \cdot LD_p) \cdot (G + H)} - C \right] - D \quad (2.57)$$

The same caveat about the variable A that was applied to equation (2.56) is equally applicable to equation (2.57).

C. EXTENSION OF THE STATIC CMOS INVERTER TRANSISTOR SIZING EQUATIONS TO GENERAL STATIC CMOS LOGIC DESIGN

The static CMOS inverter in Figures 2.8 and 2.15 involved only a single p MOSFET in the p block and a single n MOSFET in the n block. Figure 2.21 shows a compound gate that implements the logic function $F = \overline{((A \cdot B) + (C \cdot D))}$ [Weste and Eshraghian, 1985, p. 15]. There are two parallel combinations of p MOSFETs in the p block of this compound gate. The two parallel combinations are in series with one another. A similar situation exists in the n block. To apply the equations developed in Section B to a problem like translating from the schematic in Figure 2.21 to a mask level layout requires that some of the variables in equation (2.45) be modified.

Equation (2.30) is the basis for computing $Cbd_{total}\{T\}$ in the static CMOS inverter of Section B. Section B.3 states that $Cbd_{total}\{T\}$ involves all of the drain regions hard wired to the interconnection node from which the output is taken. For the static CMOS inverter of Section B this involves only one drain in the p block and one drain in the n block. For a compound gate $Cbd_{total}\{T\}$ can involve considerably more drain diffusion area than that. For example, in Figure 2.21 there are four drain regions wired to the interconnection node. If signals A and C are low and signals B and D are high in Figure 2.21, the p MOSFET fed by signal A will have to drive the load capacitance, the capacitance of its own drain, and the capacitance of the other three drains wired to the interconnection node as well. Therefore, equation (2.30) is modified for general static CMOS logic design:

$$Cbd_{total} = \#_p \cdot Cbd_p\{T\} + \#_n \cdot Cbd_n\{T\} \quad (2.58)$$

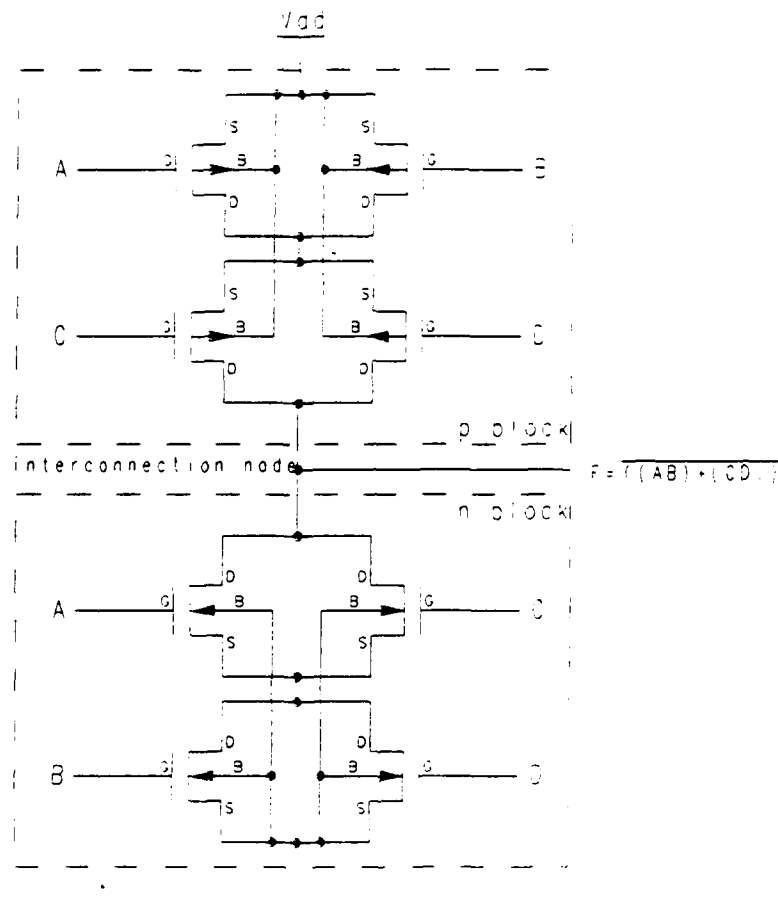


Figure 2.21 Static CMOS Compound Gate Implementation of $F = ((A \cdot B) + (C \cdot D))$.

where

$\#_p \equiv$ the total number of p drains attached to the interconnection node between the p and n blocks, each with identical dimensions.

$\#_n \equiv$ the total number of n drains attached to the interconnection node between the n and p blocks, each with identical dimensions.

Equation (2.58) can now be fully expanded according to the same procedure used to expand equation (2.30) in Section B.3.a. The result is that:

$$Cbd_{total}\{T\} = W_p \cdot C' + D' \quad [farad] \quad (2.59)$$

where C' and D' are no longer defined by equations (2.32) and (2.33):

$$\begin{aligned} C' = & \left(\#_p \cdot [L_{d,mask_p} + 2 \cdot LD_p] \cdot CJ_p\{T\} \cdot Cbdj_{avg,p}\{T\} \right. \\ & + \#_p \cdot 2 \cdot CJSW_p\{T\} \cdot Cbd_{s_{avg,p}}\{T\} \\ & + \#_n \cdot A' \cdot [L_{d,mask_n} + 2 \cdot LD_n] \cdot CJ_n\{T\} \cdot Cbdj_{avg,n}\{T\} \\ & \left. + \#_n \cdot A' \cdot 2 \cdot CJSW_n\{T\} \cdot Cbd_{s_{avg,n}}\{T\} \right) \end{aligned} \quad (2.60)$$

where A' is defined later in equation (2.64).

$$\begin{aligned} D' = \sum_x \#_x \cdot & \left[2 \cdot LD_x \cdot \left([L_{d,mask_x} + 2 \cdot LD_x] \cdot CJ_x\{T\} \cdot Cbdj_{avg,x}\{T\} \right. \right. \\ & + 2 \cdot CJSW_x\{T\} \cdot Cbd_{s_{avg,x}}\{T\} \Big) \\ & + 2 \cdot \left([L_{d,mask_x} + 2 \cdot LD_x] + N_x \cdot L_{c_x} \right) \cdot CSJW_x\{T\} \cdot Cbd_{s_{avg,x}}\{T\} \\ & \left. + N_x \cdot L_{c_x} \cdot \left([W_{c_x} + 2 \cdot LD_x] \cdot CJ_x\{T\} \cdot Cbdj_{avg,x}\{T\} + W_{c_x} \cdot C_{md_x} \right) \right] \\ & \text{for } x = p, n \end{aligned} \quad (2.61)$$

For each p transistor added in series between the supply voltage and the load the rise time at the load increases. If a single p MOSFET has the ability to drive

a load high in t_r seconds then placing k identical p MOSFETs in series would increase the rise time to $k \cdot t_r$ seconds. Similarly, placing m identical n MOSFETs in series between a load and ground increases fall time from t_f seconds to $m \cdot t_f$ seconds [Weste and Eshraghian, 1985, p. 181]. The reason for this is quite apparent from Table 2.1. Placing transistors in series is analogous to increasing the effective channel length of a single transistor. In Table 2.1 effective channel length is found in the denominator of the drain current equations. Therefore increasing effective channel length decreases drain current which implies longer rise and fall times.

In Section B.4 the variable F was calculated based on equation (2.15). Equation (2.15) was calculated for a static CMOS inverter where only a single p MOSFET stood between the supply voltage and the load. As Figure 2.21 illustrates, there may in fact be a long line of p MOSFETs in series between the supply voltage and the load. Therefore the effective channel length in equation (2.15) should be modified for general static CMOS logic design:

$$L_{effp} = \sum_{\substack{\text{longest} \\ \text{path to } V_{dd}}} (L_p - 2 \cdot LD_p) \quad (2.62)$$

where the summation is over the number of p MOSFETs that comprise the longest path between the supply voltage and the load and L_p is assumed to be the minimum mask level channel length permitted by the technology in use.

The change in equation (2.15) is reflected in the calculation of the variable F' for general static CMOS logic design:

$$F' = \frac{2 \cdot \sum_{\substack{\text{longest} \\ \text{path to } V_{dd}}} (L_p - 2 \cdot LD_p)}{(t_r) \cdot (KP_p\{T\}) \cdot (V_{dd} - |V_{to_p}\{T\}|)} \quad (2.63)$$

The change in effective channel length also makes it necessary to modify the variable A found in equation (2.19) for use in general static CMOS logic design.

Applying the same reasoning that was used to develop equation (2.63) to the calculation of the variable A gives:

$$A' = \frac{\left[\sum_{\substack{\text{longest} \\ \text{path to GND}}} (L_n - 2 \cdot LD_n) \right] \cdot (KP_p\{T\}) \cdot (Vdd - |Vto_p\{T\}|)}{\left[\sum_{\substack{\text{longest} \\ \text{path to Vdd}}} (L_p - 2 \cdot LD_p) \right] \cdot (KP_n\{T\}) \cdot (Vdd - Vto_n\{T\})} \cdot \frac{\left[\frac{(Vto_n\{T\} - 0.1 \cdot Vdd)}{(Vdd - Vto_n\{T\})} + \frac{1}{2} \cdot \log_e \left(\frac{19 \cdot Vdd - 20 \cdot Vto_n\{T\}}{Vdd} \right) \right]}{\left[\frac{(|Vto_p\{T\}| - 0.1 \cdot Vdd)}{(Vdd - |Vto_p\{T\}|)} + \frac{1}{2} \cdot \log_e \left(\frac{19 \cdot Vdd - 20 \cdot |Vto_p\{T\}|}{Vdd} \right) \right]} \quad (2.64)$$

Incorporating these modifications into equations (2.45) and (2.46) gives the final result for general static CMOS logic design:

$$W_p = \frac{F' \cdot (G + H) \cdot (B + D' + E)}{1 - F' \cdot C' \cdot (G + H)} \quad (2.65)$$

$$W_n = W_p \cdot A' \quad (2.66)$$

The equations defining the variables in equations (2.65) and (2.66) are referenced in Table 2.5.

The W_p solved for is the mask level width of the channel of each p MOSFET connected directly to the interconnection node between the p and n blocks. This width must be maintained for all MOSFETs between the loadmost p MOSFETs and the supply voltage. Similarly, the W_n solved for is the mask level width of the channel of each n MOSFET connected directly to the interconnection node between the n and p blocks. This width must be maintained for all n MOSFETs between the loadmost n MOSFETs and ground.

**TABLE 2.5 IMPORTANT EQUATIONS FOR
GENERAL STATIC CMOS LOGIC DESIGN**

Variable	Defining Equations(s)
W_p	(2.65)
W_p^p	(2.66)
A^p	(2.64)
B	(2.42) and (2.35)
C'	(2.60)
D'	(2.61)
E	(2.43)
F'	(2.63)
G	(2.38)
H	(2.39)

**D. EXTENSION OF THE TRANSISTOR SIZING EQUATIONS TO
NON-RECTANGULAR TRANSISTORS.**

To this point the equations developed for transistor sizing have been discussed only in the context of rectangular shaped transistors of the sort depicted in Figure 2.11. It is possible to apply the result obtained to other configurations such as the Manhattan geometry star in Figure 2.22 and the circular transistor in Figure 2.23. The equations in Sections B and C are based on rectangular shaped transistors but only in the sense that total channel lengths and widths and total diffusion lengths, widths, perimeters and areas were defined for rectangular areas. As long as the values assigned to these model parameters are maintained in construction it is possible to apply the results for the rectangular configuration to any configuration. For example, in Figure 2.23 the mask level channel length is $(r_2 - r_1)$ and the mask level channel width is $r_2 \cdot (2 \cdot \pi - \theta)$. These values should be made to equal L_p and W_p from the rectangular model. Similarly, the drain area should be made to equal that of the rectangular configuration. In this way the results of Sections B and C become powerful design tools.

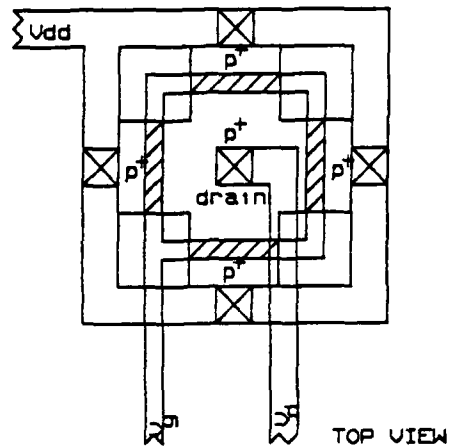


Figure 2.22 Manhattan Geometry Star Configured MOSFET

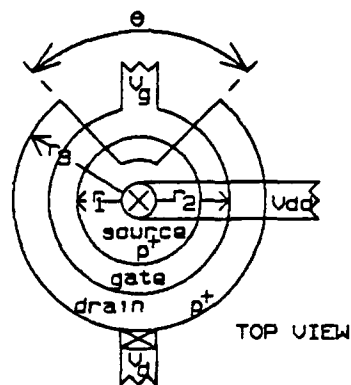


Figure 2.23 Circular MOSFET

E. CHAPTER SUMMARY

The equations presented in this chapter enable one to size transistors to meet desired timing performance standards under known loading conditions, operating temperature, and supply voltage. The equations developed for the static CMOS inverter are implemented in a computer program that is included in Appendix A.

This program is used to apply the equations to a design problem, the design of the super buffer, in the next chapter.

III. DESIGN OF A HIGH-SPEED STATIC CMOS SUPER BUFFER FOR THE MONTEREY SILICON COMPILER

A. BACKGROUND.

A need exists to create and insert into the Monterey Silicon Compiler code a mask level integrated circuit design of a static CMOS super buffer [Malagon, 1987, p. 95]. To understand the role of a super buffer it is necessary to first discuss the circuit that it is a part of. From Sedra and Smith:

"A critical aspect of the design of any logic device, particularly those using LSI (Large-Scale Integration) and VLSI (Very-Large-Scale Integration) circuit technologies, is the provision of clock signals. Difficulties arise because the clock signal (whether generated on or off the chip) must usually feed many parts of the circuit. This need for large fan-out can be met by applying the clock signal to a string of cascaded inverters and feeding the output of each inverter to a different part of the circuit, a structure known as a *branching fan-out tree*. However, problems may arise with this approach as a result of the differing time delays that the clock signal experiences on the paths to the various parts of the system. To be specific, if two physically remote segments of a logic network must intercommunicate, it is essential that the relative time variation, or *skew*, of their clocks be controlled and limited to ensure reliable operation.

The problem in VLSI circuit design is further compounded because large clock fan-out and long clock lines imply large capacitive loads and two conflicting dangers: very slow rise and fall times if drive current is inadequate or, alternatively, enormous charging and discharging currents if the driver is too capable and fast charging. Thus, the design of clock systems in VLSI circuits is a challenging problem, involving control of signals that are both large in amplitude and in rate of rise." [Sedra and Smith, 1982, p. 759]

In the Monterey Silicon Compiler architecture the effects of skew are minimized through the use of a two phase non-overlapping clocking scheme [Mullarky, 1987, pp. 11-23]. The need for large fan-out in the clock circuit is satisfied by the super buffer. The super buffer is that part of the branching fan-out tree that feeds clock signals from the pad where off-chip generated clock signals arrive, to the

data storage registers on the chip. Since the super buffer is a gate in the path of incoming clock signals, it must be guaranteed to function within specified timing constraints under given loading lest the operation of an entire chip fail due to the inability of the clock circuit to drive the on chip storage registers within an acceptable amount of time delay. Since a super buffer's sole function is to increase the drive of a propagating signal it can be constructed by cascading two inverters.

Professor Richard W. Hamming of the Naval Postgraduate School said about systems engineering, "If you optimize one component of a system you will hate yourself in the morning." The idea behind the statement is that each component of a system must be designed to fit in well with all the other system components. The clock input pads, super buffers, and storage registers form a complete subsystem within a Monterey Silicon Compiler generated circuit. CMOS replacements for the NMOS clock input pads and the NMOS storage registers already exist, therefore, the replacement CMOS super buffer must be designed with this previous work in mind.

Figure 3.1 demonstrates the concept of employment of super buffers within the Monterey Silicon Compiler architecture. In the figure each super buffer can be seen to consist of two cascaded inverters. Since the clocking scheme used involves two clocks, two clock-signals must be delivered to each register. Thus, the super buffers must be employed in pairs as can be seen in Figure 3.1. Each pair supplies both clock signals to a bank of data registers that straddles the data path.

In Figure 3.1 the inverter symbols within each super buffer are drawn so that the output stage inverter is larger than the input stage inverter. This is intended to be a reflection of the physical construction necessary to achieve the desired electrical behavior of the super buffer. The super buffer output stage must be capable of driving a large fan-out. The input stage must be capable of driving

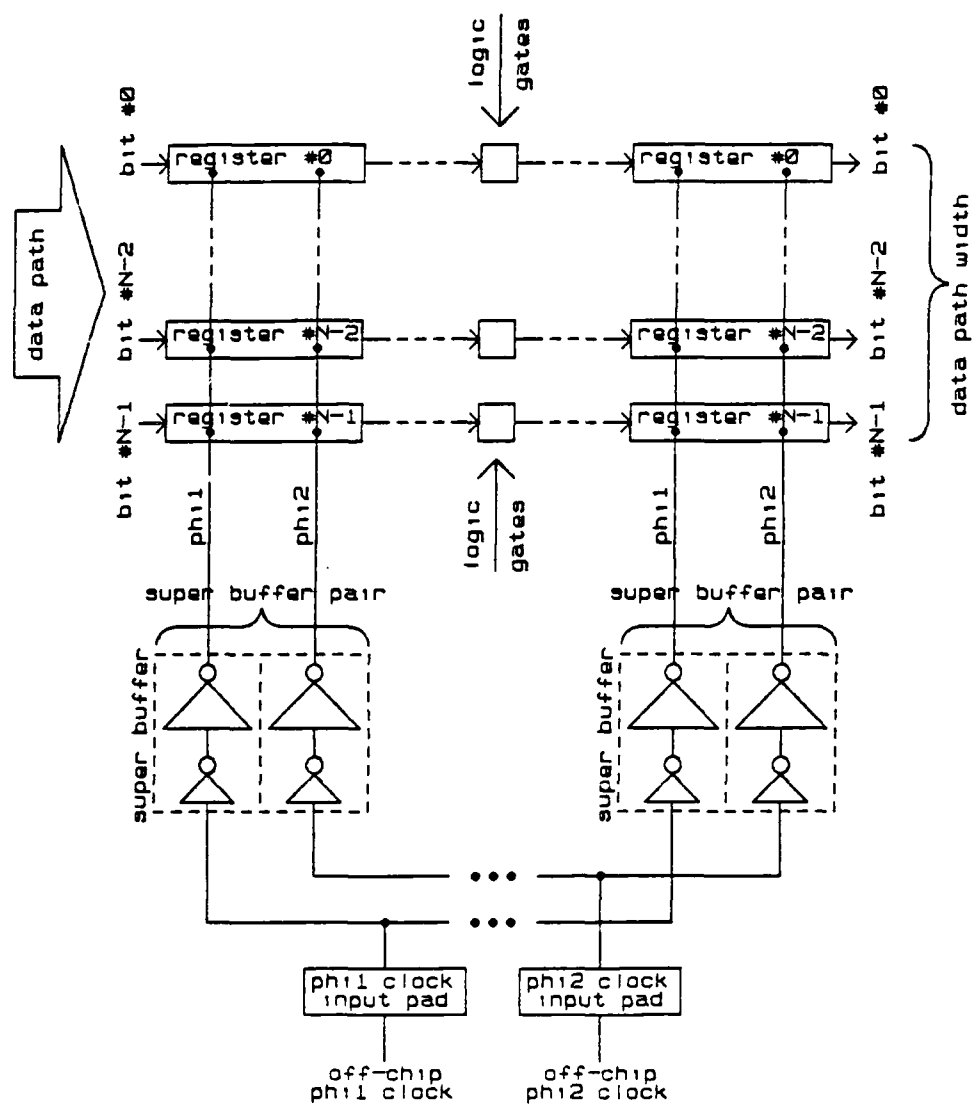


Figure 3.1 Employment of Super Buffer within the Monterey Silicon Compiler Architecture

the gate capacitance of the output stage and at the same time present an input capacitance smaller than the output stage input capacitance. The MOSFETs in the output stage must, therefore, be larger than those in the input stage.

The design task is to find all of the dimensions of the input and output stage inverters given the following:

- worst-case circuit operating temperature
- worst-case supply voltage
- worst-case gate voltage
- worst-case SPICE fabrication parameters

The equations developed in Chapter II are ideally suited to solving this problem. The procedure is documented in the next section. Worst-case conditions are referred to above because worst-case design is essential for reliable circuit operation. The performance of the super buffer with respect to time is of the utmost concern in this design. Therefore, the worst-case parameters to be used in the design process are those that restrict current flow and thereby slow down the operation of the super buffer. These include: high circuit operating temperatures, low supply voltage, low gate voltage (which is inherent to low supply voltage in fully restored static CMOS logic), and minimum current SPICE fabrication parameters (obtained from the silicon foundry where the circuit is to be constructed). A circuit designed to function properly under these punishing conditions will function faster in a less severe environment. Of course, a circuit may be designed to meet less hostile conditions if it is not necessary for the circuit to meet the design performance standards under such extreme circumstances. In that case, nominal values for the supply voltage and SPICE fabrication parameters might be used in the design specifications as well as some lesser operating temperature.

In the design of microchips intended for commercial use, semiconductor manufacturers typically guarantee their devices for operation over a temperature range of -40°C to $+85^{\circ}\text{C}$ and over a supply voltage range of 4.5 V to 6 V. [Signetics Corp., 1986, p. 5-4]. For military applications both of these ranges are broader. In keeping with industrial practice, the super buffer is designed for guaranteed operation within a specified timing constraint at 85°C (358.15 K) with a supply voltage (and gate voltage) of 4.5 V. The minimum current SPICE fabrication parameters chosen are from the Metal-Oxide-Semiconductor Implementation Service (MOSIS) sponsored by DARPA at the Information Sciences Institute, University of Southern California. The parameters are included in Appendix B. The desired rise time and fall time at the output of each stage of the super buffer is chosen to be 2.0 nanoseconds. The total average delay time desired is therefore (from equation (2.16)):

$$\begin{aligned}
 t_{d_{\text{avg},\text{total}}} &= t_{d_{\text{avg},\text{input stage}}} + t_{d_{\text{avg},\text{output stage}}} \\
 &= \frac{1}{4} \cdot (t_{r_{\text{input stage}}} + t_{f_{\text{input stage}}}) + \frac{1}{4} \cdot (t_{r_{\text{output stage}}} + t_{f_{\text{output stage}}}) \\
 &= \frac{1}{4} \cdot (2.0 \times 10^{-9} + 2.0 \times 10^{-9}) + \frac{1}{4} \cdot (2.0 \times 10^{-9} + 2.0 \times 10^{-9}) \\
 &= 2.0 \times 10^{-9} [\text{s}]
 \end{aligned}$$

B. DESIGN OF THE SUPER BUFFER.

The number of registers across the width of the data path in Figure 3.1 is equal to the number of bits in the word that propagates along the path. In order to determine the loading that the super buffer must be designed to support, an upper limit on the number of registers that can be supported under a worst-case scenario must be chosen. As this number becomes larger, the size of the super buffer required also

becomes larger. Due to the size constraint imposed by the physical layout of all floorplans designed by the Monterey Silicon Compiler, the number of supportable registers under a worst-case scenario is chosen to be four. For a number larger than that the static CMOS super buffer would have to be significantly larger than the NMOS super buffer that it replaces and it simply would not fit within the space presently allotted for it on the floorplan. This, however, is the number of registers that can be driven in 2 nanoseconds if the worst-case scenario is assumed. As discussed in Section A, the worst-case scenario implies that the circuit is constructed using worst-case minimum current SPICE fabrication parameters, that the supply voltage is only 4.5 volts, and that the circuit operates at 85° C. Since the super buffer is designed under a worst-case assumption, operating it under less hostile conditions will enhance its performance. If the capacitive loading on the super buffer remains constant but operating conditions improve, the super buffer will function faster than the 2 nanosecond delay time upper limit. The actual speed can be calculated using equation (2.56). Conversely, improved operating conditions offer the opportunity to drive more capacitance (more registers) without affecting the speed of operation of the super buffer. If the worst-case scenario does occur and the data path is wider than four bits then the super buffer will, of course, still function, but it will no longer meet the 2 nanosecond design goal. The performance of the super buffer under the loading caused by four, eight, sixteen, and thirty-two bit data paths is discussed in Section E. Thus, the Monterey Silicon Compiler is not by any means restricted to the construction of four bit circuits. As with any integrated circuit, the maximum clock frequency at which the super buffers can operate is governed by temperature, capacitive loading, supply voltage, and fabrication process. The better these conditions are, the faster the super buffers will operate; the worse they are, the slower the super buffers will operate.

Figure 3.2 shows the mask level layout of a single data register [Mullarky, 1987, p. 56]. The labels PHI1! and PHI2! on Figure 3.2 correspond to the phi1 and phi2 clocklines in Figure 3.1. The output stage of one super buffer of a super buffer pair is connected to the input labeled PHI1! in Figure 3.2. The output stage of the other super buffer in the pair is connected to the input labeled PHI2! in Figure 3.2. Looking into the register at PHI1! the super buffer sees three n MOSFETs and a p MOSFET, all in parallel and each having mask level channel dimensions ($L \times W$) equal to 3.0 microns by 4.5 microns.

The programs in Appendix A are used to calculate the gate capacitance seen by the super buffer looking into the PHI1! input of the register. To run the programs on the HP41CX they must all first be stored in extended memory and main memory must be cleared. The name "VLSI" is stored in the alpha register and execution continues as follows:

GETP then R/S are executed. The program responds:

STOP. PURGE MAIN MEMORY

The programs are so large that they cannot all be held in main memory at once. They must be swapped in and out of extended memory as needed. The prompt is saying that the program VLSI should be the only program currently in main memory. If it is not, all programs in main including VLSI must be purged and the process started over again. R/S is executed again. The program responds:

ENTER FAB. PARAM. CARD

The programs require that the SPICE fabrication parameters be entered. These should be stored on magnetic cards in accordance with the data register allocation detailed in Appendix A. The cards are entered and the program responds:

OPERATING TEMP (KELVIN) = ?

The response for worst-case operating temperature is 358.15. R/S is executed.

The program responds:

VBS (N), VOLTS = ?

Since a p^+ substrate contact will be placed on the actual device so that it abuts the n source diffusion at the ground line contact, V_{bs_n} is equal to zero. R/S is executed. The program responds:

VBS (P), VOLTS = ?

Since an n^+ substrate contact will be placed on the actual device so that it abuts the p source diffusion at the supply voltage line contact, V_{bs_p} is equal to zero. R/S is executed. The program responds:

SUPPLY VOLTAGE (VOLTS) = ?

The response for worst-case supply voltage is 4.5. R/S is executed. The program responds:

P CHNL MASK LENGTH (MTR) = ?

At the end of Section B.2 in Chapter II it is stated that the channel mask length should be chosen to be the minimum feature size for the technology being used. Since the technology being used in the Monterey Silicon Compiler is based on a p well process with three micron minimum feature size the response is 3.0×10^{-6} . R/S is executed. The program responds:

N CHNL MASK LENGTH (MTR) = ?

Again, the response is 3×10^{-6} . R/S is executed. The program responds with a menu:

WI LD

Choosing WI would go into the transistor sizing algorithm. Since the immediate goal is to find the gate capacitance seen by the super buffer looking into the PHI1!

input of the register, LD is chosen, where LD is short for "load". The program responds with an introductory line immediately followed by a query:

LOADCAP

LOAD CHNL MASK LNGTH (MTR) ?

The total gate capacitance looking in at PHI1! of the register is calculated starting with the three n MOSFETs. The length for all three is 3.0 microns. R/S is executed. The program responds:

LOAD CHNL MASK WIDTH (MTR) ?

The width for all three n MOSFETs is 4.5 microns. R/S is executed. The program responds with a query followed by a menu:

DEVICE TYPE?

N P

N is chosen to indicate to the program that the device is an n MOSFET.

The program responds with another query followed by another menu:

ANOTHER DEVICE?

Y N

The response is Y for yes. The program responds.

LOAD CHNL MASK LNGTH (MTR) ?

The same procedure is continued by responding to the prompts as appropriate until all three n MOSFETs and the p MOSFET have been entered. At that point the response to the query, "ANOTHER DEVICE", is N for no, and the program responds with the total capacitance of the four MOSFETs connected in parallel:

$C \Sigma \text{ LOAD DEV} = 43.43E - 15 \text{ (FARAD)}$

R/S is executed and the menu that gives a choice between the transistor sizing algorithm and the load capacitance algorithm appears again. Looking into the register at PHI2! the other super buffer in the pair sees three p MOSFETs and an

n MOSFET, all in parallel and each having mask level channel dimensions ($L \times W$) equal to 3.0 microns by 4.5 microns. In terms of the number of each type of device this is the opposite of what is seen by the other super buffer. This leads to a slight difference between the gate capacitance seen by each super buffer of the pair. The load capacitance algorithm determines the gate capacitance seen looking into the register at PHI2! to be 39.5 femtofarads. The difference between the capacitance seen by the two loads is not so great as to warrant the construction of two entirely different super buffers to make up the pair. It does however suggest that if only one basic super buffer is to be designed and employed in pairs then the basic super buffer should be designed to support the larger of the two loads, 43.43 femtofarads. For each super buffer to drive four registers requires that it be capable of driving four times this amount. Thus, $C \sum_{\text{load devices}} \text{gate for each super buffer} = (4) \cdot (43.43 \times 10^{-15}) = 173.7 \times 10^{-15}$ Farads. There is one other element of capacitive loading not yet determined that is required in the calculations; the routing capacitance. For a four bit data path the Monterey Silicon Compiler typically places the registers so that the metal line connecting the clock input on each register to the super buffer output is 187.5 microns long per register and 4.5 microns wide. Thus, for a four bit data path the routing capacitance of the line extending from each super buffer in the pair to the four registers it supports is:

$$C_r = (4) \cdot (4.5 \times 10^{-6}) \cdot (187.5 \times 10^{-6}) \cdot C_{md}$$

where C_{md} is the capacitance formed between metal and substrate. C_{md} is taken to be $100 \times 10^{-6} \left[\frac{F}{m^2} \right]$ [Weste and Eshraghian, 1985, p. 135]. Substituting this value for C_{md} gives:

$$C_r = 337.5 \text{ femtofarads}$$

Armed with the knowledge that $C \sum_{\text{load devices}} \text{gate} = 173.7 \times 10^{-15}$ Farads, and that $C_r = 337.5 \times 10^{-15}$ Farads for each super buffer the transistor sizing algorithm may now be used to determine the dimensions of the p and n MOSFETs in the output stage of the super buffer.

Returning once again to the menu that gives a choice between the transistor sizing algorithm and the load capacitance algorithm the choice "WI" is selected. The program responds with a query followed by a menu:

DO YOU KNOW C Σ LOAD DEV?

YES

NO

Since C Σ LOAD DEV ($= C \sum_{\text{load devices}} \text{gate}$) has already been calculated the response is YES. The program responds:

C Σ LOAD DEV (FARAD) = ?

The response is 173.7×10^{-15} . R/S is executed and the program responds:

DESIRED RISE TIME (SEC) = ?

The time that has been chosen is 2×10^{-9} seconds. R/S is executed. The program responds:

ROUTING CAP (FARAD) = ?

C_r has been calculated to be 337.5×10^{-15} Farads. It is interesting to note that this routing capacitance is about double the gate capacitance of the load. R/S is executed. The program responds:

P DRAIN MASK LENGTH (MTR) ?

The minimum drain length for the technology is selected in order to reduce drain diffusion capacitance to a minimum. The value is 3×10^{-6} . R/S is executed. The program responds:

N DRAIN MASK LENGTH (MTR) ?

As with the p drain diffusion length, the value selected is the minimum permitted. The value is 3×10^{-6} . R/S is executed. The program responds:

NO. P DIFFUSION CONTACTS

The program needs to know how many diffusion to metal contacts are going to be placed around the p drain diffusion area. The choice is three. R/S is executed and the program responds:

P DIFCTC MASK LENGTH (MTR) ?

The value requested is the length of the diffusion to metal contacts placed around the p drain diffusion. To minimize drain capacitance the minimum dimension supported by the technology is chosen. The value is 6×10^{-6} . This is the same value for the length of the diffusion to metal contacts placed around the n drain diffusion as well as for the width of the contacts placed around both drain diffusions. R/S is executed and the program responds:

PDIFCTC MASK WIDTH (MTR) ?

The response is 6×10^{-6} . R/S is executed and the program responds:

NO. N DIFFUSION CONTACTS

One diffusion to metal contact will be placed on the n drain diffusion area. R/S is executed. The program responds:

N DIFCTC MASK LENGTH (MTR) ?

The response is 6×10^{-6} . R/S is executed. The program responds:

N DIFCTC MASK WIDTH (MTR) ?

The response is 6×10^{-6} . R/S is executed. The program responds, with all the dimensions (as defined in Table 2.2) of the n and p MOSFETs in the output stage of the super buffer that are required for a complete modeling of the output stage with PSpice:

$$L \langle P \rangle = 3 \times 10^{-6} \langle \text{MTR} \rangle$$

$$W \langle P \rangle = 134.3 \times 10^{-6} \langle \text{MTR} \rangle$$

$$AD \langle P \rangle = 660.9 \times 10^{-12} \langle \text{SQ. MTR} \rangle$$

$$PD \langle P \rangle = 314.4 \times 10^{-6} \langle \text{MTR} \rangle$$

$$RD \langle P \rangle = 22.16 \langle \text{OHM} \rangle$$

$$L \langle N \rangle = 3 \times 10^{-6} \langle \text{MTR} \rangle$$

$$W \langle N \rangle = 51.93 \times 10^{-6} \langle \text{MTR} \rangle$$

$$AD \langle N \rangle = 231.2 \times 10^{-12} \langle \text{SQ. MTR} \rangle$$

$$PD \langle N \rangle = 124.4 \times 10^{-6} \langle \text{MTR} \rangle$$

$$RD \langle N \rangle = 29.19 \langle \text{OHM} \rangle$$

The program then returns to the very beginning. The program is run again in its entirety to determine the dimensions of the n and p MOSFETs in the input stage of the super buffer. $C \sum_{\text{load devices}}^{\text{gate}}$ for the input stage is that capacitance that is due to the gates of the n and p MOSFETs of the output stage. C_r is negligible for the input stage as the extent of the routing between the input and output stages is minimal. The drain diffusion length and contact dimensions are again chosen to be the minimum supportable by the technology to minimize the capacitance that must be driven. Two metal to diffusion contacts are chosen for the p drain diffusion area and one is chosen for the n drain diffusion area. The results of factoring these variables into the program in combination with the worst-case temperature, supply voltage, and fabrication parameters are all the dimensions (as defined in Table 2.2) of the n and p MOSFETs in the input stage of the super buffer that are required for a complete modeling of the input stage with PSpice:

$$L \langle P \rangle = 3 \times 10^{-6} \langle \text{MTR} \rangle$$

$$W \langle P \rangle = 106.1 \times 10^{-6} \langle \text{MTR} \rangle$$

$$AD \langle P \rangle = 507.3 \times 10^{-12} \langle \text{SQ. MTR} \rangle$$

$$PD \langle P \rangle = 246 \times 10^{-6} \langle \text{MTR} \rangle$$

$$RD \langle P \rangle = 32.76 \langle \text{OHM} \rangle$$

$$L \langle N \rangle = 3 \times 10^{-6} \langle \text{MTR} \rangle$$

$$W \langle N \rangle = 41.01 \times 10^{-6} \langle \text{MTR} \rangle$$

$$AD \langle N \rangle = 191.4 \times 10^{-12} \langle \text{SQ. MTR} \rangle$$

$$PD \langle N \rangle = 102.6 \times 10^{-6} \langle \text{MTR} \rangle$$

$$RD \langle N \rangle = 29.73 \langle \text{OHM} \rangle$$

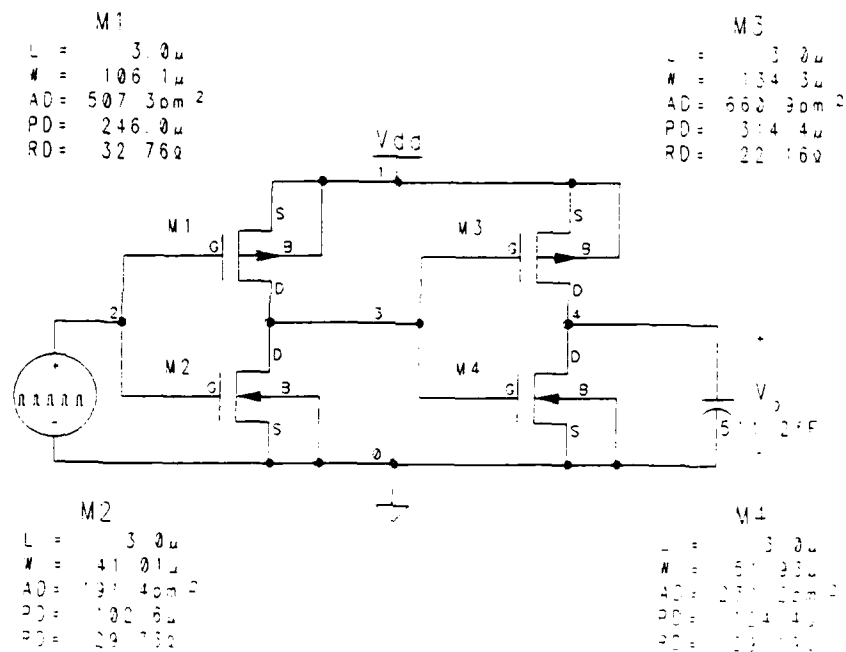


Figure 3.3 Schematic of Static CMOS Super Buffer

A schematic drawing of the super buffer with all the calculated dimensions affixed is presented in Figure 3.3. The load capacitance on the output stage is merely the sum of $C \sum_{\text{load devices}} \text{gate} + C_r$, calculated for the output stage. Note that node numbers (0,1, etc.) and transistor names (M1, M2, etc.) have been assigned in the figure. These node numbers and transistor names correspond to the nodes used in the actual PSpice deck as it appears, ready for simulation, in Appendix B. The worst-case, minimum current SPICE fabrication parameters are also included in the PSpice deck in Appendix B.

C. SIMULATION OF THE SUPER BUFFER.

The results of simulating the PSpice deck in Appendix B are displayed in Figures 3.4, 3.5, and 3.6. In each figure voltage is plotted as a function of time. The voltages displayed are referred to by node numbers which correspond to those used in Figure 3.3 and Appendix B. Voltages are measured with respect to two nodes. Where only one node is listed, the second is taken to be node 0, which in the case of this circuit is ground. Thus, Figure 3.4 shows the voltage waveforms presented to and produced by the input stage of the super buffer. The value of 1.0 volt that is subtracted from the input voltage wave form is the threshold voltage of the n device. Similarly the value of $| - 1.0 |$ volt that is subtracted from the absolute value of V(2,1) is the absolute value of the threshold voltage of the p device. These waveforms are included to assist in determining when the devices are in their various regions of operation: linear, saturation, and cutoff as discussed in Chapter II.

The simulation result in Figure 3.4 is almost identical to that predicted by theory in Figures 2.9a and 2.10a (the small spikes are due to anomalies of the model). This is an important result because the model used to prepare Figures

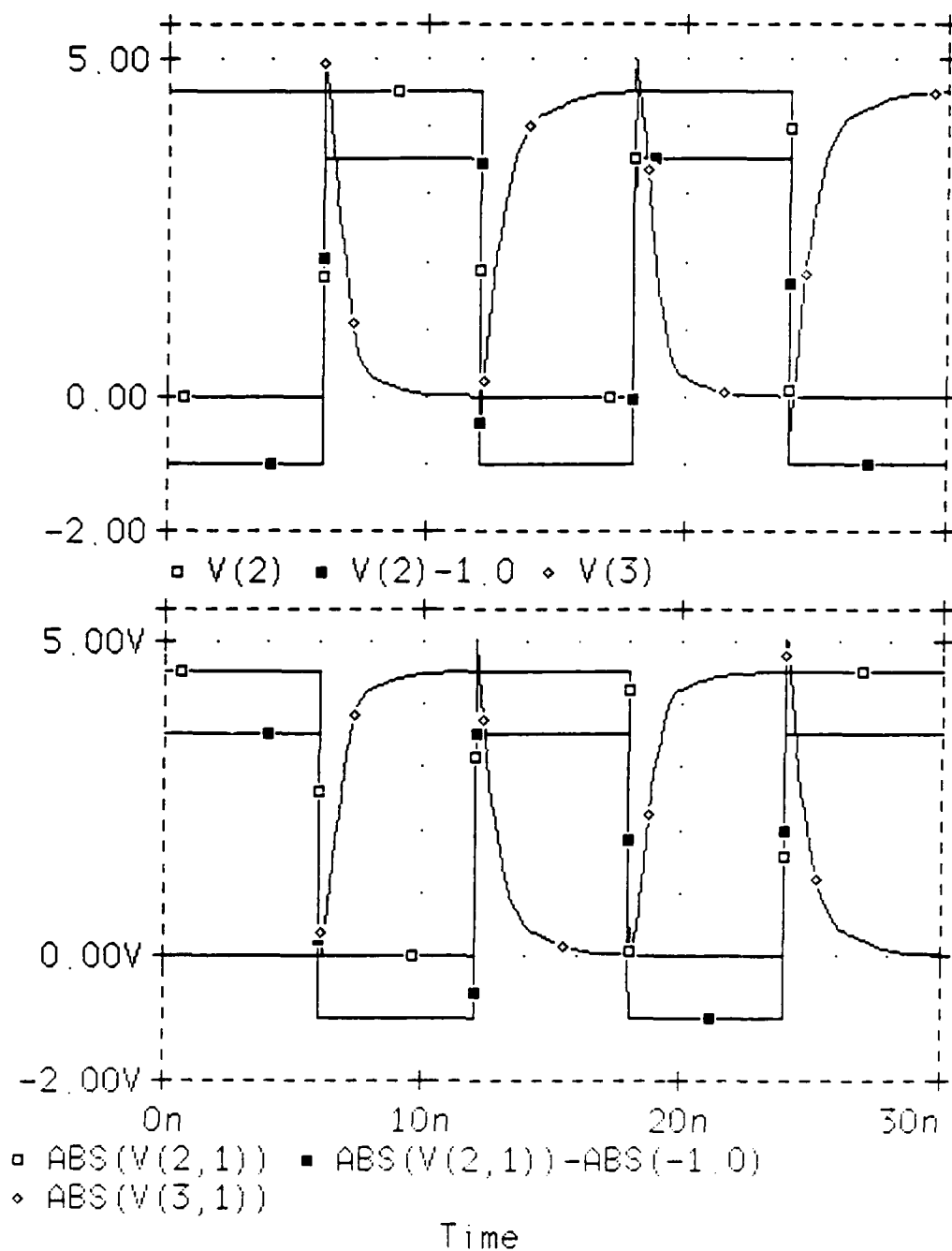


Figure 3.4 PSpice PROBE Postprocessor Simulation of Voltage Waveforms Presented to and Produced by the Input Stage of the Super Buffer Using MOSFET Level Two Model

2.9a and 2.10a was based on the Shichman-Hodges model associated with level one SPICE MOSFET simulations while the model used in the simulation that resulted in Figures 3.4, 3.5, and 3.6 was a different one. The foundation of the equations developed in Chapter II rests on the Shichman-Hodges model of MOSFET behavior. To confirm the validity of the approach taken in developing the equations of Chapter II a totally independent model was selected for simulation; the level two SPICE MOSFET model based on the work of Vladimirescu and Liu [Electronics Research Laboratory, 1980, pp. 1-23].

Figure 3.5 shows the voltage waveforms presented to and produced by the output stage of the super buffer. Figure 3.6 shows the voltage waveform presented to the input stage of the super buffer and the voltage waveform produced by the output stage of the super buffer.

Table 3.1 summarizes the rise and fall time data presented in Figures 3.4, 3.5, and 3.6. Since the performance target is that t_r and t_f for the output voltage waveforms of both the input stage and the output stage not exceed 2×10^{-9} seconds the table shows that success has been achieved. The rise time of the voltage waveform produced by the input stage is 12% faster than the 2 nanosecond goal. The fall time of this voltage waveform is 37% faster than the goal. The rise time of the voltage waveform produced by the output stage is 6% faster than the two nanosecond goal. The fall time of this waveform is 19.5% faster than the goal. Rough symmetry is achieved in rise and fall times at the output of each stage.

Delay time based on the projected rise and fall times should be 1 nanosecond for each stage or 2 nanoseconds for both stages in cascade (based on equation (2.16)). Table 3.2 summarizes the delay time data of Figures 3.4, 3.5, and 3.6. Table 3.2 shows that the average time delay through the input stage is 25% faster than predicted. The average time delay through the output stage is 27% slower

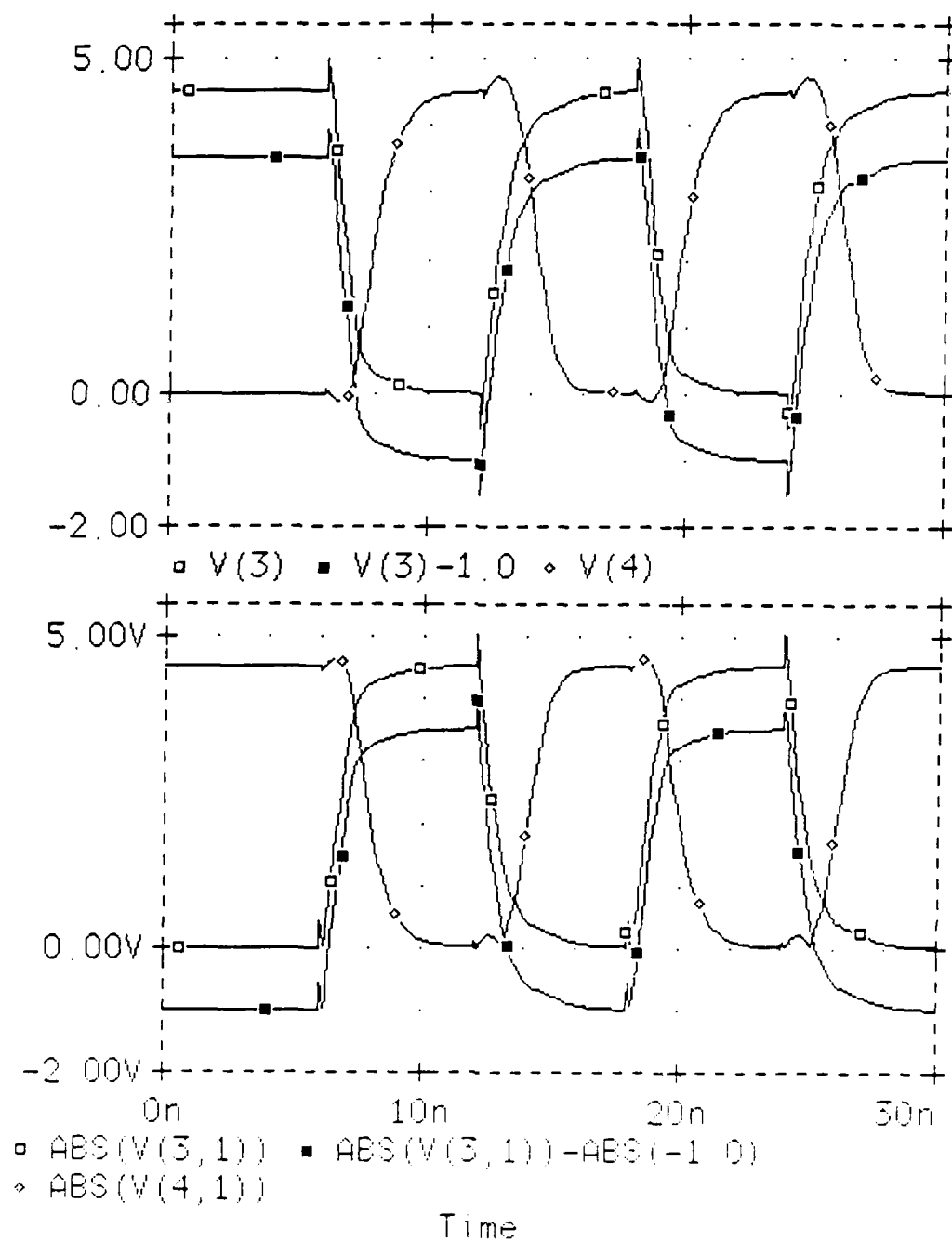


Figure 3.5 PSpice PROBE Postprocessor Simulation of Voltage Waveforms Presented to and Produced by the Output Stage of the Super Buffer Using MOSFET Level Two Model.

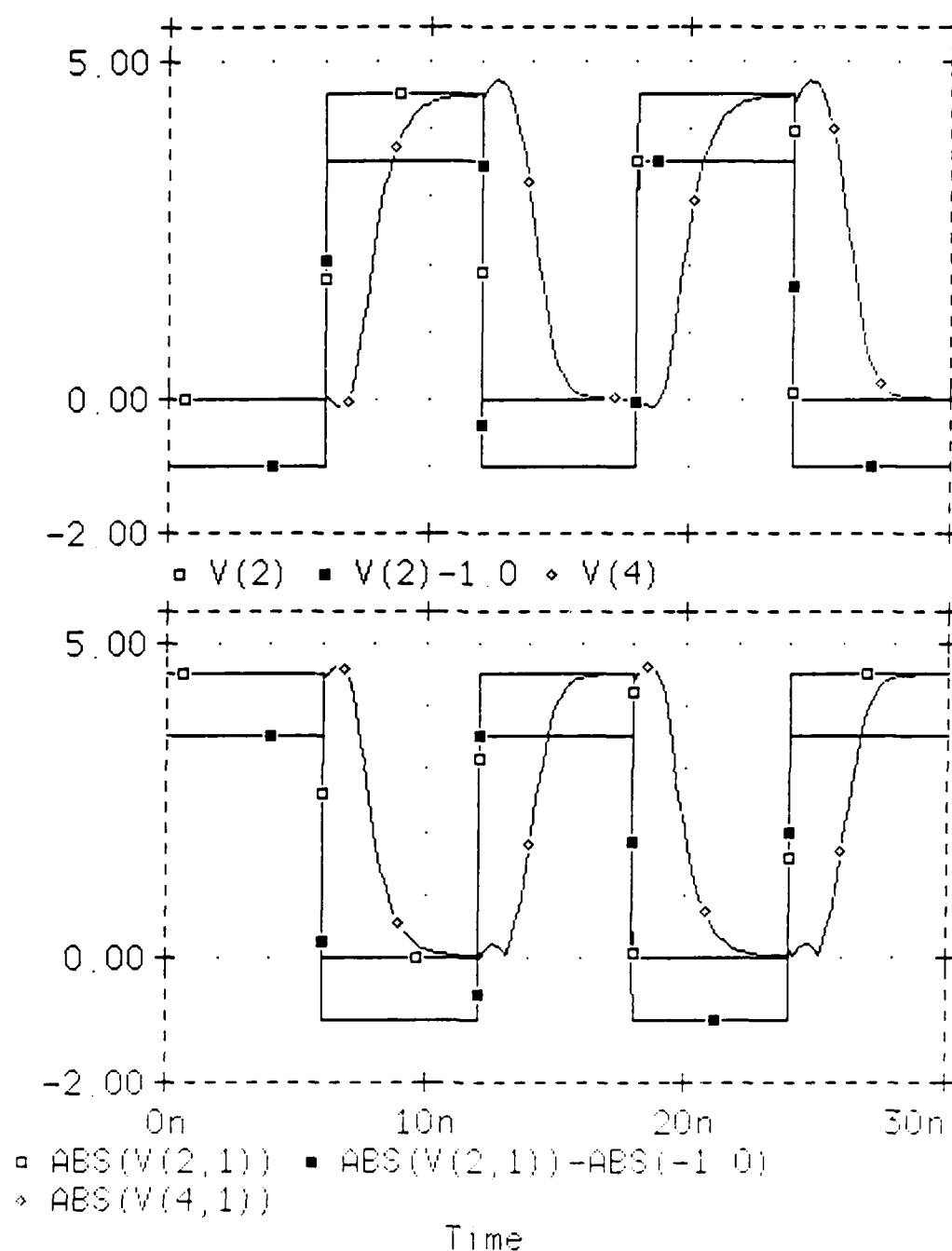


Figure 3.6 PSpice PROBE Postprocessor Simulation of Voltage Waveforms Presented to the Input Stage of the Super Buffer and Produced by the Output Stage of the Super Buffer Using MOSFET Level Two Model.

**TABLE 3.1 SUMMARY OF RISE AND FALL
TIME DATA FOR THE SUPER BUFFER**

	$t_r(\text{seconds})$	$t_f(\text{seconds})$
voltage waveform at input to input stage	8×10^{-12}	10×10^{-12}
voltage waveform at output of input stage (same as at input to the output stage)	1.76×10^{-9}	1.259×10^{-9}
voltage waveform at output of output stage	1.877×10^{-9}	1.61×10^{-9}

than predicted. Finally, the average time delay through the entire super buffer is within 1% of the projected value of two nanoseconds. Note that in Table 3.2 the sum of the column entries do not sum exactly to the values in the third row. This is because all the data in the table is taken directly from discrete data points that are used to draw the voltage waveforms in Figures 3.4, 3.5, and 3.6. Some linear interpolation is necessary in order to obtain the time at the 50% voltage levels. This accounts for the slight differences between the sums of the column entries and the third row entries.

Thus the correct timing is achieved and the validity of the equations in Chapter II is borne out by simulation with an independent model.

The low noise margin and high noise margin for both stages given a 5 volt supply voltage is calculated to be 2.6 volts and 1.7 volts, respectively [Weste & Eshraghian, 1985, pp. 507-508].

D. MASK LEVEL SUPER BUFFER IMPLEMENTATION

A mask level integrated circuit layout of the super buffer based on the dimensions calculated is shown in Figure 3.7. To reduce the possibility of latch-up,

**TABLE 3.2 SUMMARY OF DELAY TIME
DATA FOR THE SUPER BUFFER**

	$t_{dr}(\text{seconds})$	$t_{df}(\text{seconds})$	$t_{d\text{avg}} = \frac{t_{dr} + t_{df}}{2}$
delay through input stage	0.72×10^{-9}	0.773×10^{-9}	0.746×10^{-9}
delay through output stage	1.093×10^{-9}	1.45×10^{-9}	1.272×10^{-9}
delay through input and output stages in cascade	1.866×10^{-9}	2.17×10^{-9}	2.018×10^{-9}

substrate contacts are employed in the n^+ and p^+ source diffusion regions. To minimize the chip area of the super buffer requires that the transistors be laid out in serpentine patterns. As a final check of the circuit's functionality, the mask level design is simulated with the ESIM gate level simulator. The simulation indicates that the mask layout is logically correct.

To use the super buffer layout in the automated generation of custom microchips with the Monterey Silicon Compiler, the Caltech Intermediate Form (CIF) representation of the circuit is translated into an L5 form representation using a CIF to L5 conversion program created by E. Malagon [Malagon, 1987, p. 110]. CIF and L5 are two different languages used to represent the geometric shapes that comprise a mask level layout. L5 stands for Lincoln Laboratory Lisp-based Layout Language. The language was created at the Massachusetts Institute of Technology Lincoln Laboratory under the sponsorship of the US Defense Advanced Research Projects Agency. The Monterey Silicon Compiler requires that the mask level integrated circuit layout be represented in L5 form before installing the layout representation into the compiler code. After the design is translated from CIF to

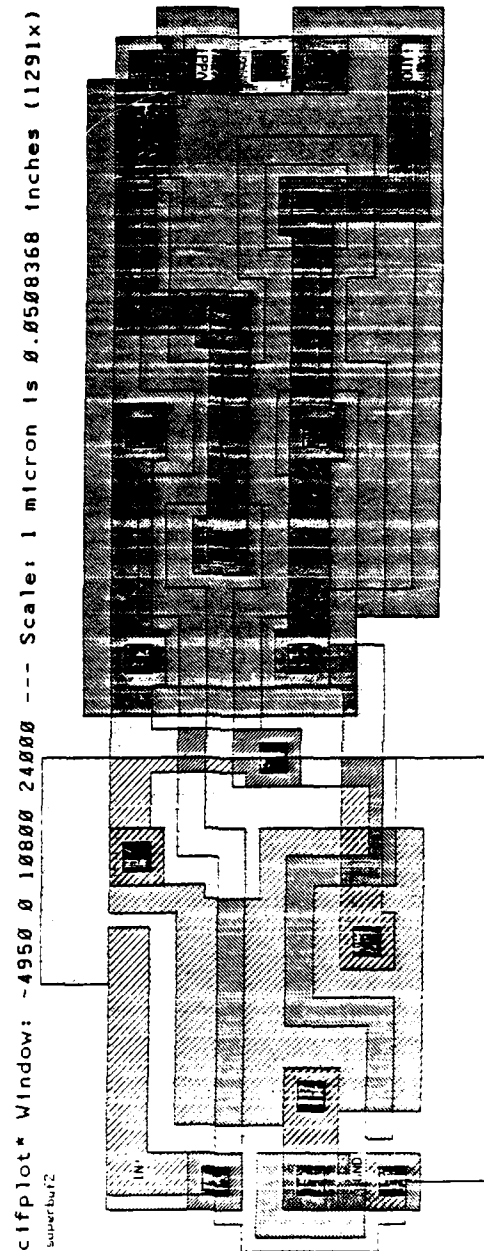


Figure 3.7 Mask Level Integrated Circuit Layout of Static CMOS Super Buffer.

L5 it is inserted into the compiler code within the program data-path.1 using a procedure proposed by Baumstarck [Baumstarck, 1987, pp. 70-81]. Some additional wiring is added in L5 code to ensure that the super buffer cell is correctly placed on the floorplan each time it is called by the compiler and to ensure that signals are properly routed to and from the super buffer.

An example of a portion of a microchip designed using the replacement static CMOS super buffer is presented in Figure 3.8. In the figure the horizontal rails at the center of the figure are the supply voltage, ground, and clock distribution rails. The outputs at the top of the two super buffers that make up the super buffer pair that straddles the rails are wired to PHI1! and PHI2! of the register directly above it in the data path.

Figure 3.9 shows an entire 4 bit shifter microchip designed with the Monterey Silicon Compiler using the static CMOS super buffer and CMOS register. This chip is in fact a hybrid chip in that both NMOS and CMOS technologies are incorporated in the chip. The input and output pads around the outer ring of the circuit are NMOS. A collection of CMOS pads for the Monterey Silicon Compiler has been obtained but has not yet been translated into L5 and inserted into the compiler code. The CMOS input pad of this collection is the one that has been referred to in this chapter. It is presented in Figure 3.10.

E. PERFORMANCE OF THE SUPER BUFFER IN MULTI-BIT DATA PATH CIRCUITS

Section C documents the performance of the super buffer under the worst-case scenario given the loading caused by a four bit data path. In section B it is stated that improving the operating conditions or the fabrication conditions of the super buffer or both results in enhanced performance. Using equation (2.56) the performance of the super buffer can be predicted under different loading conditions.

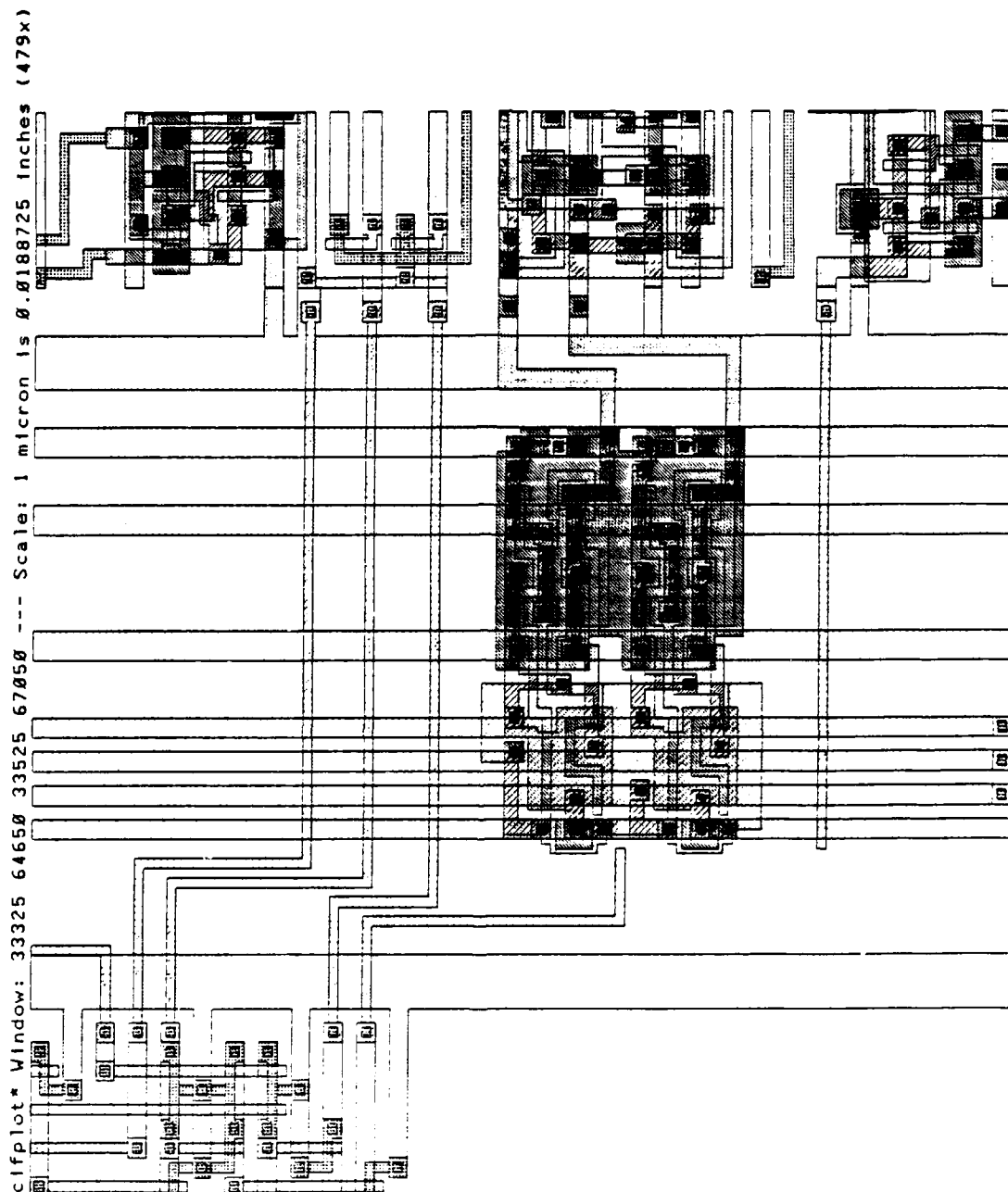


Figure 3.8 Example of a Portion of a Microchip Designed with the Monterey Silicon Compiler Showing Placement of the Static CMOS Super Buffer Below a CMOS Register.

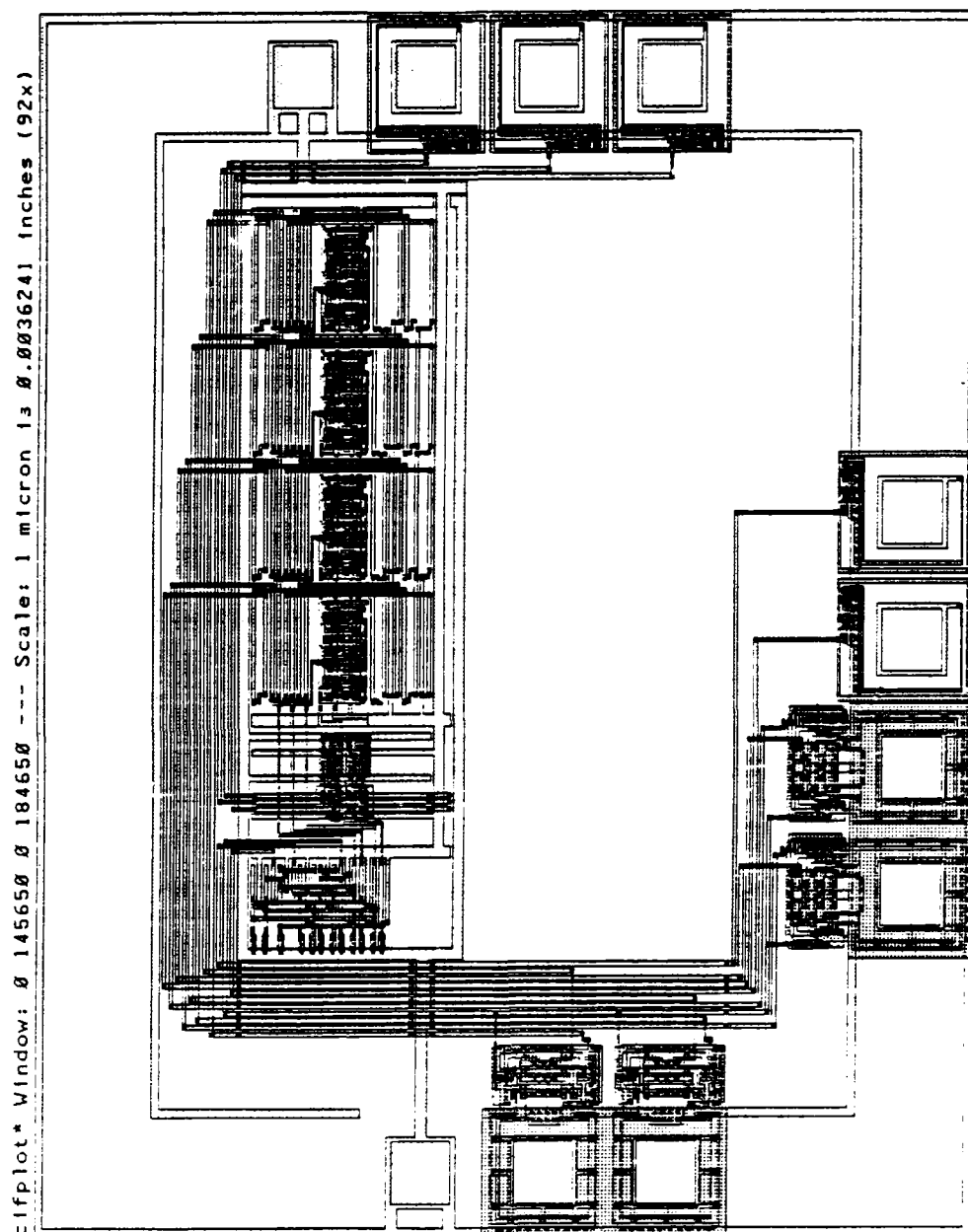


Figure 3.9 Four Bit Shifter Hybrid Microchip Designed with the Monterey Silicon Compiler.

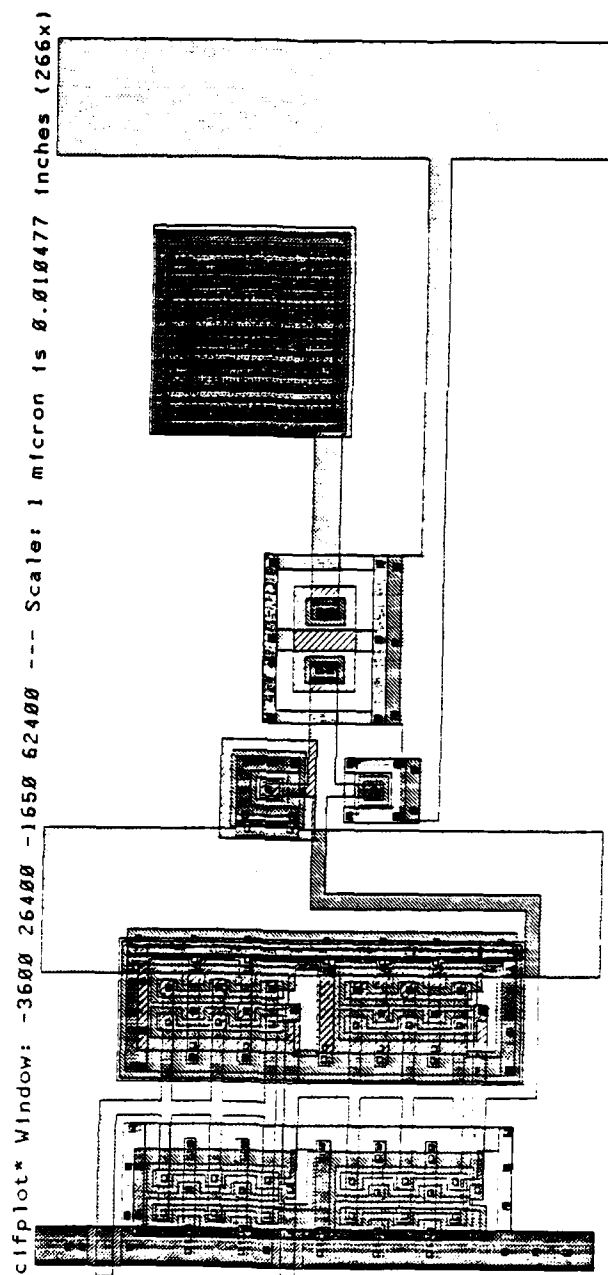


Figure 3.10 CMOS Input Pad Replacement for the Monterey Silicon Compiler.

Table 3.3 contains entries generated from equation (2.56) that predict the performance of the super buffer with the same operating temperature and fabrication process as under the worst-case scenario only the supply voltage has been raised from 4.5 volts to 6.0 volts. As can be seen in the table the effect of simply raising the supply voltage by 1.5 volts allows the super buffer to drive an eight bit data path to within 3% of the 2 nanosecond worst-case design goal.

**TABLE 3.3 SUMMARY OF RISE AND FALL TIME DATA FOR
THE SUPER BUFFER IN MULTI-BIT DATA PATH CIRCUITS
WITH VDD = 6 VOLTS**

	$t_r(=t_f)$ for 4 bits seconds	$t_r(=t_f)$ for 8 bits seconds	$t_r(=t_f)$ for 16 bits seconds	$t_r(=t_f)$ for 32 bits seconds
voltage waveform at input to input stage (ideal square wave)	0	0	0	0
voltage waveform at output of input stage (same as at input to the output stage)	1.652×10^{-9}	1.652×10^{-9}	1.652×10^{-9}	1.652×10^{-9}
voltage waveform at output of output stage	1.586×10^{-9}	2.054×10^{-9}	2.99×10^{-9}	4.862×10^{-9}

Table 3.4 contains the predicted delay time data for the super buffer under the same conditions as discussed above. The values are generated by equation (2.17) using the entries in Table 3.3. Here too, the super buffer is seen to be capable of

driving an eight bit data path in 2 nanoseconds instead of only four bits. This is due simply to the increase in the supply voltage. The table shows that even for a 32 bit data path the average delay time through the super buffer is still a very respectable 3.26 nanoseconds

**TABLE 3.4 SUMMARY OF DELAY TIME DATA FOR THE
SUPER BUFFER IN MULTI-BIT DATA PATH CIRCUITS
WITH VDD = 6 VOLTS**

	$t_{d_{avg}}$ for for 4 bits seconds	$t_{d_{avg}}$ for for 8 bits seconds	$t_{d_{avg}}$ for for 16 bits seconds	$t_{d_{avg}}$ for for 32 bits seconds
delay through input stage	0.826×10^{-9}	0.826×10^{-9}	0.826×10^{-9}	0.826×10^{-9}
delay through output stage	0.793×10^{-9}	1.027×10^{-9}	1.495×10^{-9}	2.431×10^{-9}
delay through input and output stages in cascade	1.619×10^{-9}	1.853×10^{-9}	2.321×10^{-9}	3.257×10^{-9}

Figure 3.11 shows an example of an eight bit microchip design for a taxi meter controller generated using the Monterey Silicon Compiler with the static CMOS super buffer in place [Massachusetts Institute of Technology 1982 Conference on Advanced Research in VLSI, 1982, p. 32]. Tables 3.3 and 3.4 demonstrate that by improving the supply voltage the drive of the super buffer doubles. Similar improvement in the drive of the super buffer can be realized through a fabrication process that is better than the worst-case process presumed in the design work

and through circuit operating temperatures that are lower than the worst-case temperature of 85° C. The amount of delay that is tolerable in the super buffer is largely application dependent.

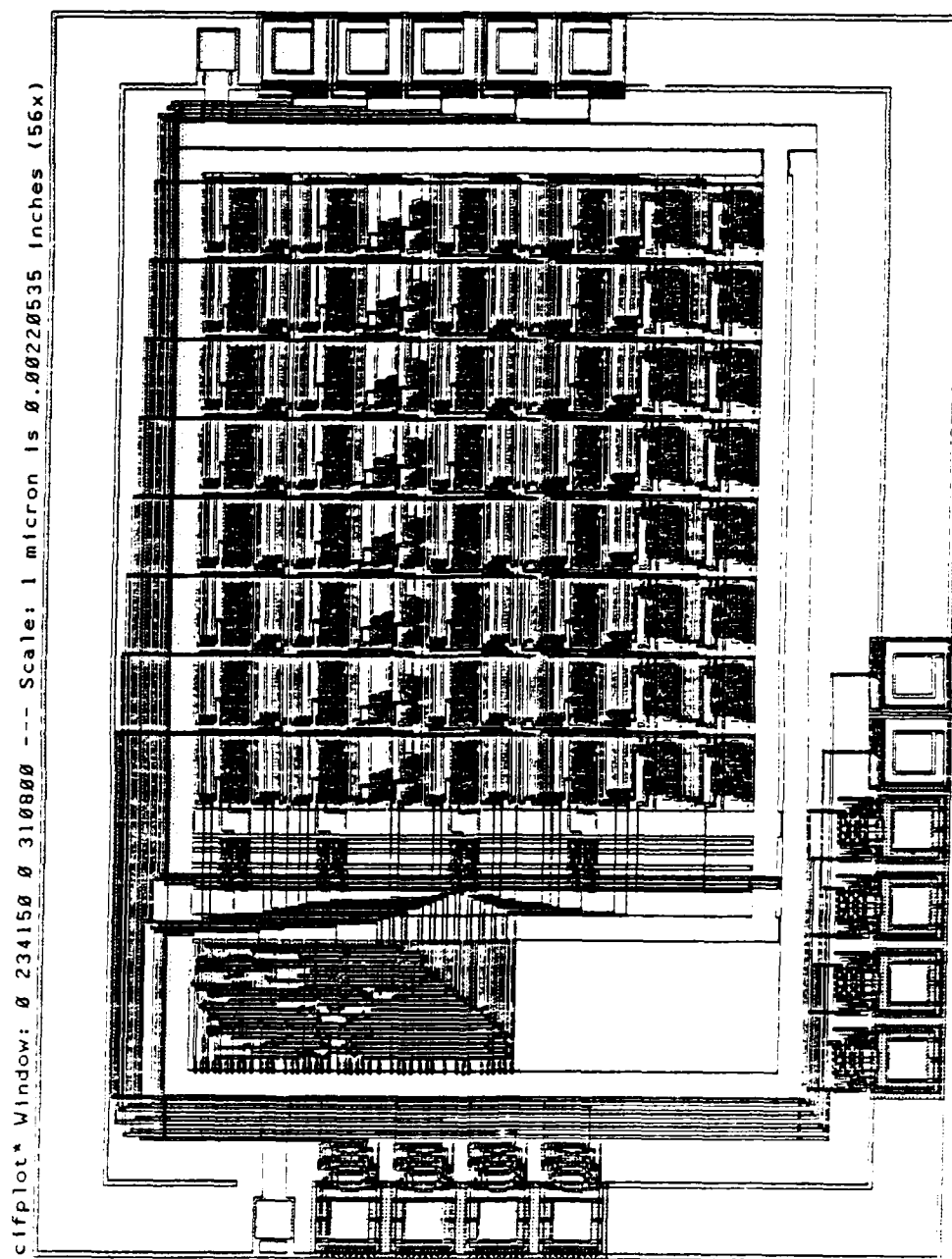


Figure 3.11 Eight Bit Taxi Meter Hybrid Microchip Designed with the Monterey Silicon Compiler.

IV. CONCLUSIONS

A. SUMMARY

This research set out to design a high-speed static CMOS super buffer for the Monterey Silicon Compiler. The problem of choosing its dimensions to achieve a desired timing result under worst-case conditions was approached analytically, and an algorithm was derived to solve the problem. The algorithm was implemented in a computer program which was used as a computer-aided-design (CAD) tool to design a hardware device. In SPICE simulations the resulting device surpassed the pre-specified timing performance standards under the worst-case scenario that it was designed to meet. Finally, a mask level integrated circuit design of this device was installed in the Monterey Silicon Compiler as a part of the technology upgrade of the MacPITTS Silicon Compiler, where it is now available for use in the automated design of custom hybrid CMOS/NMOS VLSI microchips.

The ability to use an algorithm to size transistors on a chip is an important step toward silicon compilation that results in optimal time delay circuits because computers can think in terms of algorithms, but not in terms of rules of thumb as many engineers do. Human engineers can design, simulate, and redesign until they get timing right. A silicon compiler that tries to achieve desired timing parameters for delay, rise, and fall time has to be taught how to think about the problem. That is perhaps the most exciting application of this type of approach—compilers that design chips to meet specified timing performance standards. For future research, the Monterey Silicon Compiler code that was modified to include the static CMOS super buffer can be found in the files /a/work/steele/macpitts/data-path.l

AD-A196 526

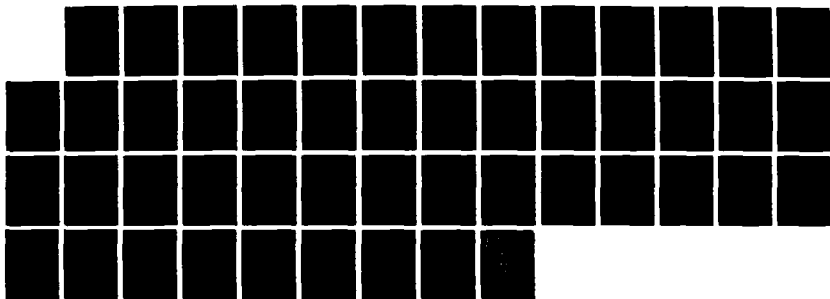
TRANSISTOR SIZING IN THE DESIGN OF HIGH-SPEED CMOS
(COMPLEMENTARY-SYMMETR. (U) NAVAL POSTGRADUATE SCHOOL
MONTEREY CA G R STEELE MAR 88

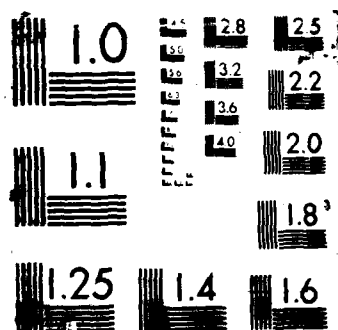
2/2

UNCLASSIFIED

F/G 28/12

NL





and /a/work/steele/macpitts/data-path.o on the Integrated Solutions CAD workstations of the Electrical and Computer Engineering Department Computer Laboratories at the Naval Postgraduate School. The NMOS logic cells in the Monterey Silicon Compiler that still require CMOS replacements are listed in Table 4.1. This table was extracted from a similar list compiled by E. Malagon [Malagon, 1985, p.95].

TABLE 4.1 MONTEREY SILICON COMPILER NMOS LOGIC CELLS REQUIRING CMOS REPLACEMENTS

ORGANELLE	LIBRARY FUNCTIONS
layout - = organelle	=
layout - equ - organelle	word - equ
layout - <> organelle	<>
layout - <> 0 organelle	<> 0
layout - = 0 organelle	= 0
lsh - zero/ lsh2/ lsh3/ lsh4/ lsh8	«
rsh - zero/ rsh2/ rsh3/ rsh4/ rsh8	»
layout - odd - operand	
layout - even - operand	
port - output 1	
bit	
layout - inverting - super - buffer	
15 contacts: pc, ndc, pdc, nsc, psc	
entire controller section	

B. RECOMMENDATIONS

An algorithm for transistor sizing in static CMOS logic design has been derived and a logic device whose dimensions were determined by the algorithm has performed successfully in SPICE simulations. It is recommended that future research in this area investigate the possibility of incorporating the following topics in the algorithm: the effects of a non-ideal input square wave, empirical adjustment of the basic drain current equations, the effects of channel length modulation and

of the body effect phenomenon, accuracy in computation and in fabrication, and stage ratios.

1. Effects of a Non-Ideal Input Square Wave

The derivation of the equations for transistor sizing in a static CMOS inverter in Chapter II assumes that the input voltage waveform is a perfect square wave—one that rises and falls instantaneously. This type of waveform causes one of the MOSFETs in the inverter to be in cutoff during switching thereby permitting the circuit simplifications represented in Figures 2.9b and 2.10b. A more realistic input voltage waveform is depicted in Figure 3.5. Applying the definitions of the three regions of operation of MOSFETs presented in Table 2.1 to the input and output voltage waveforms of Figure 3.5 shows that with a non-ideal square wave applied at the input of an inverter, both transistors of the inverter will momentarily conduct during switching—one sourcing current, the other sinking current. This obviously affects circuit timing because the rate at which charge is delivered to or taken away from the load is decreased. There are two possible solutions to this in the derivation of the equations, one difficult, the other easy. The more difficult approach is to rederive the equations of Chapter II based on a time varying input voltage waveform. The easier approach is conduct a study to find an empirical adjustment factor that would modify the value presented to the algorithm as being the desired rise time to compensate for the effects of a less than ideal input square wave.

2. Empirical Adjustment of Drain Current Equations

All of the drain current equations in Table 2.1 can be multiplied by a factor determined empirically to make the drain current equations more perfectly reflect physical device behavior as suggested by Hodges and Jackson [Hodges and Jackson, 1983, pp. 51–52]. For n channel MOSFETs the factor is $(1 + \text{LAMBDA}_n \cdot V_{ds_n})$.

For p channel MOSFETs the factor is $(1 + \text{LAMBDA}_p \cdot |V_{ds_p}|)$. Using these factors makes it necessary to rederive the transistor sizing equations of Chapter II based on these new drain current equations.

3. Channel Length Modulation

It is known that devices with channel length shorter than 10 microns saturate before the channel pinches off because the electrons (holes) reach the scattering limited velocity in the channel [Electronics Research Laboratory, 1980, p.6]. Once in the saturation region, the channel becomes shorter than L_{eff} . To compensate, the saturation region drain current equations in Table 2.1 can be divided by a channel length modulation factor. For n channel saturated MOSFETs the factor is $(1 - \text{LAMBDA}_n \cdot V_{ds_n})$ [Electronics Research Laboratory, 1980, p. 15]. For p channel saturated MOSFETs the factor is $(1 - \text{LAMBDA}_p \cdot |V_{ds_p}|)$. Making the modifications necessitates rederiving the transistor sizing equations of Chapter II based on the modified drain current equations.

4. Body Effect

In the extension of the equations derived for transistor sizing in a static CMOS inverter to general static CMOS logic design body-effect is neglected. This could perhaps be compensated for by introducing average values for V_{bs_n} and V_{bs_p} in the same manner as was used to calculate values of $C_{bdj_{avg}}\{T\}$ and $C_{bds_{avg}}\{T\}$ in equations (2.26) and (2.27).

5. Accuracy in Computation and in Fabrication

It is important to remember the first axiom of computing in using the transistor sizing algorithm presented in this thesis: "garbage in, garbage out." If for example the SPICE fabrication parameters given to the algorithm are not measured accurately, the algorithm cannot hope to produce a circuit that will behave as desired. The same is true if, for example, during fabrication the pattern

definitions created by the lithography process are inaccurate or the diffusion process is poorly controlled.

6. Stage Ratio

For consistency of approach, the input stage dimensions of the super buffer were designed using the same algorithm used to calculate the output stage dimensions. This resulted in the output stage being 1.266 times larger than the input stage. This value is known as the stage ratio which is the value by which successive transistor widths are multiplied when inverters are cascaded. Mead and Conway have written that the value of the stage ratio that minimizes overall delay for a series of cascaded inverters is given by Euler's number, $e = 2.718 \dots$ [Mead and Conway, 1908, pp. 12-14]. Thus, it may be possible to achieve slightly reduced area for the super buffer by using the algorithm to design the output stage, then using the stage ratio 2.718 to fix the dimensions of the input stage. However, Mead and Conway as well as Weste and Eshraghian have all acknowledged that other design criterion may steer a designer away from a value of 2.718 for the stage ratio [Mead and Conway, 1980, p. 14 and Weste and Eshraghian, 1895, p. 197]. Since the relative time penalty for using the stage ratio of 1.266 is slight, and since using this ratio allows a better assessment of the performance of the algorithm, the value of 1.266 was retained and the resulting circuit met its performance goals.

7. Suggested Modifications to the Monterey Silicon Compiler

In a design generated by the Monterey Silicon Compiler the area reserved for the super buffer on the floorplan is fixed. Were this area variable the compiler could be given several super buffers to choose from and it would select the one that best meets the drive requirements of the data path. This would involve modifying the body of code that defines the metal skeleton that distributes power, ground, and clock signals on chip.

The data registers currently in use are very tall and thin. Since the wires that connect the super buffer to the registers traverse the longest distance across the registers the routing capacitance has become unreasonably large. The solution is to return to the general configuration used by the original NMOS data registers. These registers were short but wide, greatly decreasing the length of the wires that connect the super buffers to the data register and thus the routing capacitance.

APPENDIX A:

STATIC CMOS INVERTER TRANSISTOR SIZING PROGRAMS

This appendix contains programs that implement the transistor sizing equations of Chapter II for a static CMOS inverter. The programs run on an HP41CX with a magnetic card reader and two extended memory modules. Main memory must be apportioned so that $SIZE \geq 076$.

Executing the programs in certain sequences occasionally results in the message "NO ROOM" and a halt to program execution. If this occurs, the following corrective actions should be taken (in the order listed):

- (1) Clear the current program from main memory.
- (2) Place the name of the program that could not be loaded in the ALPHA register.
- (3) Execute GETP.
- (4) Execute R/S.

Program execution should continue normally with data storage registers and user flags unaffected by the temporary halt in program execution.

The interrelationships of the programs are depicted in Figure A.1. To run the programs, main memory must first be entirely cleared and all programs must be placed in extended memory. The name "VLSI" is placed in the ALPHA register, GETP is executed followed by R/S. The program VLSI is responsible for loading the SPICE fabrication parameters. These parameters must be stored on magnetic data storage cards in accordance with the data register allocation given in Table A.1. The cards are loaded when they are requested by the program. The program VLSI automatically clears itself from main memory, loads the program

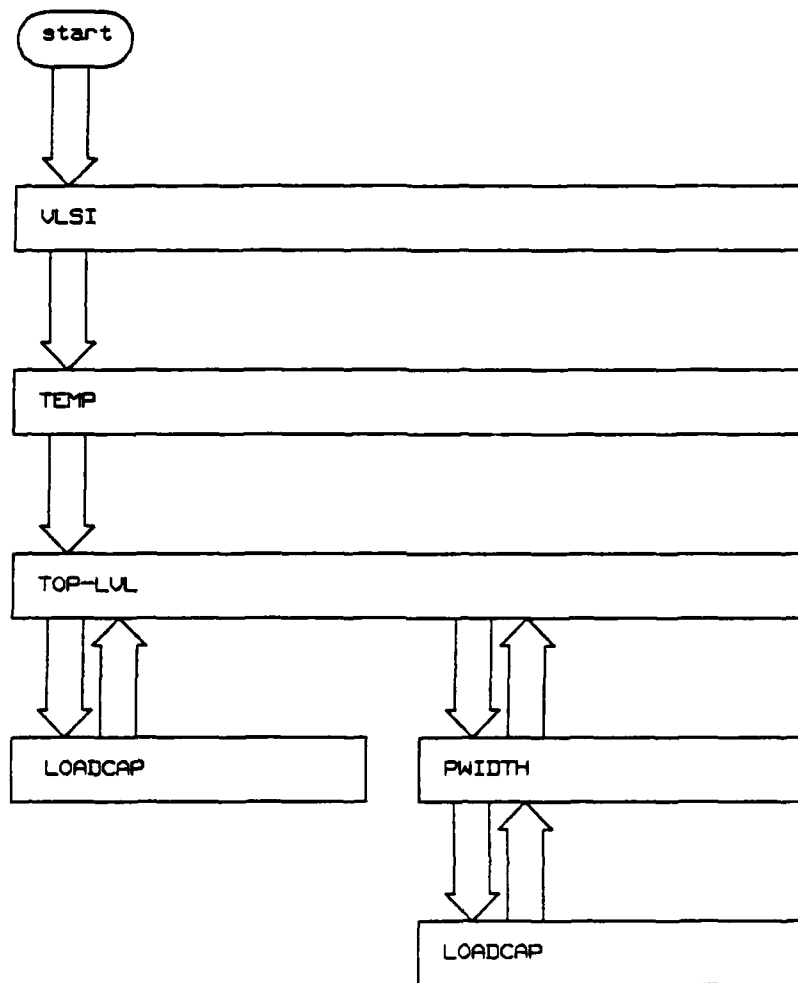


Figure A.1 Interrelationships of Transistor Sizing Programs

TEMP from extended memory, and continues execution with the first line of code in the program TEMP. The program TEMP calculates the effects of temperature on the fabrication parameters in Table A.1, overwriting the data registers of the temperature dependent parameters with their temperature altered values. Program TEMP then clears itself from main memory, loads the program TOP-LVL from extended memory, and continues execution with the first line of code in the program TOP-LVL. The program TOP-LVL acts as a memory manager, shifting the programs PWIDTH and LOADCAP in and out of main memory as required by the user. The program PWIDTH calculates all the SPICE MOSFET model dimensions and drain resistances required for the p MOSFET and the n MOSFET in a static CMOS inverter required to drive a given load capacitance. If the load capacitance is not known but the dimensions of the load MOSFETs are known, the load capacitance can be calculated using the program LOADCAP. Table A.2 details the remaining data register allocation. The source code for the programs VLSI, TEMP, TOP-LVL, PWIDTH, and LOADCAP follows Tables A.1 and A.2.

**TABLE A.1 SPICE FABRICATION PARAMETER
DATA REGISTER ALLOCATION**

SPICE PARAMETER	DATA REGISTER FOR n DEVICES	DATA REGISTER FOR p DEVICES
KP	R ₀₀	R ₁₇
VTO	R ₀₁	R ₁₈
LD	R ₀₂	R ₁₉
CJ	R ₀₃	R ₂₀
CJSW	R ₀₄	R ₂₁
FC	R ₀₅	R ₂₂
MJ	R ₀₆	R ₂₃
PB	R ₀₇	R ₂₄
MJSW	R ₀₈	R ₂₅
PHI	R ₀₉	R ₂₆
GAMMA	R ₁₀	R ₂₇
*Cmd	R ₁₁	R ₂₈
* $\epsilon_{rel,oxide}$	R ₁₂	R ₂₉
CGSO	R ₁₃	R ₃₀
CGDO	R ₁₄	R ₃₁
TOX	R ₁₅	R ₃₂
UO	R ₁₆	R ₃₃
RSH	R ₇₃	R ₇₄

* Not SPICE parameters

**TABLE A.2 DATA REGISTER ALLOCATION FOR VARIABLES
OTHER THAN SPICE FABRICATION PARAMETERS**

VARIABLE	DATA REGISTER FOR n DEVICES	DATA REGISTER FOR p DEVICES
T [Kelvin]	R ₃₄	R ₃₄
EG {T}	R ₃₅	R ₃₅
EG {T _{nom} }	R ₃₆	R ₃₆
Temporary Vto {T}	R ₃₇ , R ₃₈ , R ₃₉ , R ₄₀	R ₄₁ , R ₄₂ , R ₄₃ , R ₇₅
A	R ₃₄	R ₃₅ (abs. value)
Vdd	R ₃₆	R ₃₆
Channel Mask Length	R ₃₈	R ₃₈
Cbdj _{avg} {T}	R ₆₆	R ₄₂
Cbds _{avg} {t}	R ₄₄	R ₄₅
B	R ₄₆	R ₄₇
t _r	R ₄₈	R ₄₈
E(= C _r)	R ₄₉	R ₄₉
Drain Mask Length	R ₅₀	R ₅₀
No. Drain Diffusion Contacts	R ₅₂	R ₅₁
Diffusion Contact Mask Length	R ₅₆	R ₅₃
Diffusion Contact Mask Width	R ₅₇	R ₅₄
C	R ₅₈	R ₅₅
D	R ₅₉	R ₅₉
F	R ₆₀	R ₆₀
G	R ₆₁	R ₆₁
H	R ₆₂	R ₆₂
W	R ₆₃	R ₆₃
AD = AS	R ₆₅	R ₆₄
PD = PS	R ₇₀	R ₆₇
RD = RS	R ₇₁	R ₆₈
	R ₇₂	R ₆₉

PROGRAM VLSI

01 LBL ^T VLSI
02 ^T STOP. PURGE MAI
03 ^T ⁺ N MEMORY
04 PROMPT
05 000.074
06 ^T ENTER FAB. PARA
07 ^T ⁺ M. CARD
08 CF 09
09 CF 10
10 AVIEW
11 RDTAX
12 ^T TEMP
13 GETP
14 END

PROGRAM TEMP

```
01      LBL  $T$ TEMP
02       $T$ OPERATING TEMP (
03       $T$ KELVIN } = ?
04      PROMPT
05      STO 34
*** CALCULATE EG ( T ) ***
06      STO 37
07      XEQ  $T$ EQ( T )
08      RCL 37
09      STO 35
*** CALCULATE EG ( Tnom ) ***
10      300.15
11      STO 37
12      XEQ  $T$ EG ( T )
13      RCL 37
14      STO 36
*** CALCULATE PBn ( T ) ***
15      RCL 07
16      STO 40
17      STO 37
18      XEQ  $T$ PB ( T )
19      RCL 37
20      STO 07
*** CALCULATE PBp ( T ) ***
21      RCL 24
22      STO 41
23      STO 37
24      XEQ  $T$ PB ( T )
25      RCL 37
26      STO 24
*** CALCULATE PHIn ( T ) ***
27      RCL 09
28      STO 37
29      XEQ  $T$ PB ( T )
30      RCL 37
31      STO 09
*** CALCULATE PHIp ( T ) ***
32      RCL 26
33      STO 37
34      XEQ  $T$ PB ( T )
35      RCL 37
36      STO 26
*** CALCULATE CJn ( T ) ***
37      RCL 03
38      STO 37      ; CJn
39      RCL 06
40      STO 38      ; MJn
41      RCL 07
```

```

42      STO 39      ; PBn ( T )
43      RCL 40
44      STO 42      ; PBn
45      XEQTCJ ( T )
46      RCL 37
47      STO 03
*** CALCULATE CJp ( T ) ***
48      RCL 20
49      STO 37      ; CJp
50      RCL 23
51      STO 38      ; MJp
52      RCL 24
53      STO 39      ; PBp ( T )
54      RCL 41
55      STO 42      ; PBp
56      XEQTCJ ( T )
57      RCL 37
58      STO 20
*** CALCULATE CJSWn ( T ) ***
59      RCL 04
60      STO 37      ; CJSWn
61      RCL 08
62      STO 38      ; MJSWn
63      RCL 07
64      STO 39      ; PBn ( T )
65      RCL 40
66      STO 42      ; PBn
67      XEQTCJ ( T )
68      RCL 37
69      STO 04
*** CALCULATE CJSWp ( T ) ***
70      RCL 21
71      STO 37      ; CJSWp
72      RCL 25
73      STO 38      ; MJSWp
74      RCL 24
75      STO 39      ; PBp ( T )
76      RCL 41
77      STO 42      ; PBp
78      XEQTCJ ( T )
79      RCL 37
80      STO 21
*** CALCULATE KPn ( T ) ***
81      RCL 00
82      STO 37
83      XEQTKP ( T )
84      RCL 37
85      STO 00
*** CALCULATE KPp ( T ) ***
86      RCL 17

```

```

87      STO 37
88      XEQTKP ( T )
89      RCL 37
90      STO 17
*** CALCULATE UOn ( T ) ***
91      RCL 16
92      STO 37
93      XEQTKP ( T )
94      RCL 37
95      STO 16
*** CALCULATE UOp ( T ) ***
96      RCL 33
97      STO 37
98      XEQTKP ( T )
99      RCL 37
100     STO 33
*** CALCULATE  $\epsilon_{rel, oxide_n}$  ( T ) ***
101     RCL 00
102     STO 37      ; KPn ( T )
103     RCL 15
104     STO 38      ; TOXn
105     RCL 16
106     STO 39      ; UOn ( T )
107     XEQTEREL ( T )
108     RCL 37
109     STO 12
*** CALCULATE  $\epsilon_{rel, oxide_p}$  ( T ) ***
110     RCL 17
111     STO 37      ; KPp ( T )
112     RCL 32
113     STO 38      ; TOXp
114     RCL 33
115     STO 39      ; UOp ( T )
116     XEQTEREL ( T )
117     RCL 37
118     STO 29
119     TTOP-LVL
120     GETP
*** EG ( T ) SUBROUTINE ***
121     LBLTEG ( T )
122     RCL 37
123     X  $\nearrow$  2
124     .000702
125     *
126     RCL 37
127     1108
128     +
129     /
130     1.16
131     X ( ) Y

```



```

132      -
133      STO 37
134      RTN
135      *** PB ( T ), PHI ( T ) SUBROUTINE ***
136      LBLT PB ( T )
137      RCL 37
138      RCL 34
139      *
140      300.15
141      /
142      STO 38      ; Interim Result
143      3
144      ENTER ↗
145      8.6173468 E-05      ; K/q
146      *
147      RCL 34
148      *
149      RCL 34
150      300.15
151      /
152      LN
153      *
154      RCL 38
155      X ( ) y
156      -
157      RCL 35
158      -
159      RCL 36
160      RCL 34
161      *
162      300.15
163      /
164      +
165      STO 37
166      RTN
167      *** CJ ( T ), CJSW ( T ) SUBROUTINE ***
168      LBLT CJ ( T )
169      RCL 39
170      RCL 42
171      /
172      1
173      X ( ) Y
174      -
175      RCL 34
176      300.15
177      -
178      .0004
179      *
180      +
181      RCL 38

```

```

180      *
181      1
182      +
183      RCL 37
184      *
185      STO 37
186      RTN
187      *** KP ( T ), UO( T ) SUBROUTINE ***
188      LBL↑KP ( T )
189      RCL 34
190      300.15
191      /
192      -1.5
193      Y / X
194      RCL 37
195      *
196      STO 37
197      RTN
198      ***  $\epsilon_{rel, oxide}$  ( T ) SUBROUTINE ***
199      LBL↑EREL ( T )
200      RCL 37
201      100
202      *
203      RCL 38
204      *
205      RCL 39
206      /
207      8.854187818 E-14
208      /
209      STO 37
210      RTN
211      END

```

PROGRAM TOP-LVL

```

01      LBLT TOP-LVL
02      FS? 09
03      GTO 30
04      CF 02
05      CF 03
06      ENG 3
*** CALCULATE  $V_{to_n}$  ( T ) ***
07      RCL 01
08      STO 37      ;  $V_{TO_n}$ 
09      RCL 10
10      STO 39      ;  $\text{GAMMA}_n$ 
11      RCL 09
12      STO 40      ;  $\text{PHI}_n$  ( T )
13      TVBS ( N ), VOLTS = ?
14      PROMPT
15      ABS
16      STO 41      ; |  $V_{bs_n}$  |
17      XEQT VTO ( T )
18      RCL 37
19      STO 34
*** CALCULATE  $V_{to_p}$  ( T ) ***
20      RCL 18
21      ABS
22      STO 37      ; |  $V_{TO_p}$  |
23      RCL 27
24      STO 39      ;  $\text{GAMMA}_p$ 
25      RCL 26
26      STO 40      ;  $\text{PHI}_p$  ( T )
27      TVBS ( P ), VOLTS = ?
28      PROMPT
29      STO 41      ;  $V_{bs_p}$ 
30      XEQT VTO ( T )
31      RCL 37
32      STO 35
*** INPUT  $V_{dd}$  ***
33      TSUPPLY VOLTAGE (
34      TVOLTS ) = ?
35      PROMPT
36      STO 38
*** CALCULATE RATIO "A"; ***
***  $W_n = W_p \cdot A$  for  $t_r \simeq t_f$  ***
37      19
38      RCL 38
39      *
40      20
41      RCL 34
42      *

```

43	-	
44	RCL 38	
45	/	
46	LN	
47	2	
48	/	
49	STO 39	; Interim Result
50	RCL 34	
51	.1	
52	RCL 38	
53	*	
54	-	
55	RCL 38	
56	RCL 34	
57	-	
58	/	
59	RCL 39	
60	+	
61	RCL 38	
62	RCL 35	
63	-	
64	*	
65	RCL 17	
66	*	
67	STO 39	; Interim Result
68	19	
69	RCL 38	
70	*	
71	20	
72	RCL 35	
73	*	
74	-	
75	RCL 38	
76	/	
77	LN	
78	2	
79	/	
80	STO 40	; Interim Result
81	RCL 35	
82	.1	
83	RCL 38	
84	*	
85	-	
86	RCL 38	
87	RCL 35	
88	-	
89	/	
90	RCL 40	
91	+	
92	RCL 38	
93	RCL 34	

```

94      -
95      *
96      RCL 00
97      *
98      STO 40      ; Interim Result
99       $\uparrow$ P CHNL MASK LNG
100      $\uparrow$ TH ( MTR ) = ?
101     PROMPT
102     STO 42
103      $\uparrow$ N CHNL MASK LNG
104      $\uparrow$ TH ( MTR ) = ?
105     PROMPT
106     STO 66
107     2
108     RCL 02
109     *
110     -
111     RCL 39
112     *
113     STO 39      ; Interim Result
114     RCL 42
115     2
116     RCL 19
117     *
118     -
119     RCL 40
120     *
121     1/X
122     RCL 39
123     *
124     STO 36
*** MENU ***
125     LBL 01
126     SF 27
127      $\uparrow$ WI ----- LD
128     PROMPT
*** CALL TO PWIDTH ***
129     LBL A
130     CF 27
131      $\uparrow$ PWIDTH
132     GETP
133     GTO 01
*** CALL TO LOADCAP ***
134     LBL E
135     CF 03
136     CF 27
137     SF 09
138      $\uparrow$ LOADCAP
139     GETSUB
140     XEQ  $\uparrow$ LOADCAP
141     LBL 30

```

```

142      CF 09
143      ↑LOADCAP
144      PCLPS
145      CF 02
146      GTO 01
*** VTO ( T ) SUBROUTINE ***
147      LBL↑VTO ( T )
148      RCL 40
149      RCL 41
150      +
151      SQRT
152      RCL 40
153      SQRT
154      -
155      RCL 39
156      *
157      RCL 37
158      +
159      STO 37
160      RTN
161      END

```

PROGRAM PWIDTH

```
01      LBLTPWIDTH
02      FS? 10
03      GTO 40
04      CF 02
*** CALCULATE Cbdjavg, n ( T ) ***
05      RCL 05
06      STO 39      ; FCn
07      RCL 06
08      STO 40      ; MJn
09      RCL 38      ; Vdd
10      .9
11      *
12      STO 41
13      RCL 07
14      STO 75      ; PBn ( T )
15      XEQTCBDJ
16      RCL 37
17      STO 43
18      RCL 38
19      .1
20      *
21      STO 41
22      XEQTCBDJ
23      RCL 37
24      RCL 43
25      +
26      2
27      /
28      STO 44
*** CALCULATE Cbdjavg, p ( T ) ***
29      RCL 22
30      STO 39      ; FCp
31      RCL 23
32      STO 40      ; MJp
33      RCL 38      ; Vdd
34      .9
35      *
36      STO 41
37      RCL 24
38      STO 75      ; PBp ( T )
39      XEQTCBDJ
40      RCL 37
41      STO 43
42      RCL 38
43      .1
44      *
45      STO 41
46      XEQTCBDJ
```

```

47      RCL 37
48      RCL 43
49      +
50      2
51      /
52      STO 45
*** CALCULATE Cbdsavg, n ( T ) ***
53      RCL 05
54      STO 39      ; FCn
55      RCL 08
56      STO 40      ; MJSWn
57      RCL 38      ; Vdd
58      .9
59      *
60      STO 41
61      RCL 07
62      STO 75      ; PBn ( T )
63      XEQTCBDJ
64      RCL 37
65      STO 43
66      RCL 38
67      .1
68      *
69      STO 41
70      XEQTCBDJ
71      RCL 37
72      RCL 43
73      +
74      2
75      /
76      STO 46
*** CALCULATE Cbdsavg, p ( T ) ***
77      RCL 22
78      STO 39      ; FCp
79      RCL 25
80      STO 40      ; MJSWp
81      RCL 38      ; Vdd
82      .9
83      *
84      STO 41
85      RCL 24
86      STO 75      ; PBp ( T )
87      XEQTCBDJ
88      RCL 37
89      STO 43
90      RCL 38
91      .1
92      *
93      STO 41
94      XEQTCBDJ

```



```

95      RCL 37
96      RCL 43
97      +
98      2
99      /
100     STO 47
*** CALCULATE C  $\sum_{\text{load devices}}$  gate ***

101     LBL 00
102      $\uparrow$ DO YOU KNOW CΣ L
103      $\uparrow$ LOAD DEV ?
104     AVIEW
105     PSE
106     SF 27
107      $\uparrow$ YES ----- NO
108     PROMPT
109     LBL E
110     CF 27
111     SF 10
112      $\uparrow$ LOADCAP
113     GETSUB
114     SF 03
115     XEQ  $\uparrow$ LOADCAP
116     LBL 40
117     CF 10
118      $\uparrow$ LOADCAP
119     PCLPS
120     GTO 00
121     LBL A
122     CF 27
123     FC? 02
124     GTO 03
125     LBL 04
*** ENTER MASK GEOMETRY DATA ***
126      $\uparrow$ DESIRED RISE TI
127      $\uparrow$ ME ( SEC ) = ?
128     PROMPT
129     STO 49
130      $\uparrow$ ROUTING CAP ( FAR
131      $\uparrow$ AD ) = ?
132     PROMPT
133     STO 50
134      $\uparrow$ P DRAIN MASK LN
135      $\uparrow$ GTH ( MTR ) ?
136     PROMPT
137     STO 51
138      $\uparrow$ N DRAIN MASK LN
139      $\uparrow$ GTH ( MTR ) ?
140     PROMPT
141     STO 52

```

```

142      TNO. P DIFFUSION
143      TH_CONTACTS
144      PROMPT
145      STO 53
146      TPDIFCTC MASK LN
147      THGTH ( MTR ) ?
148      PROMPT
149      STO 54
150      TPDIFCTC MASK WI
151      THDTH ( MTR ) ?
152      PROMPT
153      STO 55
154      NO. N DIFFUSION
155      TH_CONTACTS
156      PROMPT
157      STO 56
158      TNDIFCTC MASK LN
159      THGTH ( MTR ) ?
160      PROMPT
161      STO 57
162      TNDIFCTC MASK WI
163      THDTH ( MTR )
164      PROMPT
165      STO 58
*** CALCULATE "C" ***
166      RCL 51
167      RCL 19
168      2
169      *
170      +
171      RCL 20
172      *
173      RCL 45
174      *
175      RCL 21
176      2
177      *
178      RCL 47
179      *
180      +
181      RCL 52
182      RCL 02
183      2
184      *
185      +
186      RCL 36
187      *
188      RCL 03
189      *
190      RCL 44
191      *

```

192	+
193	RCL 36
194	2
195	*
196	RCL 04
197	*
198	RCL 46
199	*
200	+
201	STO 59
* * * CALCULATE "D" * * *	
202	RCL 51
203	RCL 19
204	2
205	*
206	+
207	RCL 20
208	*
209	RCL 45
210	*
211	RCL 21
212	2
213	*
214	RCL 47
215	*
216	+
217	RCL 19
218	*
219	2
220	*
221	STO 60
222	RCL 52
223	RCL 02
224	2
225	*
226	+
227	RCL 03
228	*
229	RCL 44
230	*
231	RCL 04
232	2
233	*
234	RCL 46
235	*
236	+
237	RCL 02
238	*
239	2
240	*
241	ST+ 60

242	RCL 51
243	RCL 19
244	2
245	*
246	+
247	RCL 53
248	RCL 54
249	*
250	+
251	2
252	*
253	RCL 21
254	*
255	RCL 47
256	*
257	ST+ 60
258	RCL 52
259	RCL 02
260	2
261	*
262	+
263	RCL 56
264	RCL 57
265	*
266	+
267	2
268	*
269	RCL 04
270	*
271	RCL 46
272	*
273	ST+ 60
274	RCL 55
275	RCL 19
276	2
277	*
278	+
279	RCL 20
280	*
281	RCL 45
282	*
283	RCL 55
284	RCL 23
285	*
286	+
287	RCL 54
288	*
289	RCL 53
290	*
291	ST+ 60
292	RCL 58

```

293      RCL 02
294      2
295      *
296      +
297      RCL 03
298      *
299      RCL 44
300      *
301      RCL 58
302      RCL 11
303      *
304      +
305      RCL 57
306      *
307      RCL 56
308      *
309      ST+ 60
*** CALCULATE "F" ***
310      RCL 42
311      2
312      RCL 19
313      *
314      -
315      2
316      *
317      RCL 49
318      /
319      RCL 17
320      /
321      RCL 38
322      RCL 35
323      -
324      /
325      STO 61
*** CALCULATE "G" ***
326      RCL 35
327      RCL 38
328      .1
329      *
330      -
331      RCL 38
332      RCL 35
333      -
334      /
335      STO 62
*** CALCULATE "H" ***
336      RCL 38
337      19
338      *
339      RCL 35
340      20

```

```

341      *
342      -
343      RCL 38
344      /
345      LN
346      2
347      /
348      STO 63
*** CALCULATE  $W_p$  AND  $W_n$  ***
349      RCL 62
350      RCL 63
351      +
352      RCL 59
353      *
354      RCL 61
355      *
356      1
357      X ( ) Y
358      -
359      1/X
360      RCL 61
361      *
362      RCL 62
363      RCL 63
364      +
365      *
366      RCL 48
367      RCL 60
368      +
369      RCL 50
370      +
371      *
372      STO 64
373      RCL 36
374      *
375      STO 65
*** CALCULATE OUTPUT ***
*** PARAMETERS, OUTPUT ***
*** RESULTS, & RETURN TO ***
*** TOP-LVL ***

*** CALCULATE  $AD_p = AS_p$  ***
376      RCL 64
377      RCL 19
378      2
379      *
380      +
381      RCL 51
382      RCL 19
383      2

```

```

384      *
385      +
386      *
387      RCL 55
388      RCL 19
389      2
390      *
391      +
392      RCL 53
393      *
394      RCL 54
395      *
396      +
397      STO 67
*** CALCULATE  $AD_n = AS_n$  ***
398      RCL 65
399      RCL 02
400      2
401      *
402      +
403      RCL 52
404      RCL 02
405      2
406      *
407      +
408      *
409      RCL 58
410      RCL 02
411      2
412      *
413      +
414      RCL 56
415      *
416      RCL 57
417      *
418      +
419      STO 70
*** CALCULATE  $PD_p = PS_p$  ***
420      RCL 51
421      RCL 19
422      2
423      *
424      +
425      RCL 53
426      RCL 54
427      *
428      +
429      2
430      *
431      RCL 64
432      RCL 19

```

```

433      2
434      *
435      +
436      2
437      *
438      +
439      STO 68
*** CALCULATE  $PD_n = PS_n$  ***
440      RCL 52
441      RCL 02
442      2
443      *
444      +
445      RCL 56
446      RCL 57
447      *
448      +
449      2
450      *
451      RCL 65
452      RCL 02
453      2
454      *
455      +
456      2
457      *
458      +
459      STO 71
*** CALCULATE  $RD_p = RS_p$  ***
460      RCL 55
461      RCL 19
462      2
463      *
464      +
465      1/X
466      RCL 54
467      *
468      RCL 53
469      /
470      STO 37
471      RCL 64
472      RCL 19
473      2
474      *
475      +
476      1/X
477      RCL 51
478      RCL 19
479      2
480      *
481      +

```



```

482      *
483      RCL 37
484      +
485      RCL 74
486      *
487      STO 69
*** CALCULATE  $RD_n = RS_n$  ***
488      RCL 58
489      RCL 02
490      2
491      *
492      +
493      1/X
494      RCL 57
495      *
496      RCL 56
497      /
498      STO 37
499      RCL 65
500      RCL 02
501      2
502      *
503      +
504      1/X
505      RCL 52
506      RCL 02
507      2
508      *
509      +
510      *
511      RCL 37
512      +
513      RCL 73
514      *
515      STO 72
*** OUTPUT SPICE MOSFET PARAMETERS ***
516       $T_L(P) =$ 
517      ARCL 42
518       $T_H(MTR)$ 
519      PROMPT
520       $T_W(P) =$ 
521      ARCL 64
522       $T_H(MTR)$ 
523      PROMPT
524       $T_{AD}(P) =$ 
525      ARCL 67
526       $T_H(SQ. MTR)$ 
527      PROMPT
528       $T_{PD}(P) =$ 
529      ARCL 68
530       $T_H(MTR)$ 

```

```

531      PROMPT
532       $\uparrow$ RD ( P ) =
533      ARCL 69
534       $\uparrow$ -( OHM )
535      PROMPT
536       $\uparrow$ L ( N ) =
537      ARCL 66
538       $\uparrow$ -( MTR )
539      PROMPT
540       $\uparrow$ W ( N ) =
541      ARCL 65
542       $\uparrow$ -( MTR )
543      PROMPT
544       $\uparrow$ AD ( N ) =
545      ARCL 70
546       $\uparrow$ -( SQ. MTR )
547      PROMPT
548       $\uparrow$ PD ( N ) =
549      ARCL 71
550       $\uparrow$ -( MTR )
551      PROMPT
552       $\uparrow$ RD ( N ) =
553      ARCL 72
554       $\uparrow$ -( OHM )
555      PROMPT
556       $\uparrow$ TOP-LVL
557      GETP
*** Cbdj ( T, Vbd ), Cbds ( T, Vbd ) SUBROUTINE ***
558      LBL  $\uparrow$ CBDJ
559      RCL 41
560      RCL 40
561      *
562      RCL 75
563      /
564      RCL 40
565      1
566      +
567      RCL 39
568      *
569      1
570      X ( ) Y
571      -
572      +
573      1
574      RCL 39
575      -
576      1
577      RCL 40
578      +
579      CHS
580      Y  $\nearrow$  X

```

```
581      *  
582      STO 37  
583      RTN  
584      LBL 03  
585      TC Σ LOAD DEV ( FARA  
586      T-D ) = ?  
587      PROMPT  
588      STO 48  
589      GTO 04  
590      END
```

PROGRAM LOADCAP

```
01      LBLTLOADCAP
02      SF 02
03      TLOADCAP
04      AVIEW
05      PSE
06      0
07      STO 37
08      LBL 05
09      TLD CHNL MASK LN
10      T←GTH ( MTR )
11      PROMPT
12      STO 39
13      TLD CHNL MASK WI
14      TDTH ( MTR )
15      PROMPT
16      STO 40
17      TDEVICE TYPE?
18      AVIEW
19      PSE
20      SF 27
21      TN-----P
22      PROMPT
    *** CALCULATE WITH N DATA ***
23      LBL A
24      CF 27
25      RCL 39
26      2
27      RCL 02
28      *
29      -
30      8.854187818 E-12
31      *
32      RCL 12
33      *
34      RCL 15
35      /
36      RCL 40
37      *
38      RCL 13
39      RCL 40
40      *
41      +
42      RCL 14
43      RCL 40
44      *
45      +
46      ST+ 37
47      TANOTHER DEVICE?
```

```

48      AVIEW
49      PSE
50      SF 27
51      T      Y      N
52      PROMPT
53      LBL B
54      CF 27
55      GTO 05
56      LBL D
57      CF 27
58      GTO 06
    *** CALCULATE WITH P DATA ***
59      LBL E
60      CF 27
61      RCL 39
62      2
63      RCL 19
64      *
65      -
66      8.854187818 E-12
67      *
68      RCL 29
69      *
70      RCL 32
71      /
72      RCL 40
73      *
74      RCL 30
75      RCL 40
76      *
77      +
78      RCL 31
79      RCL 40
80      *
81      +
82      ST + 37
83      T ANOTHER DEVICE?
84      AVIEW
85      PSE
86      SF 27
87      T      Y      N
88      PROMPT
89      LBL 06
90      RCL 37
91      STO 48
92      FC? 03
93      GTO 07
94      RTN
95      LBL 07
96      T C Σ LOAD DEV=
97      ARCL 48

```

```
98      TF( FARAD )  
99      PROMPT  
100     FS? 09  
101     XEQTTOP-LVL  
102     XEQTPWIDTH  
102     END
```

APPENDIX B

STATIC CMOS SUPER BUFFER PSPICE DECK

This appendix contains the actual PSpice deck used for the simulation of the super buffer designed in Chapter 3. The worst-case minimum current MOSIS SPICE fabrication parameters are included in the deck.

```
SUPER BUFFER
M1 3 2 1 1 M1 L=3.0Um W=106.1Um AD=507.3P PD=246.0Um
M2 3 2 0 0 M2 L=3.0Um W=41.01Um AD=191.4P PD=102.6Um
M3 4 3 1 1 M3 L=3.0Um W=134.3Um AD=660.9P PD=314.4Um
M4 4 3 0 0 M4 L=3.0Um W=51.93Um AD=231.2P PD=124.4Um
C1 4 0 511.2FF
VDD 1 0 4.5
VIN 2 0
+PULSE 0 4.5 6Ns 0.01Ns 0.01Ns 6Ns 12Ns
.TEMP 85.0
.TRAN/OP 1.0NS 42NS 0NS 0.1NS
.PROBE
.PLOT TRAN V(2,0) V(4,0)
.PRINT TRAN V(2,0) V(4,0)
.OPTIONS NODE LIST OPTS ACCT LIMPTS=2000 NUMDGT=8 ITL5=0 ITL4=40
.WIDTH OUT = 80
.OP
*
*
* MOSIS CMOS WORST MINIMUM CURRENT CASE SPICE PARAMETERS
*
*
.MODEL M1 PMOS
+RD      =      32.76
+LEVEL   =      2.000
+VTO     =     -1.000
+KP      =     1.26D-05
+GAMMA   =      0.700
+PH      =      0.600
+LAMBDA  =     4.70D-02
+CGSO    =     4.00D-10
+CGDO    =     4.00D-10
+RSH     =     70.000
+CJ      =     3.50D-04
```

```

+MJ      =      0.500
+CJSW    =     2.00D-10
+MJSW    =      0.330
+TOX     =     5.50D-08
+NSUB    =     1.12D+14
+NSS     =     0.00D+00
+NFS     =     8.80D+11
+TPG     =     -1.000
+XJ      =     4.00D-07
+LD      =     4.80D-07
+UO      =     200.000
+UCRIT   =     1.60D+04
+UEXP    =      0.150
+VMAX    =     1.00D+05
+NEFF    =      0.010
+DELTA   =      1.900

```

*

.MODEL M2 NMOS

```

+RD      =      29.73
+LEVEL   =      2.000
+VTO     =      1.000
+KP      =     3.77D-05
+GAMMA   =      1.500
+PHI     =      0.600
+LAMBDA  =     1.60D-02
+CGSO    =     5.20D-10
+CGDO    =     5.20D-10
+RSH     =     30.000
+CJ      =     2.20D-04
+MJ      =      0.500
+CJSW    =     3.00D-10
+MJSW    =      0.330
+TOX     =     5.50D-08
+NSUB    =     1.00D+16
+NSS     =     0.00D+00
+NFS     =     1.20D+12
+TPG     =      1.000
+XJ      =     6.00D-07
+LD      =     3.20D-07
+UO      =     600.000
+UCRIT   =     9.99D+05
+UEXP    =      0.001
+VMAX    =     1.00D+05
+NEFF    =      0.010
+DELTA   =      1.200

```

*

.MODEL M3 PMOS

```

+RD      =      22.16
+LEVEL   =      2.000
+VTO     =     -1.000
+KP      =     1.26D-05

```


+GAMMA = 0.700
 +PHI = 0.600
 +LAMBDA = 4.70D-02
 +CGSO = 4.00D-10
 +CGDO = 4.00D-10
 +RSH = 70.000
 +CJ = 3.50D-04
 +MJ = 0.500
 +CJSW = 2.00D-10
 +MJSW = 0.330
 +TOX = 5.50D-08
 +NSUB = 1.12D+14
 +NSS = 0.00D+00
 +NFS = 8.80D+11
 +TPG = -1.000
 +XJ = 4.00D-07
 +LD = 4.80D-07
 +UO = 200.000
 +UCRIT = 1.60D+04
 +UEXP = 0.150
 +VMAX = 1.00D+05
 +NEFF = 0.010
 +DELTA = 1.900
 *

.MODEL M4 NMOS

+RD = 29.19
 +LEVEL = 2.000
 +VTO = 1.000
 +KP = 3.77D-05
 +GAMMA = 1.500
 +PHI = 0.600
 +LAMBDA = 1.60D-02
 +CGSO = 5.20D-10
 +CGDO = 5.20D-10
 +RSH = 30.000
 +CJ = 2.20D-04
 +MJ = 0.500
 +CJSW = 3.00D-10
 +MJSW = 0.330
 +TOX = 5.50D-08
 +NSUB = 1.00D+16
 +NSS = 0.00D+00
 +NFS = 1.20D+12
 +TPG = 1.000
 +XJ = 6.00D-07
 +LD = 3.20D-07
 +UO = 600.000
 +UCRIT = 9.99D+05
 +UEXP = 0.001
 +VMAX = 1.00D+05
 +NEFF = 0.010

```

+DELTA    =    1.200
*
*
*      SPICE node  Signal name
*
*          0      GND
*          1      VDD
*          2      VIN
*          3      OUT
*          4      INTERMEDIATE
.END

```

LIST OF REFERENCES

Baumstarck, J. E., *SCMOS Silicon Compiler Organelle Design and Insertion*, M.S.E.E. Thesis, Naval Postgraduate School, Monterey, California, December 1987.

Electronics Research Laboratory, College of Engineering, University of California at Berkeley, Memo No. UCB/ERL M80/7, *The Simulationn of MOS Integrated Circuits Using SPICE2*, by A. Vlademirescu and S. Liu, February 1980.

Hodges, D. A. and Jackson, H. G., *Analysis and Design of Digital Integrated Circuits*, McGraw-Hill Book Company, 1983.

Information Sciences Institute, University of Southern California, The MOSIS Project ISI/TM-84-128, *The MOSIS System (What it is and How to Use it)*, March 1984.

Malagon, E. G., *Technology Upgrade of a Silicon Compiler*, M.S.E.E. Thesis, Naval Postgraduate School, Monterey, California, June 1987.

Massachusetts Institute of Technology 1982 Conference on Advanced Research in VLSI, *Generating Custom High Performance VLSI Designs from Succinct Algorithmic Descriptions*, by J. M. Siskind, J. R. Southard, and K. W. Crouch, 25 January 1982.

McCarthy, O. J., *MOS Devices and Circuit Design*, John Wiley & Sons, 1982.

Mead, C. and Conway, L., *Introduction to VLSI Systems*, Addison-Wesley Publishing Company, 1980.

MicroSim Corp., *PSpice*, 1987.

Mullarky, A. J., *CMOS Cell Library for a Silicon Compiler*, M.S.E.E. Thesis, Naval Postgraduate School, Monterey, California, March 1987.

Pollack, S., Erickson, B., and Mazor, S., "Silicon Compilers Ease Complex VLSI Design," *Computer Design*, pp. 79-82, 15 September 1986.

Sedra, A. S. and Smith, K. C., *Micro-Electronic Circuits*, Holt, Rinehart and Winston, 1982.

Signetics Corp., *High-Speed CMOS Data Manual*, 1986.

Weste, N. H. E. and Eshraghian, K., *Principles of CMOS VLSI Design: A Systems Perspective*, Addison-Wesley Publishing Company, 1985.

Wyatt Jr., J. L., "*The Practical Engineer's No-Nonsense Guide to On-Chip Signal Delay Calculations*," VLSI Memo No. 87-381, Massachusetts Institute of Technology, Cambridge, Massachusetts, May 1987 (private communication).

BIBLIOGRAPHY

- Annaratone, M., *Digital CMOS Circuit Design*, Klewer Academic Publishers, 1986.
- Baumstarck, J. E., *SCMOS Silicon Compiler Organelle Design and Insertion*, M.S.E.E. Thesis, Naval Postgraduate School, Monterey, California, December 1987.
- Boylestead, R. and Nashelsky, L., *Electronic Devices and Circuit Theory*, 3rd ed., Prentice Hall, Inc., 1972.
- Carlson, D. J., *Application of a Silicon Compiler to VLSI Design of Digital Pipelined Multipliers*, M.S.E.E. Thesis, Naval Postgraduate School, Monterey, California, June 1984.
- Electronics Research Laboratory, College of Engineering, University of California at Berkeley, Memo No. UCB/ERL M80/7, *The Simulation of MOS Integrated Circuits Using SPICE2*, by A. Vlademirescu and S. Liu, February 1980.
- Hodges, D. A. and Jackson, H. G., *Analysis and Design of Digital Integrated Circuits*, McGraw-Hill Book Company, 1983.
- Information Sciences Institute, University of Southern California, The MOSIS Project ISI/TM-84-128, *The MOSIS System (What it is and How to Use it)*, March 1984.
- Kim, J., "PATH: A Simulation-Based Transistor Sizer," VLSI Memo No. 87-412, Massachusetts Institute of Technology, Cambridge, Massachusetts, September 1987 (private communication).
- Lincoln Laboratory, Massachusetts Institute of Technology, Project Report RVLSI-3, *An Introduction to MacPITTS*, by J. R. Southard, 10 February 1983.
- Lincoln Laboratory, Massachusetts Institute of Technology, Project Report RVLSI-5, *L5 User's Guide*, by K. W. Crouch, 7 March 1984.
- Malagon, E. G., *Technology Upgrade of a Silicon Compiler*, M.S.E.E. Thesis, Naval Postgraduate School, Monterey, California, June 1987.
- Malagon-Fajar, M. A., *Silicon Compilation Using a Lisp-Based Layout Language*, M.S.E.E. Thesis, Naval Postgraduate School, Monterey, California, June 1986.
- Massachusetts Institute of Technology 1982 Conference on Advanced Research in VLSI, *Generating Custom High Performance VLSI Designs from Succinct Algorithmic Descriptions*, by J. M. Siskind, J. R. Southard, and K. W. Crouch, 25 January 1982.

- McCarthy, O. J., *MOS Devices and Circuit Design*, John Wiley & Sons, 1982.
- Mead, C. and Conway, L., *Introduction to VLSI Systems*, Addison-Wesley Publishing Company, 1980.
- Meindl, J. D., "Chips for Advanced Computing," *Scientific American*, v. 257, pp. 78-88, October 1987.
- MicroSim Corp., *PSpice*, 1987.
- Motorola Inc., *CMOS Integrated Circuits*, 1978.
- Motorola Inc., *CMOS/NMOS Special Functions Data*, 1986.
- Mullarky, A. J., *CMOS Cell Library for a Silicon Compiler*, M.S.E.E. Thesis, Naval Postgraduate School, Monterey, California, March 1987.
- Muller, R.S. and Kamins T. I., *Device Electronics for Integrated Circuits*, John Wiley & Sons, 1977.
- Mulvey, J., *Semiconductor Device Measurements*, TEKTRONIX, Inc., Beaverton, Oregon, 1968.
- National Semiconductor Corp., *CMOS Integrated Circuits*, 1975.
- National Semiconductor Corp., *CMOS Databook*, 1981.
- Nilsson, J. W., *Electric Circuits*, Addison-Wesley Publishing Company, 1984.
- Pollack, S., Erickson, B., and Mazor, S., "Silicon Compilers Ease Complex VLSI Design," *Computer Design*, pp. 79-82, 15 September 1986.
- RCA Corp. Solid State, *CMOS Integrated Circuits Databook*, 1983.
- Sedra, A. S. and Smith, K. C., *Micro-Electronic Circuits*, Holt, Rinehart and Winston, 1982.
- Signetics Corp., *High-Speed CMOS Data Manual*, 1986.
- Texas Instruments Inc., *High-Speed CMOS Logic Data Book (Silicon-Gate Complementary MOS)*, 1984.

University of California at Berkeley Report No. UCB/CSD 86/272, *1986 VLSI Tools: Still More Works by the Original Artists*, edited by W. S. Scott, R. N. Mayo, G. Hamachi, and J. K. Ousterhoot, December 1985.

Weste, N. H. E. and Eshraghian, K., *Principles of CMOS VLSI Design: A Systems Perspective*, Addison-Wesley Publishing Company, 1985.

Wilensky R., *LISPcraft*, W. W. Norton & Company, 1984.

Wyatt Jr., J. L., "*The Practical Engineer's No-Nonsense Guide to On-Chip Signal Delay Calculations*," VLSI Memo No. 87-381, Massachusetts Institute of Technology, Cambridge, Massachusetts, May 1987 (private communication).

INITIAL DISTRIBUTION LIST

	No. Copies
1. Defense Technical Information Center Cameron Station Alexandria, VA 22304-6145	2
2. Library, Code 0142 Naval Postgraduate School Monterey, CA 93943-5002	2
3. Department Chairman, Code 62 Department of Electrical and Computer Engineering Naval Postgraduate School Monterey, CA 93943-5000	1
4. Dr. D. E. Kirk, Code 62Ki Department of Electrical and Computer Engineering Naval Postgraduate School Monterey, CA 93943-5000	2
5. Dr. H. H. Loomis, Jr., Code 62Lm Department of Electrical and Computer Engineering Naval Postgraduate School Monterey, CA 93943-5000	2
6. Dr. C. Yang, Code 62Ya Department of Electrical and Computer Engineering Naval Postgraduate School Monterey, CA 93943-5000	1
7. Mr. D. Schaeffer, Code 62 Department of Electrical and Computer Engineering Naval Postgraduate School Monterey, CA 93943-5000	1
8. Dr. B. Wei Department of Electrical Engineering San Jose State University San Jose, CA 95192-0080	1

9. Mr. P. Blankenship 1
Massachusetts Institute of Technology
Lincoln Laboratory
P. O. Box 73
Lexington, MA 02173-0073

10. Mr. J. O'Leary 1
Massachusetts Institute of Technology
Lincoln Laboratory
P. O. Box 73
Lexington, MA 02173-0073

11. Dr. T. Bestul 1
Naval Research Laboratories
Code 7590
Washington, D. C. 20375

12. Mr. A. DeGroot 1
Lawrence Livermore National Laboratory
P. O. Box 808
Livermore, CA 94550

13. Lt Col A. Ross, USAF 1
Naval Research Laboratory, Code 9110
4555 Overlook Ave., S. W.
Washington, D. C. 20375

14. CDR D. Southworth, USN 1
Office of Naval Technology, Code ONT227
800 N. Quincy (BT#1)
Arlington, VA 22217-5000

15. Mr. J. Hall 1
Office of Naval Technology, Code ONT20P4
800 N. Quincy (BT#1)
Arlington, VA 22217-5000

16. Deputy Commanding General 1
Marine Corps Research, Development, and Acquisition Command
Code C2IS
Quantico, VA 22134

17. Commandant of the Marine Corps 1
Headquarters, United States Marine Corps
Code INTS
Washington, D. C. 20380-0001

- | | | |
|-----|--|---|
| 18. | Mrs. B. Steele
Digital Equipment Corporation
MK02-2/F10
Continental Boulevard
Merrimack, NH 03054 | 1 |
| 19. | Mr. J. McCracken
United States Department of Labor
Room S 1310
Frances Perkins Building
200 Constitution Ave. N. W.
Washington, D. C. 20210 | 1 |
| 20. | LtCol W. H. Keller, III, USMC
110 Owings Hill Court
Owings, MD 20736 | 1 |
| 21. | Mrs. Robert Limes
411 Evergreen Road
Pacific Grove, CA 93950 | 1 |
| 22. | Col M. Sanger, USA
1803 Rupert Street
MacLean, VA 22101 | 1 |
| 23. | Capt G. Steele, USMC
Marine Corps Research, Development, and Acquisition Command
Code C2IS
Quantico, VA 22134 | 3 |